Computational modelling of particulate composites using meshless methods

Md. Sultanul Islam

Supervisors: Dr. Sivakumar Kulasegaram
Prof. David Kennedy

A thesis submitted to the graduate school in fulfilment of the requirements for the degree of Doctor of Philosophy

November 28, 2011

Institute of Mechanics and Advanced Materials
Theoretical and Computational Mechanics

Cardiff, Wales, U.K.

Abstract

This thesis deals with the numerical simulation of particulate composites using one of the more stable and accurate meshless methods namely the element free Galerkin (EFG) method. To accurately describe the material inhomogeneities present in particulate composites, an extrinsic enrichment function is incorporated into the approximation of the EFG method which produces more versatile, robust and effective computational methodology. The effectiveness of the proposed numerical model is then investigated by employing the model to analyse different configurations of particulate composites. The accuracy and efficiency of this enriched EFG method are studied numerically by comparing the results obtained with the available analytical solutions and other numerical techniques. Further, it is demonstrated that the method developed in this work has the potential to efficiently model syntactic foam, a type of particulate composites. This is illustrated by performing multi-scale modelling using homogenisation technique which confirms satisfactory comparison of the numerical method with experimental results. To further explore the applicability of the developed methodology, an enriched or extended finite element method (XFEM) based technique, is applied to study crack inclusion and interaction of crack propagation with matrix and particles within particle reinforced composite material.

Declaration

This work has not previously been accepted in substance for any degree and is not concurrently submitted in candidature for any degree.

Signed ……..... (candidate) Date ……

Statement 1

This thesis is being submitted in partial fulfillment of the requirements for the degree of Doctor of Philosophy (PhD).

Signed ……..... (candidate) Date ……

Statement 2

This thesis is the result of my own independent work/investigation, except where otherwise stated. Other sources are acknowledged by explicit references.

Signed ……..... (candidate) Date ……

Statement 3

I hereby give consent for my thesis, if accepted, to be available for photocopying and for inter-library loan, and for the title and summary to be made available to outside organisations.

Signed ……..... (candidate) Date ……

Acknowledgements

This thesis is the result of several years interesting work. It would not have been completed, without the support of many people who encouraged and assisted me throughout its completion.

I would like to express my deepest gratitude to my supervisor Dr. Sivakumar Kulasegaram, who mentored me patiently and diligently along this academic journey. He has been patient throughout this endeavour, and his constant encouragement keeps me motivated throughout this long journey. I am very thankful to Prof. David Kennedy for his support and advice.

I owe special gratitude to Prof. Stephane Bordas whose tremendous support and advice has been invaluable for this thesis. Words are simply not enough to express my gratefulness to him the way he guided me. I would like to thank my colleague and friend Dr. Sundararajan Natarajan for his enormous contribution in completing this thesis. I would like to acknowledge all of my research group members Ahmad, Chang-Kye, Haojie and Olivier for the great friendship they have demonstrated with me and helped me in so many ways over the last couple of years. In particular I would like to show my heartfelt appreciation to Ahmad who has been always with me in difficult times.

I would like to thank everyone from the school of engineering who have helped me throughout the PhD. A especial and heartily thanks to Chris Lee for the love and support she has given me through the hard times in dealing with the paper works. I would like to thank all of my friends that I have made throughout my post graduate life in Cardiff, especially Shakil, Alam, Faisal, Sumon bhai, Hasan, Zico, Zeeshan, Riaz, Sadi, Mehedi, Tousif, Rahat, Sagor, Sayem, Saikat, Nusrat, Shams, Kashfia, Sanjana, Bulbul bhai and family, Shishir bhai and family(Afra), Sharif bhai and family, Sadeque bhai and family, Imtiaz bhai and family, Fasih bhai and Family,

Kamrul bhai and family, Ketan bhai and family, Barna apa and family, Mamun bhai and family, Rajib bhai and family, Saiful bhai and family, Sumi apa, Motiar bhai, Shishir bhai and family, Buppi bhai and family, Rashid uncle and family, Hasan uncle, Lulu aunty, Shoaib, Sabrina, Musa uncle and family, Mesbah uncle and family for their love, warmth and affection during these years.

I would like to express my profound gratitude to my uncle Dr. Mofiz, my aunt Dr. Nargis and my cousin Dip, who have always supported me, believed in me and showered me with so much love and adoreness that I did not feel to be away from home. I would like to pay sincere tribute to my late grandfather, my sister Dr. Daisy, brother-in-law Dr. Raju and my adorable nieces Nafisa and Nabila. Without their support, love and encouragement, I would not be the person I am today. Finally and most importantly I would like to thank my mother for the endless support she has given me through the hard times and praise she has given me during the good times. Your support, both moral and financial, has been very much appreciated.

I dedicate this work to my greatest teachers, my father late Abul Quasem and my mother Sultana Razia, to whom I owe everything in my life.

Contents

List of figures

List of tables

List of Abbreviations and Nomenclature

Greek letters

s	Stress tensor, unit
e	Strain tensor
l	Lagrange multipliers
f	EFG shape function
y	Enrichment function
j	Level set function
Ω	Structural domain
Γ	Boundary
u	Poisson's ratio
c	Lame constant
m	Lame constant

Conventions

A	Cross-sectional area
H	Heaviside function
R	Ramp function
V	Volume fraction
a	Enriched nodal variables associated to material interface enrichment

x	Co-ordinates in Cartesian co-ordinate system
b	Body force vector
n	Unit outward normal vector
E	Young's modulus of elasticity, unit
D	Material matrix modulus, unit
K	Global stiffness matrix
f	Force vector
u	Vector of unknown coefficients
d	Size of the domain of influence

Acronyms

FEM	Finite element method
FDM	Finite difference method
FVM	Finite volume method
MLS	Moving least square
PDE	Partial differential equation
RKPM	Reproducing kernel particle method
EFG	Element free Galerkin
SPH	Smoothed particle hydrodynamics
MLPG	Meshless local Petrov Galerkin
DEM	Diffuse element method

PUM	Partition of unity method
MMC	Metal matrix composites
FGM	Functionally graded materials
SEM	Scanning electron microscopic
RVE	Representative volume element
XFEM	Extended finite element method
BEM	Boundary element method

Chapter 1

INTRODUCTION

1.1 Composite materials

Contemporary engineering tools and applications have been significantly improved by the use of composite materials that are specially designed to provide the desired mechanical behaviour. Composite materials have introduced a new dimension in the field of mechanics because of their distinctive characteristics and wide range of applicability. These materials are heterogeneous man-made mixtures of two or more homogeneous phases that are bonded together. Multi-phase composites have attracted more attention in recent years due to their tailorable properties of stiffness, fracture toughness and other favourable characteristics [1]. Composite materials (often called composites) are engineered materials with significantly new physical or chemical properties. The first phase or base material is called the matrix and is usually a light metal (e.g. aluminium, titanium etc.) while the other phase is the reinforcement and is commonly either particles or fibres, the former being the more widely used. In general, the second phase substance or particles has much higher stiffness than the matrix.

The term "composite" is usually reserved for those materials in which the distinct phases are separated on a scale larger than the atomic, and in which properties such as the elastic modulus are significantly altered in comparison with those of a homogeneous material. Composite materials offer a variety of advantages in comparison with homogeneous materials. These include the ability for scientists or engineers to exercise considerable control over material properties, the potential to produce stiffer, stronger, lightweight materials as well as for highly resilient and compliant materials. For this reason increasing interest in composite materials exists in engineering.

Composite materials can be classified based on a number of criteria. Based on the type of matrix materials used, composite materials can be divided into three types:

1. *Metal matrix composites*
2. *Polymer matrix composites*
3. *Ceramic matrix composites*

Based on the nature of reinforcement, common composite materials can be classified as follows:

i. Fibres as the reinforcement (Fibrous Composites)

Fibre reinforced composites provide improved strength, strength-to-weight ratio and other mechanical properties by incorporating strong, stiff but brittle fibres into a softer, more ductile matrix. The matrix material acts as a medium to transfer the load to the fibres, which carry most of the applied load. These composites are classified into two types:

a. *Random fibre (short fibre) reinforced composites* (Figure 1.1(a))
b. *Continuous fibre (long fibre) reinforced composites* (Figure 1.1(b))

ii. Particles as the reinforcement (Particulate composites)

Particulate Composites consist of a matrix reinforced with a dispersed phase in the form of particles (Figure 1.1(c)). Plastics, cermets and metals are examples of particles.

iii. Flat flakes as the reinforcement (Flake composites)

Flake composites consist of thin, flat flakes held together by a binder or placed in a matrix (Figure 1.1(d)). Almost all flake composite matrices are plastic resins. The most commonly used flake materials are glass, mica and aluminium.

iv. Fillers as the reinforcement (Filler composites)

In filler composites, filler materials are added to a composite result in strengthening the composite and reducing weight (Figure 1.1(e)).

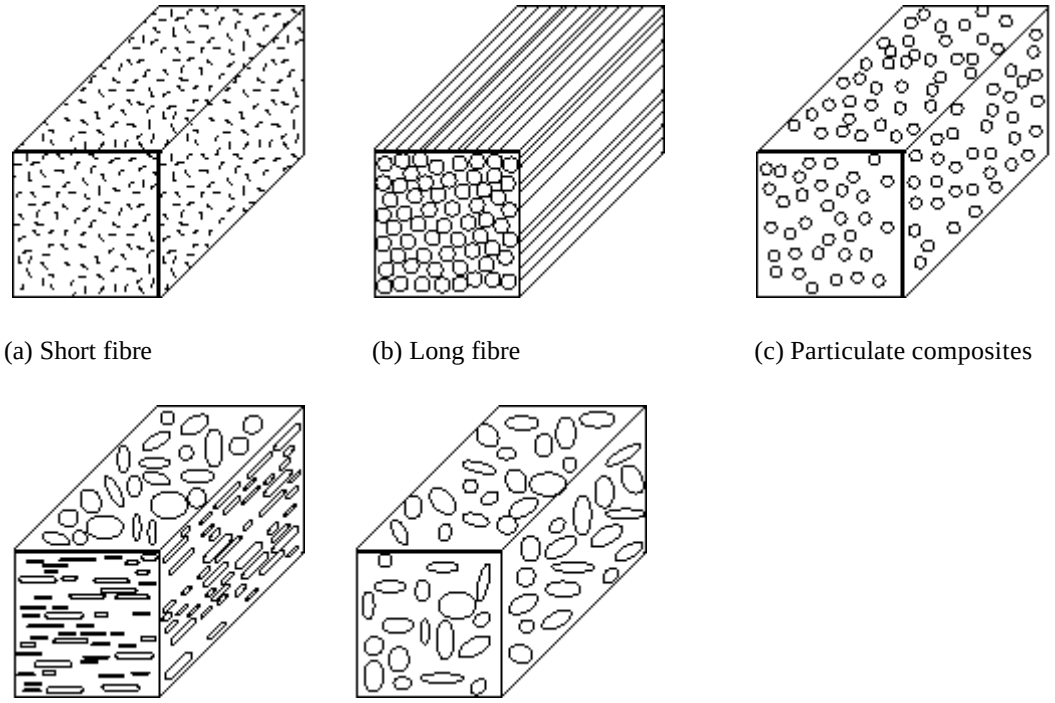

(a) Short fibre (b) Long fibre (c) Particulate composites

(d) Flake composites (e) Filler composites

Figure 1.1: Schematic diagrams of different types of composites [2]

Particulate Composites have the potential to enable the development of new materials, and alter some of their properties and property combinations to unprecedented level. The high costs and technical difficulties involved with the fabrication of many fibre-reinforced composites often limit their use in many practical applications [3]. Particulate composites can be regarded as viable alternatives to them. They can be processed to the desired shape and can have improved stiffness, strength and fracture toughness characteristics. They hold high potential where shock or impact properties are important. For example, particle-reinforced metal matrix composites have shown great potential for many automotive applications [4]. In this proposed research, particulate composites will be discussed as they have been more widely used as composite materials.

1.2 Particulate Composites

As the name itself indicates, the reinforcement is of particulate nature. It may be spherical, cubic, tetragonal, a platelet, or of other regular or irregular shape. However,

particulate composites are slightly less broad than ordinary composites. A particulate composite has homogenous properties. For example it would make no difference if a force was applied to the front, back or side of the object as the material would have the same properties throughout. Soil is the most common example of natural particulate composites; where as concrete is the most widely used man-made particulate composites for past several decades. This particular material can be considered as extensively understood because of the amount of research and experimental work that have been done on it in the past decades.

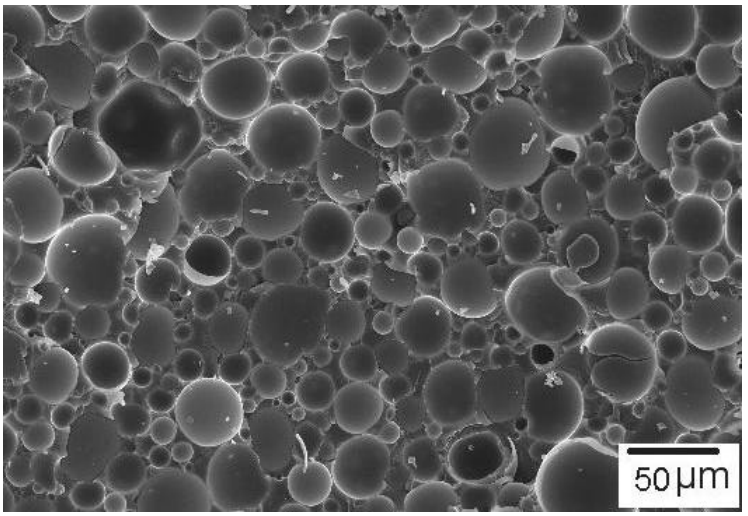

Figure 1.2: The microstructure of syntactic foam containing 60% microballoons by volume [5]

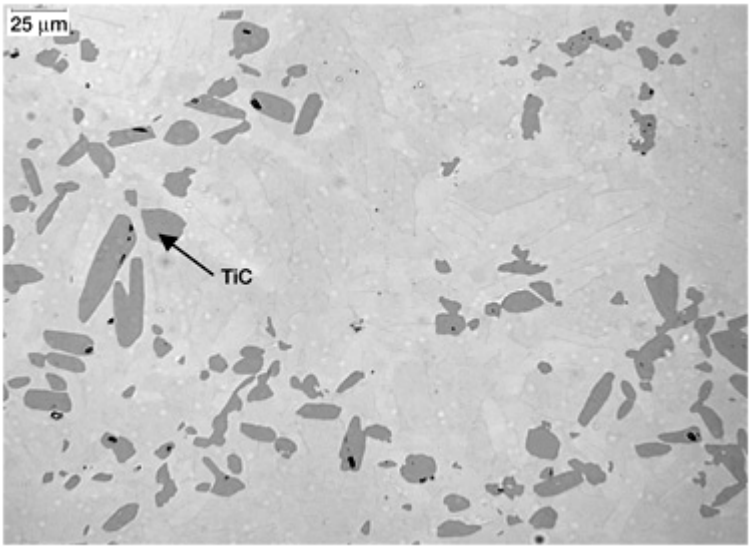

Figure 1.3: Distribution of titanium carbide particles in a matrix of titanium alloy, Ti-6Al-4V [6]

Figure 1.2 and 1.3 illustrate scanning electron microscopic (SEM) pictures of two different types of particulate composites.

Particulate composites are designed not only to improve the strength, but also to produce specific performance oriented applications. One approach to predict the effective mechanical properties of a two-phase composite is to apply the rule of mixtures [7]. According to the rule of mixtures, each of the constituent phases of the composite contributes to the effective mechanical property to an extent depending on the volume fraction of the constituent phase. Mechanical properties, such as modulus of elasticity, of particulate composites are achievable within the range defined by rule of mixtures as follows:

Upper bound is represented by: $E_c(upper) = E_m V_m + E_p V_p$

And lower bound is represented by: $E_c(lower) = \dfrac{E_m E_p}{E_p V_m + E_m V_p}$

where E and V denote modulus of elasticity and volume fractions respectively while subscripts c, m, p represent composite, matrix and particulate phases respectively. From Figure 1.4, it can be seen that for a given volume fraction, the moduli of various conceivable composites lie between an upper bound given by isostrain condition and a lower bound given by isostress condition.

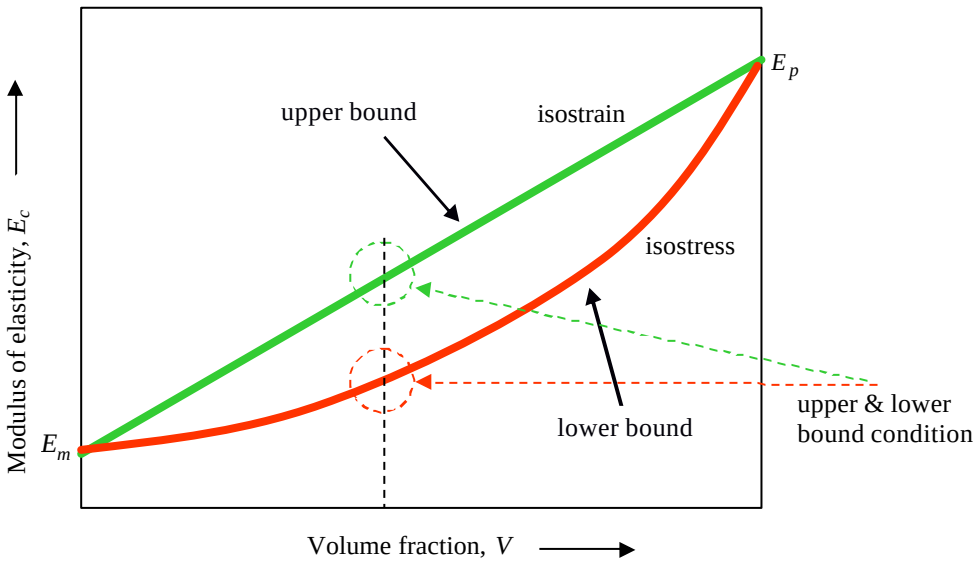

Figure 1.4: Rule of mixtures for particulate composites [8]

Functionally graded materials (FGMs), produced from particulate composites, are attracting considerable attention due to the increasing performance demands in modern engineering applications [9]. Such materials have been used in various fields, for example in biomedical [10], sensor and energy applications [11]. FGMs contain either a gradual or a stepwise change in material properties along a given direction. In particulate composites a graded structure can be obtained by either changing (a) the particle volume fraction or (b) the particle size along the thickness of the composite [12].

1.3 Application of particulate composites

Composite materials are continuously replacing traditional engineering materials because of their advantages of high stiffness and strength over homogeneous materials. The type, shape and spatial arrangement of the reinforcing phase in particulate composites are the key parameters in determining their mechanical behaviour. In the processing of particulate composites, one of the subjects of interest is to choose a suitable matrix and a reinforcement material. In some cases, chemical reactions that occur at the interface between the matrix and its reinforcement materials have been considered harmful to the final mechanical properties and are usually avoided. Sometimes, the interfacial reactions are intentionally induced, because, the new layer formed at the interface acts as a strong bond between the phases [13].

Particulate composites are used with all three matrix material types – metals, polymers and ceramics. One of the major applications of particulate composites have been in the metal matrix composites (MMCs), where silicon carbide, silicon nitride, alumina, and other inorganic particles are used as reinforcements for aluminium alloys and for higher temperature materials such as the nickel base alloys and titanium. Various applications of the MMCs are listed in Table 1.1.

Table 1.1: Features and applications of metal matrix composites (MMCs) [13]

MMC Types	Industrial applications	Special features
Graphite reinforced in aluminium	Bearings	Cheaper, lighter, self-lubricating, conserves copper, lead, tin, zinc
Graphite reinforced in aluminium, silicon carbide reinforced in aluminium, aluminium oxide reinforced in aluminium	Automobile pistons, cylinder liners, piston rings, connecting rods	Reduced wear, anti seizing, cold start, lighter, conserves fuel, improved efficiency.
Graphite reinforced in copper	Sliding electrical contacts	Excellent conductivity and anti seizing properties.
Silicon carbide reinforced in aluminium	Turbocharger impellers	High temperature use
Glass or carbon bubbles reinforced in aluminium		Ultra light material.
Cast carbon fibre reinforced magnesium fibre composites	Tubular composites for space structures	Zero thermal expansion, high temperature strength, good specific strength and specific stiffness.
Zircon reinforced in aluminium-silicon alloy, aluminium silicate reinforced in aluminium	Cutting tool, machine shrouds, impellers	Hard, abrasion-resistant materials.

During the production of MMCs, several oxides are used as reinforcements, in the form of particulates. For example, alumina, zirconium oxide and thorium oxide particulates are used as reinforcements in aluminium, magnesium and other metallic matrices. Because of their high specific stiffness, lightweight, and high thermal conductivity, boron in an aluminium matrix have been used for structural tubular

supports in the space shuttle orbiter. MMCs having silicon carbide and a titanium matrix are being used for the skin, beams, stiffeners and frames of the hypersonic aircraft under development [13].

The cermets are the examples of ceramic–metal composites. Cermets contain hard ceramic particles dispersed in a metallic matrix, e.g., titanium carbide (TiC) or tungsten carbide (WC) embedded in cobalt or nickel. They are utilised extensively as cutting tools for hardened steels. The hard carbide particles provide the cutting surface but, being extremely brittle, are not themselves capable of withstanding the cutting stresses. Toughness is enhanced by their inclusion in the ductile metal matrix, which isolates the carbide particles from one another and prevents particle to particle crack propagation [14].

The most common cermet is the cemented carbide. In cemented carbides, particles of tungsten, titanium or tantalum-carbide of dimensions 0.8-5 micrometers are dispersed in cobalt or other metals of the iron group with concentrations up to 94% by volume [14]. Because of utilising relatively large volume fraction of the particulate phase, it maximises the abrasive action of the composite.

Polymers are frequently reinforced with various particulate materials such as carbon black. Carbon black consists of very small and essentially spherical particles of carbon, produced by the combustion of natural gas or oil in an atmosphere that has only a limited air supply. When added to vulcanized rubber, carbon black enhances tensile strength, toughness, tear and abrasion resistance of the rubber. Automobile tires contain in the order of 15 to 30 % volume of carbon black [15]. Aluminium alloy castings containing dispersed SiC particles are widely used for automotive components including pistons and brake applications.

Particulate composites have many engineering applications because they are easy to mould (depending on the type and application) and they have significantly improved stiffness. However, a major drawback is that damage and cracks may occur in the particles and the matrix and at the particle/matrix interface depending on the relative stiffness and the strength of the two constituent materials and the interface strength. If the embedded particles are much stronger and stiffer than the matrix, matrix cracking

and particle/matrix interface debonding (often refer to as dewetting) become the major damage modes [16]. On the other hand, if both constituent materials have material properties in the same order of magnitude, particle cracking can occur. These damages will influence the nature of load response characteristics or in other words non-linear stress-strain relation curve of a particulate composite material [17].

1.4 Importance of numerical simulation

The attractive features of particulate composites have been exploited to investigate their applicability in different branches of engineering. More sophisticated particulate composites have become significantly important in materials engineering over the last couple of decades. They have excelled in certain industries such as the aviation and locomotive industries and other specialist applications such as in space shuttle design. The materials used in these industries are generally on the forefront of technology and are constantly being modified to enhance their material properties as they become better understood. As these materials are relatively new, the development of their behaviour is relatively unknown. Therefore, when designing new applications or modifying material properties of these particulate composites, it is essential that their material properties can be predicted accurately to obtain the desired behaviour.

The investigation of the characteristics and effective material parameters could be done by either performing experiments with the existing material sample or by using analytical methods making rather strong assumptions on the mechanical field variables. However quite often, analytical methods do not lead to sufficiently accurate results. Moreover, they are very few in numbers to be present for a number of applications. The experimental procedure can be expensive and time-consuming as the processing costs can be extremely high to produce them. Hence numerical or computational modelling techniques are preferred. Numerical simulation can play an important role in providing a validation for theories, offers insights to the experimental results and assists in the interpretation or even the discovery of new phenomena. Numerical tools are often more useful than traditional experimental methods in terms of providing an insightful and complete information that can not be directly measured or observed, or difficult to obtain through other means. In the next

section of this chapter, research carried out in the past on particulate composites and modelling heterogeneities using computational modelling and numerical simulations will be discussed.

1.5 Previous research on particulate composites

The main aim will be to focus on the previous work that has been done in modelling particulate composites using numerical simulation. An overview of these research works is presented below:

Scalon [18] stated that a great deal of attention and study has been devoted to the understanding of particulate composite materials. This attention derives from the fact that these materials have achieved a dominant position in the metal matrix composite area because of their relative low cost and easier fabrication when compared with the fibre reinforced materials. Furthermore, these materials have potential in automotive and aerospace applications.

Lloyd [19] and Prangnell [20] showed that the particles in particulate composites were not uniformly distributed in space due to, for instance, the molten metal mixing route in metal matrix composites. As a result, some particle-rich regions, which are usually called clusters, were formed. It has been observed that damage evolution tended to originate preferentially in clustered regions [19] and that different particle shapes show different susceptibility to interfacial decohesion [21].

Kwon et al [16] studied the crack initiation and propagation for particulate composite specimens with a notch. A numerical simulation was conducted to predict the crack behaviour based on the damage initiation, growth and local saturation; and the results were compared to those obtained from the experimental study. It was indicated in the study that an inhomogeneous material property, which usually results from a non-uniform particle distribution in a matrix material, significantly affected the crack behaviour in a particulate composite.

Wilkins and Shen [22] studied the evolution of stresses inside the native inclusion particles in silicon carbide (SiC) particulate reinforced aluminium matrix composites

computationally by recourse to the finite element method. The analyses were performed for a simplistic model. The simplistic model was found to be able to predict the stress enhancement in the inclusion that is consistent with the measured propensity of fatigue crack initiation when elasticity dominates.

Chen et al [23] proposed an effective analytical approach which was developed for the problem of particulate composites containing spherical inclusion with imperfect interface between the matrix and spherical inclusions. In case of thin elastic interphase, the displacement field and the stress field in the inclusion and the matrix was exactly solved for the boundary problem of hydrostatic compression of an infinite spherical symmetrical body.

Okada et al [24] proposed a new boundary element method (BEM) formulation for the analysis of particulate composite materials. Homogenisation analysis based on representative volume element (RVE) was carried out considering a unit cell which contained a number of distributed particles (up to 1000). The effective properties obtained by the approach were accurate when the volume fraction of the particles was less than about 25%.

Tan et al [25] proposed a cohesive particle/matrix interface model for high explosive composite materials and determined the model parameters by experiments. Their model is based on a bilinear cohesive law with three stages, namely, the rising, descending and complete debonding sections which are governed by three parameters (i.e. interface cohesive strength and two moduli for rising and descending linear stages) [26].

Adopting this cohesive interface model, Inglis and Geubelle [27] studied the effect of damage due to particle debonding on the constitutive response of particulate composite materials by using the micromechanics solution and compared it with the multi-scale finite element analysis. Tan et al. [28] studied the interface debonding and its effect on particulate composite materials that are subjected to uniaxial tension.

Chen and Kulasegaram [26] developed a smooth particle hydrodynamics (SPH) [29] based numerical technique to investigate the mechanical properties and evolution of

debonding process in particulate composites. A Lagrangian corrected SPH method was presented together with an appropriate numerical model for treating material interface discontinuity within the particulate composites.

Studies showed that particulate composites have the advantage of simplicity of fabrication and low cost compared with fibrous and laminate composites [30]. Particulates chosen as reinforcement are usually harder and stiffer than the matrix material. This improves the hardness and stiffness of polymeric composites. However, owing to the limited surface area of contact, the load transfer from matrix to particles occurs to a smaller extent. This could lead to insignificant improvement in strength and impact resistance [30].

Rabczuk and Zi [31] presented an extended element free Galerkin (EFG) [32] method for dealing with cohesive cracks. The cracks were described by a jump in the displacement field for particles whose domain of influence was cut by the crack. Particles with partially cut domain of influence were enriched with branch functions. The accuracy of the method, due to the smoothness and higher order continuity, was demonstrated by several quasi static and dynamic crack propagation examples.

Rabczuk et al [33] proposed a three-dimensional extended EFG method for arbitrary crack initiation and propagation that ensured crack path continuity for non-linear material models and cohesive laws. An extrinsic enrichment of the meshfree shape functions was used with discontinuous and near-front branch functions to close the crack front and improve accuracy. The crack was modelled as a jump in the displacement field. The method was applied to several static, quasi-static and dynamic crack problems, illustrating very accurate numerical results compared with available experimental and analytical results.

Yvonnet et al [34] proposed an efficient numerical procedure for computing the effective thermal conductivities of a particulate composite in which the inclusions have different sizes and arbitrary shapes and the interfaces are highly conducting. The elaborated numerical procedure, tested and validated by means of relevant analytical exact and approximate results as benchmarks, has been applied to quantify the size

and shape effects on the effective thermal conductivities of particular composites where the inclusions are coated by a highly conducting interface.

Huynh and Belytschko [35] described the methods for treating fracture in composite materials by the extended finite element method (XFEM) [36, 37] with meshes that are independent of matrix/inclusion interfaces. All discontinuities and near-tip enrichments were modelled using the framework of local partition of unity. Level sets were used to describe the geometry of the interfaces and cracks so that no explicit representation of either the cracks or the material interfaces is needed. A number of numerical results for both two-dimensional and three-dimensional examples illustrated that interface enrichment is sufficient to model the correct mechanics of an interface crack.

Gupta et al [9] studied hollow particle filled composites, called syntactic foams to fabricate functionally gradient composites based on a new approach, which relies on creating a gradient of particles as per their wall thickness. Since this approach is independent of volume fractions, the dimensional stability will be better for such composites. Experimental results, compared with theoretical and finite element analysis, showed that the flexural properties of functionally graded syntactic foams (FGSF) based on wall thickness approach can be controlled more effectively.

Du et al [38] adapted enrichment techniques to account for the material interfaces in the framework of the XFEM for particle reinforced composites. The level set function was used to describe the geometry of material distribution, as well as to construct enrichment function for material boundaries. A plate with multi-circular inclusions under uniaxial tension was simulated by finite element method (FEM) and XFEM respectively where the results showed that XFEM was highly effective and efficient.

Ying et al [39] showed that for particle reinforced composites, the enrichment technique for the XFEM was used to account for the material interfaces. It was demonstrated that the particle reinforced composites with three kinds of distributions of particles under uniaxial tension was simulated by XFEM and FEM, respectively. The comparison showed the effectiveness of the XFEM.

Zhu et al [40] proposed an efficient three dimensional numerical approach based on the extended finite element method to model linear spring-layer curved imperfect interfaces and then applied to predict the effective bulk and shear moduli of spherical particle composites in which such imperfect interfaces intervene. The computed effective bulk and shear moduli of composites were compared with the analytical upper and lower bounds derived by Hashin [41].

Wang et al [42] developed a numerical technique for modelling the interaction between propagating cracks and the second phase particles by using the XFEM. The numerical results showed that the energy release rate may substantially be affected by the presence of the particles. Consequently the crack growth trajectories are also changed. A pre-existing flaw on the interface of a particle could attract the crack, to promote rapid crack propagation and increase the energy release rate.

There is a plethora of literature available in modelling composite materials. However, the above review has only highlighted a number of key numerical methodologies mainly adopted for modelling particulate composites.

There have been many techniques developed in order to exploit the attractive features of particulate composites. However, for a number of engineering applications which involve large deformation of material or complicated boundaries, meshless methods can be best suited due to their unique characteristics. Moreover, for irregular shape particles, meshless methods would be more suitable compared to the mesh-based methods due to the burden of mesh generation. In this particular study, one of the most popular, stable and accurate meshless methods namely the EFG method will be used.

1.6 Scopes and objectives of the thesis

The objectives of the research presented in this thesis are to:

- Develop an EFG based numerical model to simulate particulate composites.
- Determine the accuracy of the model and investigate possible improvements.

- Explore the characteristics of enriched EFG formulation for particulate composites and compare with general EFG formulation.
- Validate the accuracy of the model by comparing the results obtained with analytical and other numerical methods.
- Make a comparison between two enrichment based methods – enriched EFG and XFEM.

1.7 Outline of the thesis

This thesis is organised as follows. Chapter 2 reviews the general background of the meshless methods along with a brief description of some of the well known meshless methods. Then a detailed formulation of the EFG method is presented, followed by the numerical discretisation of a 2-D linear elastic problem. This chapter concludes with different types of enrichment techniques that can be applied into the EFG method.

Chapter 3 reviews the problem dealing with heterogeneous materials. A numerical model which can simulate particulate composites is developed and presented in this chapter. The discontinuity in the model is tackled by the enrichment function, which was implemented by the level set methods. Level set functions for circular discontinuity are presented, along with their formulations.

Numerical results obtained from the simulation of particulate composites are presented in chapter 4. The accuracy of the model is compared with suitable analytical solutions available in the literature, and the convergence analysis of the method is carried out by validating the results against similar results produced in other numerical methods.

Chapter 5 reviews the findings from this research, which emphasises the main contributions of this PhD research work. A brief summary of the key findings and recommendations are presented, where perspectives of the possible future directions that could be developed in this research field are discussed.

References

1. Carol, I., Lopez, C. and Roa, O., *Micromechanical analysis of quasi-brittle materials using fracture-based interfae elements.* International Journal for Numerical Methods in Engineering, 2001. **52**(12): p. 193-215.
2. eFunda. *Introduction to composite materials. available at: http://www.efunda.com/formulae/solid_mechanics/composites/comp_intro.cfm* [Accessed 10 April 2010].
3. Mital, S.K., and Murthy, P.L.N., *Uncertainties in the thermal and mechanical properties of particulate composites quantified.* Glenn Research Centre, NASA, 1999.
4. Mital, S.K., and Murthy, P.L.N., *Quantifying uncertainties in the thermo-mechanical properties of particulate reinforced composites.* Journal of Reinforced Plastics and Composites, 2000. **19**: p. 657-678.
5. Gupta, N., and Nagorny, R., *Tensile properties of glass microballoon-epoxy resin syntactic foams.* Journal of Applied Polymer Science, 2006. **102**(2): p. 1254-1261.
6. Glenn Research Centre, NASA. *Particulate titanium matrix composites tested. available at: http://www.grc.nasa.gov/WWW/RT/RT2002/5000/5920thesken2.html* [Accessed 30 June 2011].
7. Pal, R., *New models for effective Young's modulus of particulate composites.* Composites Part B: Engineering, 2005. **36**(6-7): p. 513-523.
8. Krock, R.H., *ASTM proceedings.* 1963. **63**.
9. Gupta, N., Gupta, S.K., Mueller, B.J., *Analysis of a functionally graded particulate composite under flexural loading conditions.* Materials Science and Engineering A, 2008. **485**: p. 439-447.
10. Pompe, W., Worch, H., Epple, M., Friess, W., Gelinsky, M., Greil, P., Hempel, U., Scharnweber, D., Schulte, K., *Functionally graded materials for biomedical applications.* Materials Science and Engineering A, 2003. **362**(1-2): p. 40-60.

11. Müller, E., Drasar, C., Schilz, J., Kaysser, W. A., *Functionally graded materials for sensor and energy applications.* Materials Science and Engineering A, 2003. **362**(1-2): p. 17-39.
12. Hashmi, S.A.R. and U.K. Dwivedi, *Estimation of concentration of particles in polymerizing fluid during centrifugal casting of functionally graded polymer composites.* Journal of Polymer Research, 2007. **14**(1): p. 75-81.
13. Vijayaram, T.R., *Metallurgical applications of metal matrix composites.* Article published in The Metallurgist, 2004.
14. Lee, S.M., *Handbook of composite reinforcements.* Wiley-VCH publishers Inc., 1993.
15. Callister, W.D., *Fundamentals of Materials Science and Engineering*. Fifth ed 2000, Toronto: John Wiley & Sons, Inc.
16. Kwon, Y.W., Lee, J.H., and Liu, C.T., *Study of damage and crack in particulate composites.* Composites Part B: Engineering, 1998. **29**(4): p. 443-450.
17. Basaran, C., and Nie, S. , *A thermodynamics based damage mechanics model for particulate composites.* International Journal of Solids and Structures 2007. **44**: p. 1099-1114.
18. Scalon, J.D., *Spatial and size distributions of particles in composite materials.* Ph.D. Thesis. Department of Probability & Statistics, University of Sheffield, U.K., 1998.
19. Lloyd, D.J., *Intrinsic fracture mechanisms in inorganic composite systems.* TMS annual meeting, Las Vegas, USA, 1995: p. 39-47.
20. Prangnell, P.B., Barnes, S. J., Roberts, S. M., Withers, P. J., *The effect of particle distribution on damage formation in particulate reinforced metal matrix composites deformed in compression.* Materials Science and Engineering A, 1996. **220**(1-2): p. 41-56.
21. Whitehouse, A.F., and Clyne, T.W., *Cavity formation during tensile straining of particulate and short fibre metal matrix composites.* Acta Metallurgica et Materialia, 1993. **41**: p. 1701-1711.
22. Wilkins, T., and Shen, Y.L., *Stress enhancement at inclusion particles in aluminium matrix composites:computational modelling and implications to fatigue damage.* Computational Materials Science, 2001. **22**: p. 291-299.

23. Chen, J., Tong, J. and Chen, Y., *Elastic properties of particulate composites with imperfect interface.* Journal of Wuhan University of Technology - Materials Science Edition, 2002. **17**(2): p. 78-82.
24. Okada, H., Fukui, Y., and Kumazawa, N., *Homogenization analysis for particulate composite materials using the boundary element method.* Computer Modeling in Engineering and Sciences, 2004. **5**(2): p. 135-149.
25. Tan, H., Liu, C., Huang, Y., Geubelle, P.H., *The cohesive law for the particle/matrix interfaces in high explosives.* Journal of the Mechanics and Physics of Solids, 2005. **53**: p. 1892–1917.
26. Chen, Y., and Kulasegaram, S., *Numerical modelling of fracture of particulate composites using SPH method.* Computational Materials Science, 2009. **47**(1): p. 60-70.
27. Inglis, H.M., Geubelle, P. H., Matous, K., Tan, H., Huang, Y., *Cohesive modeling of dewetting in particulate composites: micromechanics vs. multiscale finite element analysis.* Mechanics of Materials, 2007. **39**(6): p. 580-595.
28. Tan, H., Huang, Y., Liu, C., Ravichandran, G., Inglis, H.M., Geubelle, P.H., *The uniaxial tension of particle-reinforced composite materials with nonlinear interface debonding.* International Journal of Solids and Structures, 2007. **44**(6): p. 1809–1822.
29. Lucy, L.B., *Numerical approach to testing the fission hypothesis.* Astronomical Journal, 1977. **82**: p. 1013-1024.
30. Agarwal, B.D., Broutman, L. T., and Chandrashekhara, K., *Analysis and performance of fibre composites, 3rd edition, 2006* (John Wiley, New York).
31. Rabczuk, T., and Zi, G., *A meshfree method based on the local partition of unity for cohesive cracks* Computational Mechanics, 2007. **39**(6): p. 743-760.
32. Belytschko, T., Lu, Y.Y., and Gu, L., *Element Free Galerkin Methods.* International Journal for Numerical Methods in Engineering, 1994. **37**: p. 229-256.
33. Rabczuk, T., Bordas, S., and Zi, G., *A three-dimensional meshfree method for continuous multiple-crack initiation, propagation and junction in statics and dynamics.* Computational Mechanics, 2007. **40**(3): p. 473-495.
34. Yvonnet, J., Q.C. He, and C. Toulemonde, *Numerical modelling of the effective conductivities of composites with arbitrarily shaped inclusions and*

highly conducting interface. Composites Science and Technology, 2008. **68**(13): p. 2818-2825.

35. Huynh, D.B.P., and Belytschko, T., *The extended finite element method for fracture in composite materials.* International Journal for Numerical Methods in Engineering, 2008. **77**(2): p. 214-239.
36. Belytschko, T., and Black, T., *Elastic crack growth in finite elements with minimal remeshing.* International Journal for Numerical Methods in Engineering, 1999. **45**: p. 601-620.
37. Moës, N., Dolbow, J., and Belytschko, T., *A finite element method for crack growth without remeshing.* International Journal for Numerical Methods in Engineering, 1999. **46**: p. 131-150.
38. Du, C., Ying, Z., and Jiang, S., *Extended finite element method and its application in heterogeneous materials with inclusions.* Materials Science and Engineering, 2010. **10**(1): p. IOP Conference Series.
39. Ying, Z., Du, C., and Wang, Y., *Numerical simulation of particle reinforced composite using extended finite element method.* . Journal of Hydraulic Engineering, 2011. **42**(2): p. 198-203.
40. Zhu, Q.Z., Gu, S.T., Yvonnet, J., Shao, J.F., He, Q.C., *Three-dimensional numerical modelling by XFEM of spring-layer imperfect curved interfaces with applications to linearly elastic composite materials.* International Journal for Numerical Methods in Engineering, 2011. **88**: p. 307-328.
41. Hashin, Z., *Extremum principles for elastic heterogenous media with imperfect interfaces and their application to bounding of effective moduli.* Journal of the Mechanics and Physics of Solids, 1992. **40**: p. 767-781.
42. Wang, Z., Ma, L., and Wu, L., *Numerical simulation of crack growth through particulate clusters in brittle matrix using the XFEM technique.* Procedia Engineering, 2011. **10**: p. 786-791.

Chapter 2

MESHLESS METHODS

2.1 General background

A mesh is defined as any of the open spaces or interstices between the strands of a net that is formed by connecting nodes in a predefined manner [1]. In finite difference method (FDM), the meshes used are often called grids; in finite volume method (FVM), they are called volumes or cells; and in finite element method (FEM), they are called elements. The terminologies of grids, volumes, cells and elements carry certain physical meanings as they are defined for different physical problems. However, all these notations - grids, volumes, cells, and elements can be termed meshes according to the above definition of mesh. The key aspect is that a mesh must be predefined to provide a certain relationship between the nodes, which is the core of the formulation of these conventional numerical methods.

A recent strong interest is focused on the development of the next generation of computational methods - meshless methods, which are expected to be more suitable than the conventional grid-based methods for a number of applications. Meshless methods use a set of nodes scattered within the problem domain as well as set of nodes scattered on the boundaries of the domain to represent the problem domain and its boundaries. These set of scattered nodes do not form a mesh, which means that no information between the nodes is required at least for field variable interpolation. The key idea of the meshless methods is to provide accurate and stable numerical solutions with all types of possible boundary conditions with a set of arbitrarily distributed nodes (or particles) without using any mesh that provides the connectivity of these nodes or particles. One important goal of the initial research to perform meshless method is to modify the internal structure of the grid-based FDM and FEM to become more adaptive, versatile and robust. Much effort is concentrated on problems to which the conventional FDM and FEM are difficult to apply, such as problems with free surface, deformable boundary, moving interfaces (for FDM), large deformation (for FEM), complex mesh generation, mesh adaptivity, and multi-scale resolution (for both FDM and FEM) [2]. To overcome these problems, a number of meshless methods have been proposed for analysing solids and structures as well as fluid flows. These meshless methods share some common features, but are different in the means of function approximation and implementation procedures.

2.2 Classification of meshless methods

Based on the formulation, meshless methods can generally be divided into two major categories: methods based on strong form formulations and methods based on weak form formulations. Most of the current meshless applications have been based on the Galerkin (global weak-form) formulation. Galerkin based meshless methods are similar to FEM in that they both require numerical integration to form the disrectised system of equations. However, unlike FEM where the basis functions are simple piecewise polynomials, the basis functions used for meshless methods are often highly nonlinear and not in closed form, as they must satisfy a number of stringent requirements [3].

Some commonly used methods for generating the basis functions include the moving least square (MLS) method [4], the reproducing kernel particle method (RKPM) [3] and point interpolation method [1]. In general, Galerkin-based meshless methods require higher-order numerical integration and a background mesh (though unlike the mesh in FEM, it is not totally dependent of the nodes) for the global integration, which tends to increase the computational cost. In addition to that, most of the basis functions in meshless methods do not satisfy Kronecker delta property (refer to page 35), which often makes it difficult to directly apply the essential boundary conditions.

The strong form methods such as point collocation method [5] and finite point method [6, 7] have attractive advantages of being simple to implement, computationally efficient and "truly" meshfree, as it does not even require a background mesh since no integration is required in establishing the discrete system of equations. Such distinct features facilitate the implementation of the refinement or coarsening scheme as node can be easily inserted or removed without concerning too much about the nodal connectivity. However, they are often unstable and less accurate, especially when irregularly distributed nodes are used for problems governed by partial differential equations (PDEs) with Neumann (derivative) boundary conditions, such as in solid mechanics problems with stress (natural) boundary conditions.

On the other hand, weak form methods, such as the EFG method and meshless local Petrov Galerkin (MLPG) method, are well-established methods due to the advantage of excellent stability and accuracy. The Neumann boundary conditions can be naturally satisfied due to the use of the weak form that involves smoothing (integral) operators. However, the weak form method is said not to be "truly" meshfree, as a background mesh (local or global) is required for the integration of the weak form. An extensive overview of these methods can be found in [8, 9]. A very brief description of some of the popular meshless methods is given below:

2.2.1 Smoothed particle hydrodynamics (SPH) method

The oldest of the meshless methods is the SPH method [10, 11]. SPH, as a meshfree and particle method, was originally invented for modelling astrophysical phenomena, and later extended for applications to problems of continuum solid and fluid mechanics [11]. Gingold and Monaghan [12] provided a rationale for this method by invoking a notion of a kernel approximation which is illustrated below.

In SPH, a kernel interpolation is used to approximate the field variables at any point in a domain. The spatial discretisation of the state variables is provided by a set of particles (points). These particles have a spatial distance (known as the "smoothing length"), over which their properties are "smoothed" by a kernel function. This means that the physical quantity of any particle can be obtained by summing the relevant properties of all the particles which lie within the range of the kernel. For example, an approximation of the value of a function f at the location $\mathbf{x}$ is given in a continuous form by an integral of the product of the function and a kernel (weighting) function $W(\mathbf{x}-\mathbf{x}', r)$:

$$\langle f(\mathbf{x}) \rangle = \int f(\mathbf{x}')\, W(\mathbf{x}-\mathbf{x}', r)\, d\mathbf{x}' \tag{2.1}$$

where the angle brackets $\langle\ \rangle$ denote a kernel approximation, r is a parameter that defines size of the kernel support known as the smoothing length, and $\mathbf{x}'$ is the new independent variable.

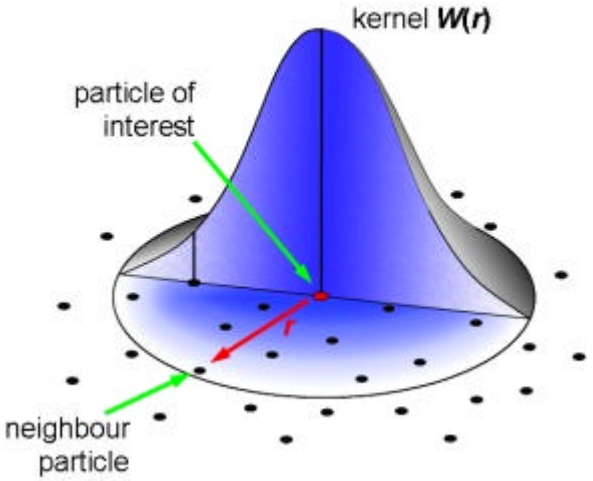

Figure 2.1: Principles of the SPH kernel function [13]

The kernel function usually has the property of compact support, which means it is zero everywhere, but on a finite domain inside the range of the smoothing length $2r$:

$$W(\mathbf{x}-\mathbf{x}',r)=0 \; for \left|\mathbf{x}-\mathbf{x}'\right| \geq 2r \tag{2.2}$$

In a normalised form, it can be written as:

$$\int W(\mathbf{x}-\mathbf{x}',r)d\mathbf{x}'=1 \tag{2.3}$$

2.2.2 Element free Galerkin (EFG) method

The EFG method [4], an innovative approach, can be categorised as a meshless method as discrete equations can be generated with a set of nodes and the description of the internal and external surfaces of the domain, i.e., boundary of the model. This method is based on MLS approximation. Nayroles et al. [14] are the first to use moving least square approximations in a Galerkin method to formulate the so-called diffuse element method (DEM). Based on the idea of Nayroles and motivated by the purpose to model arbitrary crack propagation without computationally expensive remeshing, Belytschko and his co-workers developed the EFG method in 1994 [2]. More detailed description of EFG method is given later in this chapter.

2.2.3 Meshless local Petrov Galerkin (MLPG) method

Atluri and Zhu [15] have proposed the MLPG method that requires only local background cells for the integration. The MLPG method is based on a local weak form and MLS approximation. Because the MLPG does not need any element or mesh either for interpolation or for integration purposes, it has been applied for a number of applications, for example, two-dimensional elasto-statics [16], the analysis of beam and plate structures [17], fluid flows [18] etc. However, the drawback of the MLPG method is the difficulty in handling of the numerical integration near the boundary and the asymmetry of the discretised system matrix.

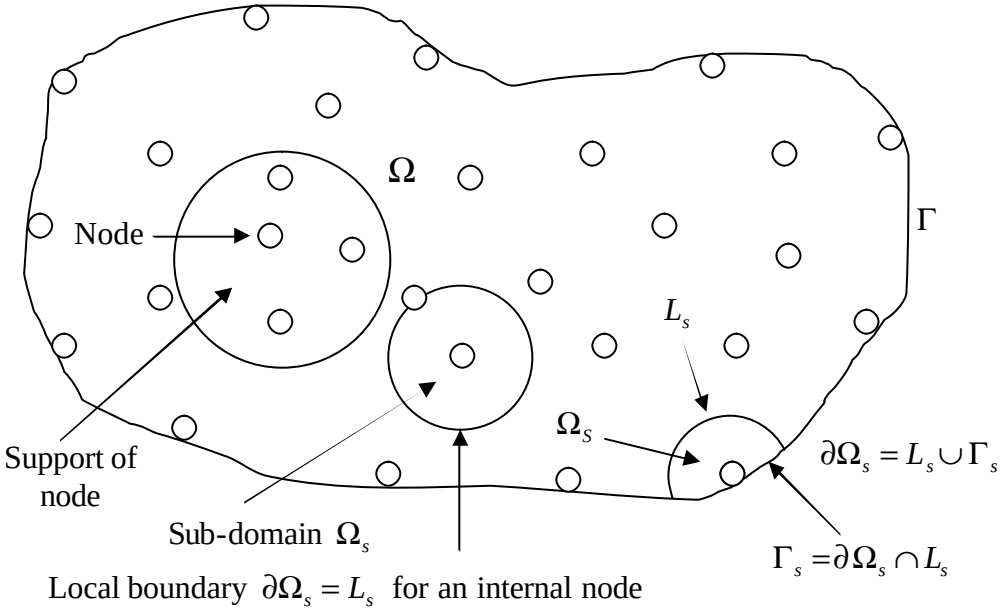

Figure 2.2: The MLPG scheme for a two dimensional domain [19]

Apart from the afore-mentioned meshless methods, many other methods were proposed, such as the reproducing kernel particle method (RKPM) [20], the natural element method [21], the free mesh method [22], method of finite spheres [23], the *h-p* cloud method [24] etc. On the basis of these proposed methods and theoretical development, meshless methods have been applied to many engineering areas, such as fracture mechanics [25-27], fluid mechanics [28, 29] etc.

In our proposed study, the EFG method will be used, because of its potential to be modified and developed for the efficient, reliable and accurate solution for the analysis of static problems in solid mechanics. The EFG method utilises moving least square interpolants, in which only nodes are required to construct the shape function. Cordes and Moran [30] showed that in solid mechanics problems containing material discontinuities, the EFG method was proven to have higher convergence rates over the finite element method. Moreover, moving discontinuities or interfaces can usually be treated without remeshing with minor costs and accuracy degradation (for instance, see Belytschko and Organ [31]).

2.3 Element Free Galerkin (EFG) Method

The EFG method was proposed by Belytschko et al. [4] as an improved version of the DEM as introduced by Nayroles et al. [14]. This is categorised as a meshless method as discrete equations can be generated with a set of nodes and the description of the internal and external surfaces of the domain, i.e., boundary of the model.

Belytschko et al. [4] identified the spatial discretisation mentioned by Nayroles et al. [14] as moving least squares and made three alterations to enhance the accuracy of the method:

1. MLS approximation is employed for the construction of the shape function.
2. Lagrangian multipliers are introduced in the potential energy function to enforce the essential boundary condition.
3. Background mesh, which is flexible in terms of dependency of nodes is corncerned, is required to carry out the integration to calculate system matrices.

The resulting formulation is then called the EFG method. Although EFG is considered meshless while referring to the shape function approximation, an ‘auxiliary’ mesh will be required for solving the PDEs derived from the Galerkin approach [32] . Either a regular background mesh or cell structure is applied while computing the integrals in the weak form, hence it partially opposes the original mesh-free philosophy.

In the traditional mesh-based method, the approximation is based on the rigid connectivity defined by elements. This is one reason why it is difficult to handle large material distortions. The meshless methods, which construct the interpolation in terms of a set of particles rather than elements, are less susceptible to distortion difficulties. Because of the advantages in handling problems which are difficult for the finite element method, the meshless approach has attracted much attention. For instance, EFG method was successfully used in evaluating fracture and crack propagation problems [33-36].

2.3.1 Moving least squares (MLS) approximation

The EFG method is based on the MLS technique introduced by Shepard [37] and Lancaster and Salkauskas [38]. It consists of three components: a basis function, a weight function associated with each node, and a set of coefficients that depends on node position. In this section the main characteristics of the MLS approximation are given. In the MLS approximation, we let

$$\mathbf{u}^h(\mathbf{x}) = \sum_{i=1}^{m} p_i(\mathbf{x}) a_i(\mathbf{x}) = \mathbf{p}^T(\mathbf{x})\mathbf{a}(\mathbf{x}) \tag{2.4}$$

where $\mathbf{u}^h(\mathbf{x})$ is the approximation of the function $\mathbf{u}$, m is the number of terms in the basis, $p_i(\mathbf{x}) = [p_1(\mathbf{x}), p_2(\mathbf{x}), p_3(\mathbf{x}),..., p_m(\mathbf{x})]$ is a polynomial basis function, and $a_i(\mathbf{x}) = [a_1(\mathbf{x}), a_2(\mathbf{x}), a_3(\mathbf{x}),..., a_m(\mathbf{x})]$ is a vector of unknown coefficients, which are functions of the spatial coordinates $\mathbf{x}$.

The basis is usually a complete set of polynomial functions of specific order. Examples of commonly used one dimensional linear and quadratic basis are:

$$\mathbf{p}^T(\mathbf{x}) = (1, x) \qquad \text{(Linear basis)} \tag{2.5}$$

$$\mathbf{p}^T(\mathbf{x}) = (1, x, x^2) \qquad \text{(Quadratic basis)} \tag{2.6}$$

Similarly in two dimensions ($\mathbf{x} = (x, y)$), linear and quadratic bases are used which are

$$\mathbf{p}^T(\mathbf{x}) = (1, x, y) \qquad \text{(Linear basis)} \tag{2.7}$$

$$\mathbf{p}^T(\mathbf{x}) = (1, x, y, xy, x^2, y^2) \quad \text{(Quadratic basis)} \tag{2.8}$$

For example, the approximation $u^h(\mathbf{x})$ with a quadratic basis can be expressed explicitly as:

$$u^h(x, y) = a_1(x, y) + a_2(x, y).x + a_3(x, y).y + a_4(x, y).xy + a_5(x, y).x^2 + a_6(x, y).y^2 \tag{2.9}$$

This type of approximation is commonly known as curve-fitting or surface fitting approximation.

Now let us consider any point $\mathbf{x}$ in the domain Ω and all the nodes (n) $\mathbf{x}_I$ whose domain of influence contain this point. The vector of coefficients $\mathbf{a}(\mathbf{x})$ are obtained by performing a weighted least-square fit for the local approximation, which is obtained by minimising the difference between the local approximation and the function. This yields a quadratic form:

$$J(\mathbf{x}) = \sum_{I=1}^{n} w(\mathbf{x} - \mathbf{x}_I)(\mathbf{u}^h(\mathbf{x}, \mathbf{x}_I) - \mathbf{u}(\mathbf{x}_I))^2 \tag{2.10}$$

$$= \sum_{I=1}^{n} w(\mathbf{x} - \mathbf{x}_I)[\mathbf{p}^T(\mathbf{x}_I)\mathbf{a}(\mathbf{x}) - \mathbf{u}_I]^2 \tag{2.11}$$

where $\mathbf{x}_I$ denotes coordinates of node I, $w_I(\mathbf{x})$ is the weight function of node I at point $\mathbf{x}$, n is the number of nodes in the neighbourhood of $\mathbf{x}$ for which the weight function $w(\mathbf{x} - \mathbf{x}_I)$ is non-zero, $\mathbf{u}_I$ representing unknown parameters associated with node I. The neighbourhood of $\mathbf{x}$ is called the domain of influence of $\mathbf{x}$, providing the compact support associated with it. It is desirable that the weight function $w(\mathbf{x} - \mathbf{x}_I)$ is smooth.

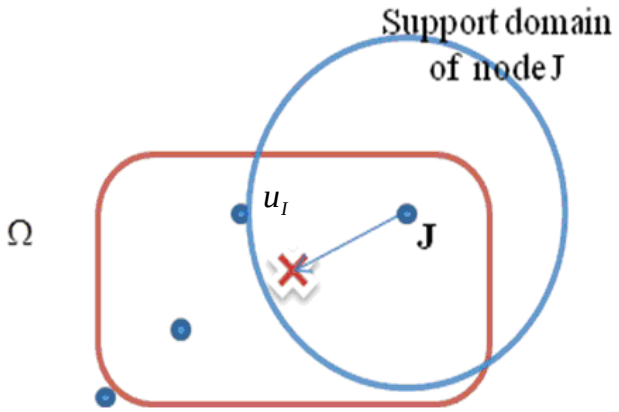

Figure 2.3: Definition of domain of influence

The weight functions are defined so that their overlapping compact supports will cover the entire domain. The overlap of nodal domains of influence defines the nodal connectivity [39].

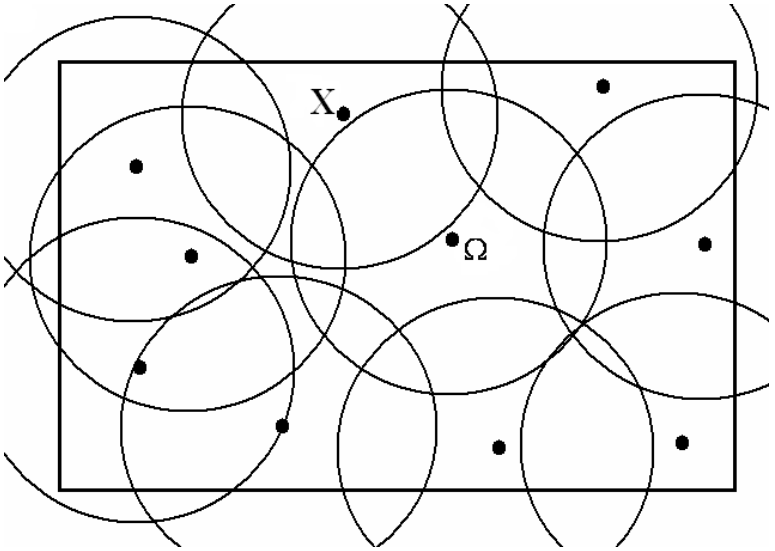

Figure 2.4: Division of domain Ω on overlapping nodal domains of influence [39]

The minimisation of J with respect to $\mathbf{a}(\mathbf{x})$ leads to the following expression:

$$\frac{\partial J(\mathbf{x})}{\partial \mathbf{a}(\mathbf{x})} = \mathbf{A}(\mathbf{x})\mathbf{a}(\mathbf{x}) - \mathbf{B}(\mathbf{x})\mathbf{u} = 0 \tag{2.12}$$

or, $$\mathbf{A}(\mathbf{x})\mathbf{a}(\mathbf{x}) = \mathbf{B}(\mathbf{x})\mathbf{u} \tag{2.13}$$

or, $$\mathbf{a}(\mathbf{x}) = \mathbf{A}^{-1}(\mathbf{x})\mathbf{B}(\mathbf{x})\mathbf{u} \tag{2.14}$$

where

$$\mathbf{A}(\mathbf{x}) = \sum_{I=1}^{n} w_I(\mathbf{x})\, \mathbf{p}^T(\mathbf{x}_I)\, \mathbf{p}(\mathbf{x}_I) \tag{2.15}$$

$$w_I(\mathbf{x}) \equiv w(\mathbf{x} - \mathbf{x}_I) \tag{2.16}$$

$$\mathbf{B}(\mathbf{x}) = [w_1(\mathbf{x})p(\mathbf{x}_1), w_2(\mathbf{x})p(\mathbf{x}_2), ..., w_n(\mathbf{x})p(\mathbf{x}_n)] \tag{2.17}$$

$$\mathbf{u}^T = \{u_1, u_2, ...u_n\} \tag{2.18}$$

Substituting $\mathbf{a}(\mathbf{x})$ into equation (2.3), the approximation $\mathbf{u}^h(\mathbf{x})$ can be rewritten as a sum of nodal components:

$$\mathbf{u}^h(\mathbf{x}) = \sum_{I=1}^{n} f_I(\mathbf{x})\mathbf{u}_I \tag{2.19}$$

where f_I is the shape function given by:

$$f_I(\mathbf{x}) = \mathbf{p}^T(\mathbf{x})\mathbf{A}^{-1}(\mathbf{x})\mathbf{B}_I(\mathbf{x}) \tag{2.20}$$

where $\mathbf{B}_I(\mathbf{x})$ is the I-th column of $\mathbf{B}(\mathbf{x})$.

The spatial derivatives of the shape functions are obtained by

$$f_{I,i} = (\mathbf{p}^T(\mathbf{x})\mathbf{A}^{-1}(\mathbf{x})\mathbf{B}_I(\mathbf{x}))_{,i} \tag{2.21}$$

$$f_{I,i} = \mathbf{p}_{,i}{}^T(\mathbf{x})\mathbf{A}^{-1}(\mathbf{x})\mathbf{B}_1(\mathbf{x}) + \mathbf{p}^T(\mathbf{x})[\mathbf{A}_{,i}{}^{-1}(\mathbf{x})\mathbf{B}_I(\mathbf{x}) + \mathbf{A}^{-1}(\mathbf{x})\mathbf{B}_{I,i}(\mathbf{x})] \tag{2.22}$$

where

$$\mathbf{A}_{,i}{}^{-1}(\mathbf{x}) = -\mathbf{A}^{-1}\mathbf{A}_{,i}\,\mathbf{A}^{-1} \tag{2.23}$$

and the index following a comma is a special derivative.

Weight functions $w_I(\mathbf{x}) \equiv w(\mathbf{x}-\mathbf{x}_I)$ play an important role in the performance of the method [4]. They should be constructed so that they are positive, they should be relatively large for the $\mathbf{x}_I$ close to $\mathbf{x}$ and their magnitude should be decreased as the distance from $\mathbf{x}$ to $\mathbf{x}_I$ increases. In other words, one has to consider weight functions which will depend only the distance between two nodes as follows:

$$w_I(d) \equiv w(\mathbf{x}-\mathbf{x}_I) \tag{2.24}$$

where $d = \|\mathbf{x}-\mathbf{x}_I\|$ is the distance between point $\mathbf{x}$ and node point $\mathbf{x}_I$.

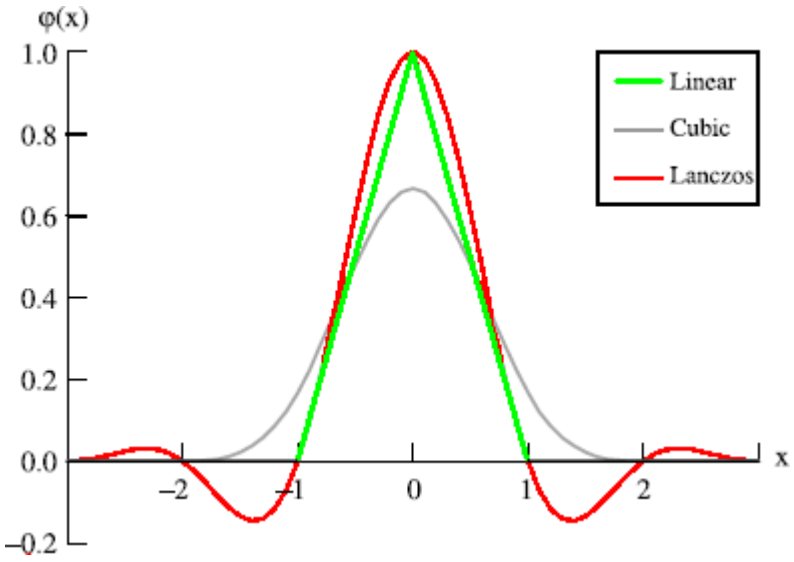

Figure 2.5: Different types of weight function [40]

In this thesis, the cubic spline weight function is chosen which is given by:

$$w(\mathbf{x}-\mathbf{x}_I) \equiv w(r) = \begin{cases} \frac{2}{3} - 4r^2 + 4r^3 & for\ r \le \frac{1}{2} \\ \frac{4}{3} - 4r + 4r^2 - \frac{4}{3}r^3 & for\ \frac{1}{2} < r \le 1 \\ 0 & for\ r > 1 \end{cases}$$

where $r = \frac{\|\mathbf{x} - \mathbf{x}_I\|}{d_{mI}}$, d_{mI} is the size of the domain of influence of the I^{th} node and is computed by:

$$d_{mI} = d_{\max} c_I \tag{2.25}$$

where $d_{\max}$ is a scaling parameter which is typically 2.0-4.0 for a static analysis [32], c_I is the nodal spacing which is a distance to the second nearest node for equally spaced nodes. $d_{\max}$ = 2.5 was shown in [41, 42] as optimal for various static and dynamic fracture mechanics problems.

2.4 Discretisation

In this thesis, only materials with linear elastic behaviour are considered. Hence, the approaches and criteria of linear elastic materials are used. The linear elasticity assumes that displacements in a body are small and that there is a linear relation between stress and strain. For static problems of linear elasticity, this is formulated by the following fundamental system of differential equations and boundary conditions (2.26)-(2.31).

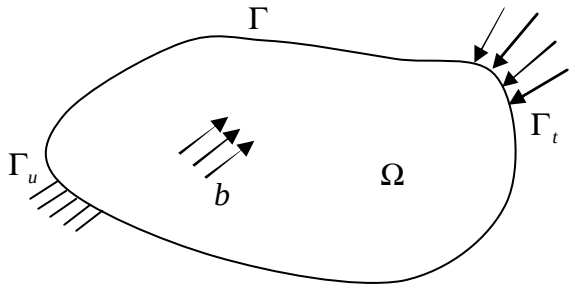

Figure 2.6: An elastic body subject to boundary conditions

The following two dimensional problem of a homogeneous isotropic body is considered on the domain O bounded by the G, as shown in figure 2.6, for which the equation of equilibrium is:

$$s_{ij,j} + b_j = 0 \text{ in } \Omega \tag{2.26}$$

where s_{ij} are the component of the stress tensor and b_j is the body force vector.

The essential boundary conditions are chosen as:

$$u_i = \overline{u}_i \text{ on } \Gamma_{u_i} \tag{2.27}$$

while the natural boundary conditions are written as:

$$s_{ij} n_j = \overline{t}_i \text{ on } \Gamma_{t_i} \tag{2.28}$$

where $\overline{u}_i$ and $\overline{t}_i$ being the prescribed displacements and tractions respectively, and n_j is the unit normal outward vector on the boundary G. The subscripts u and t on Γ denote parts of the boundary on which essential and natural boundary conditions are defined respectively.

The linear stress-strain relation (constitutive relation) is given by the equation:

$$\begin{Bmatrix} s_{xx} \\ s_{yy} \\ s_{xy} \end{Bmatrix} = \mathbf{D} \begin{Bmatrix} e_{xx} \\ e_{yy} \\ e_{xy} \end{Bmatrix} \tag{2.29}$$

where $\mathbf{D}$ is the fourth order elastic tensor, which is given as:

$$\mathbf{D} = \frac{E}{(1+n)(1-2n)} \begin{bmatrix} 1-n & n & 0 \\ n & 1-n & 0 \\ 0 & 0 & \frac{1-2n}{2} \end{bmatrix}, \text{ for plane strain} \tag{2.30a}$$

$$\mathbf{D} = \frac{E}{1-n^2}\begin{bmatrix} 1 & n & 0 \\ n & 1 & 0 \\ 0 & 0 & \frac{1-n}{2} \end{bmatrix}, \text{ for plane stress} \tag{2.30b}$$

where E is the Young's modulus of elasticity and n is the Poisson's ratio.

For small displacements, the strain components can be written as:

$$e_{ij} = \frac{1}{2}\left(u_{j,i} + u_{i,j}\right) \tag{2.31}$$

where u_i are the components of the displacement.

Equation (2.26) is called the 'strong form' and computational solutions of equation (2.26) rely on a process called 'discretisation' which converts the problem into system of algebraic equations.

The variational (or weak) form for the equilibrium equation (2.26) can be written as:

$$dW(\mathbf{u}) = \int_{\Omega} d u_{i,j} s_{ij} d\Omega - \int_{\Omega} d u_i b_i d\Omega - \int_{\Gamma_t} d u_i \bar{t}_i d\Gamma - dW_u(\mathbf{u}) = 0 \tag{2.32}$$

where $dW_u(\mathbf{u})$ represents a term to enforce the essential boundary conditions.

It should be noted that the EFG method does not satisfy the Kronecker delta property, i.e.

$$f_I(\mathbf{x}_J) \neq d_{IJ} = \begin{cases} 1 & if\ I = J \\ 0 & otherwise \end{cases} \tag{2.33}$$

where $f_I(\mathbf{x}_J)$ is the shape function corresponding to the node at $\mathbf{x}_I$, evaluated at a nodal point, $\mathbf{x}_J$, and d_{IJ} is the Kronecker delta. Therefore they are not interpolants,

and the term 'approximants' is used. Hence $u^h(\mathbf{x}_I) \neq u_I$, i.e., the nodal parameters u_I are not the nodal values of $u^h(\mathbf{x}_I)$. The approximation to the displacement at the I^{th} node depends on the nodal parameter u_I as well as the nodal parameters u_1 through u_n corresponding to all other nodes within the domain of influence of node *I*. Therefore the essential boundary conditions can not be imposed directly. To overcome the problem, a number of techniques were developed for enforcing the essential boundary conditions. These are: the Lagrange multiplier method [4], the modified variational principle method [43], the penalty method [35], and coupling with the finite element method [44].

In the proposed study, the Lagrange multiplier method will be used to enforce the essential boundary conditions, since this method is relatively stable and sufficiently accurate. According to this method, dW_u in the variational form can be defined as:

$$dW_u(\mathbf{u}) = \int_{\Gamma_u} dl_i(u_i - \overline{u}_i)d\Gamma - \int_{\Gamma_u} du_i l_i d\Gamma \tag{2.34}$$

where l_i is the Lagrange multiplier.

Hence the governing equation of the weak form can be written as:

$$\int_{\Omega} du_{i,j} s_{ij} d\Omega - \int_{\Omega} du_i b_i d\Omega - \int_{\Gamma_t} du_i \overline{t}_i d\Gamma - \int_{\Gamma_u} dl_i (u_i - \overline{u}_i) d\Gamma - \int_{\Gamma_u} du_i l_i d\Gamma = 0 \tag{2.35}$$

The discrete form of the equation (2.35) is given as:

$$\begin{bmatrix} \mathbf{K} & \mathbf{G} \\ \mathbf{G}^T & 0 \end{bmatrix} \begin{Bmatrix} \mathbf{u} \\ \mathrm{l} \end{Bmatrix} = \begin{Bmatrix} \mathbf{f} \\ \mathbf{q} \end{Bmatrix} \tag{2.36}$$

where **K**, **u** and **f** are the stiffness matrix, the displacement vector and the force vector respectively, and are defined as:

$$\mathbf{K}_{IJ} = \int_{\Omega} \mathbf{B}_I^T \mathbf{D} \mathbf{B}_J \, d\Omega \tag{2.37}$$

where I and J represent I-th and J-th node respectively, and $\mathbf{B}_I$ is the matrix of the shape function derivatives:

$$\mathbf{B}_I = \begin{bmatrix} f_{I,x} & 0 \\ 0 & f_{I,y} \\ f_{I,y} & f_{I,x} \end{bmatrix} \tag{2.38}$$

where a comma designates a partial derivative with respect to the indicated spatial variable.

$$\mathbf{G}_{IK} = \int_{\Gamma_u} f_I \mathbf{N}_K \, d\Gamma \tag{2.39}$$

$$\mathbf{q}_K = -\int_{\Gamma_u} \mathbf{N}_K \bar{\mathbf{u}} \, d\Gamma \tag{2.40}$$

$$\mathbf{N}_K = \begin{bmatrix} N_K & 0 \\ 0 & N_K \end{bmatrix} \tag{2.41}$$

where $\mathbf{N}_K$ is the Lagrange interpolant for node K

$$\mathbf{f}_I = \int_{\Omega} f_I \mathbf{b} \, d\Omega + \int_{\Gamma_t} f_I \bar{\mathbf{t}} \, d\Gamma \tag{2.42}$$

It can be noticed that $\mathbf{K}_{IJ}$ will be non-zero only when f_I and f_J are non-zero on a common part of Ω. Hence, when each weight function (and therefore each shape function) is only non-zero on a small part of Ω, the matrix $\mathbf{K}$ will be sparse.

The enriched EFG method, an extended EFG technique, has been utilised for the approximation of solutions with discontinuities, singularities, or other locally non-

polynomial phenomena. Thereby, optimal convergence rates are achieved for solutions that involve kinks, jumps, and also high gradients within elements. The simulation is typically carried out on simple (often regular) meshes without mesh alignment or refinement near the discontinuities. Two types of enrichment functions will be discussed in the next section.

2.5 Enriched element free Galerkin (EFG) method

The enriched EFG method is designed to enhance the conventional EFG method in order to solve problems that exhibit strong and weak discontinuities in material and geometric behaviour, while preserving the EFG original advantages. In comparison to the EFG method, the enriched EFG method has the following differences [9]:

- Detection of enriched and non-enriched nodes
- Treatment of enriched (additional degrees of freedom)
- Computation of stiffness matrices

Theoretically, enrichment can be regarded as the principal of increasing the order of completeness that can be achieved. In terms of computation, it may simply target higher accuracy of the approximation by including the information obtained from the analytical solution. The choice of the enriched functions depends on the *a priori* solution of the problem. For instance, in a crack analysis this is equivalent to an increase in accuracy of the approximation if analytical near crack tip solutions are somehow included in the enrichment terms [45].

The basic idea of the enrichment is to transform equation (2.3) into a more appropriate form to enhance the way approximation is constructed. The enhancement may be attributed to the degree of consistency of the approximation, or to the capability of approximation to reproduce a given complex field of interest.

There are basically two ways of enriching an EFG approximation: (a) intrinsic enrichment, where the enrichment functions are included in the EFG basis; and (b) extrinsic enrichment, where the approximation is enriched by adding functions externally to the EFG basis.

2.5.1 Intrinsic enrichment

Meshless approximations can be intrinsically enriched by including the enrichment functions in the basis. The MLS approximations used in the EFG method allows the number of bases to be independent of the number of degree of freedom. The field can, therefore, be enriched in an intrinsic way without introducing any extra unknowns. In terms of computational cost, intrinsic method is very much desirable in this aspect.

The basic idea in this approach is to enhance the approximation equation (2.4) by transforming the basis function $\mathbf{p}$ to include new terms so that a certain condition of reproducing a complex field can be satisfied [46]. For instance, for a first order standard linear basis function $\mathbf{p}^{lin} = \{1, x, y\}$; new enrichment terms $\mathbf{p}^{enr} = \{f_1, f_2\}$ are added so that

$$\mathbf{p} = \{\mathbf{p}^{lin}, \mathbf{p}^{enr}\} = \{1, x, y, f_1, f_2\} \tag{2.43}$$

2.5.2 Coupling enriched and linear approximation

Enriching the approximation for the entire domain of a problem is generally unnecessary and increases computational cost. A special technique is presented for coupling the enriched and the linear approximations. The technique involves coupling the approximation over a transition region as a linear basis combination of the enriched linear approximation (this is similar to the way Belytschko et al. [9] coupled EFG to finite elements). The approximation is written as:

$$\mathbf{u}^h(\mathbf{x}) = R\mathbf{u}^{enr}(\mathbf{x}) + (1-R)\mathbf{u}^{lin}(\mathbf{x}) \tag{2.44}$$

where $\mathbf{u}^{enr}(\mathbf{x})$ is the enriched approximation, $\mathbf{u}^{lin}(\mathbf{x})$ is the linear approximation; R is a ramp function which is equal to unity on the enriched boundary of the coupling domain and 0 on the linear boundary of the coupling domain. This is the only requirement imposed on the variable R.

The coupled approximation for the enriched intrinsic basis is then written as:

$$\mathbf{u}^{h}(\mathbf{x}) = \sum_{I=1}^{n} \tilde{f}_I(\mathbf{x})\mathbf{u}_I \tag{2.45}$$

where

$$\tilde{f}_I(\mathbf{x}) = R f_I^{enr}(\mathbf{x}) + (1-R) f_I^{lin}(\mathbf{x}) \tag{2.46}$$

where f_I^{enr} is the shape function formed from the enriched basis and f_I^{lin} is the shape function formed from a linear basis. One of the advantages of this method is that it ensures a compatible displacement field. However, the continuity of the strain field depends on the continuity of the ramp function, R [47].

Belytschko and Fleming [47] found out that mixing the enriched and linear approximations was found to work better for the intrinsically enriched basis than for the extrinsic MLS enrichment. The extrinsic MLS enrichment is sensitive to discontinuities and some loss of accuracy was noticed.

2.5.3 Extrinsic enrichment

Another form of enrichment is based on a so-called extrinsic enrichment. This uses extrinsic bases $p_k(\mathbf{x})$ to increase the order of completeness.

$$\mathbf{u}^{h}(\mathbf{x}) = \sum_{i=1}^{n} f_i(\mathbf{x})\mathbf{u}_i + \sum_{k=1}^{m} p_k(\mathbf{x})\mathbf{a}_k \tag{2.47}$$

where $\mathbf{a}_k$ are additional unknowns or degrees of freedom associated to the enriched solution. It should be noted that the enrichment should be added to each node whose domain of influence extends into the region to be enriched. In a general partition of unity enrichment, equation (2.47) is rewritten as,

$$\mathbf{u}^{h}(\mathbf{x}) = \sum_{i=1}^{n} f_i(\mathbf{x})\mathbf{u}_i + \sum_{k=1}^{m} f_k^{pu}(\mathbf{x})\mathbf{p}(\mathbf{x})\mathbf{a}_k \tag{2.48}$$

2.5.4 Double nodes

In addition to the enrichment strategy that is added to the approximation function in the EFG method, double nodes or pair nodes technique can also be used for solving problems which exhibit material discontinuities. The detailed formulation of this technique will be presented in the next chapter.

2.6 Conclusion

A rigorous description of meshless methods is given in this chapter. Some of the popular meshless methods are described briefly. The EFG method has been illustrated in details, so as the MLS technique. Later it was shown how the enrichment function can be incorporated into the EFG method to solve problems regarding material discontinuity.

A numerical model which can simulate particulate composites will be developed using the enriched EFG method as well as the EFG with double nodes technique in the next chapter.

References

1. Liu, G.R., *Mesh free methods: moving beyond the finite element method*. Boca Raton, Fla.: CRC Press, 2003.
2. Belytschko, T., Krongauz, Y., Dolbow, J., Gerlach, C., *On the completeness of meshfree particle methods.* International Journal for Numerical Methods in Engineering, 1998. **43**(5): p. 785-819.
3. Liu, W.K., and Chen, Y., *Wavelet and multiple scale reproducing kernel methods.* international Journal for Numerical Methods in Fluids, 1995. **21**: p. 901-916.
4. Belytschko, T., Lu, Y.Y., and Gu, L., *Element Free Galerkin Methods.* International Journal for Numerical Methods in Engineering, 1994. **37**: p. 229-256.

5. Aluru, N.R., *A point collocation method based on reproducing kernel approximations.* International Journal for Numerical Methods in Engineering, 2000. **47**: p. 1083-1121.
6. Oñate, E., Idelsohn, S., Zienkiewicz, O.C., and Taylor, R.L., *A finite point method in computational mechanics. Applications to convective transport and fluid flow.* International Journal for Numerical Methods in Engineering, 1996. **39**(22): p. 3839-3866.
7. Oñate, E., Perazzo, F., and Miquel, J. , *A finite point method for elasticity problems.* Computational Structures, 2001. **79**: p. 2153-63.
8. Belytchko, T., Krongauz, Y., Organ, D., Fleming, M. and Krysl, P., *Meshless Methods: An Overview and Recent Developments.* Computer Methods in Applied Mechanics and Engineering, 1996. **139**: p. 3-47.
9. Nguyen, V.P., Rabczuk, T., Bordas, S., Duflot, M., *Meshless methods: A review and computer implementation aspects.* Mathematics and Computers in Simulation 2008. **79**: p. 763-813.
10. Lucy, L.B., *Numerical approach to testing the fission hypothesis.* Astronomical Journal, 1977. **82**: p. 1013-1024.
11. Monaghan, J.J., *Smoothed Particle Hydrodynamics.* Annu. Rev. Astron. Astrophys, 1972. **30**: p. 543-574.
12. Gingold, R.A., and Monaghan, J.J., *Smoothed Particle Hydrodynamics: theory and application to non-spherical stars.* Monthly notices of the Royal Astronomical Society, 1977. **181**: p. 375-391.
13. NUIGalway. *Mesh-free computational fluid dynamics. available at: http://www.nuigalway.ie/mechbio/research/meshfree.html.* [Accessed 15 July 2011].
14. Nayroles, B., Touzot, G., and Villon, P. , *Generalizing the finite element methods: diffuse approximation and diffuse elements.* Computational mechanics, 1992. **10**: p. 307-318.
15. Atluri, S.N., and Zhu, T. , *A new meshless local Petrov-Galerkin (MPLG) approach in computational mechanics.* Computational Mechanics, 1998. **22**: p. 117-127.
16. Atluri S.N., a.Z., T., *The meshless local Petrov-Galerkin (MLPG) approach for solving problems in elsto-statics.* Computational Mechanics, 2000b. **225**: p. 169-179.

17. Kim, H.G., Cho, J.Y., Atluri, S.N., *Analysis of Thin Beams Using the Meshless Local Petrov-Galerkin Method with Generalized Moving Least Squares Interpolations,*. Computational Mechanics, 1999. **24:(5)**: p. 334-347.
18. Lin, H., and Atluri, S.N., *Meshless local Petrov-Galerkin (MLPG) method for convection-diffusion problems.* Computer Modeling in Engineering and Sciences, 2000a. **1**(2): p. 45-60.
19. Rahmabadi, A.A., Bagri, A., Bordas, S.P.A., Rabczuk, T., *Analysis of Thermoelastic Waves in a Two-Dimensional Functionally Graded Materials Domain by the Meshless Local Petrov-Galerkin (MLPG) Method.* Computer Modeling in Engineering and Sciences, 2010. **65**(1): p. 27-74.
20. Liu, W., Jun, S., and Zhang, Y.F., *Reproducing Kernel Particle Methods.* International Journal for Numerical Methods in Engineering, 1995. **20**: p. 1081-1106.
21. Sukumar, N., Moran, B., and Belytschko, T., *The Natural Element Method in Solid Mechanics.* International Journal for Numerical Methods in Engineering, 1998. **43**: p. 839-887.
22. Yagawa, G., and Yamada, T., *Free mesh method: A new meshless finite element method* Computational Mechanics, 1996. **18**: p. 383-386.
23. De, S., and Bathe, K.J., *The method of finite spheres.* Computational Mechanics, 2000. **25**: p. 329-345.
24. Duarte, C.A., and Oden, J.T., *h-p adaptive method using clouds.* Computer Methods in Applied Mechanics and Engineering, 1996. **139**: p. 237-262.
25. Rao, B.N., and Rahman, S., *Mesh-free analysis of cracks in isotropic functionally graded materials.* Engineering Fracture Mechanics, 2003. **70**: p. 1-27.
26. Duflot, M., and Nguyen-Dang, H., *A meshless method with enriched weight functions for fatigue crack growth.* International Journal for Numerical Methods in Engineering, 2004. **59**: p. 1945-1960.
27. Chen, Y.P., Lee, J.D., and Eskandarian, A., *Dynamic meshless method applied to nonlocal crack problems.* Theoretical and Applied Fracture Mechanics, 2002. **38**: p. 293-300.
28. Martinez, M.A., Cueto, E., Alfaro, I., Doblare, M., Chinesta, F., *Updated lagrangian free surface flow simulations with natural neighbour galerkin*

methods. international Journal for Numerical Methods in Engineering, 2004. **60**: p. 2105-2119.

29. Singh, I.V., *The numerical solution of viscous fluid problems using meshless method.* Heat and Technology, 2004. **22**: p. 137-151.
30. Cordes, L.W., and Moran, B. , *Treatment of material discontinuity in the Element-free Galerkin method.* Computer Methods in Applied Mechanics and Engineering, 1996. **139**: p. 75-89.
31. Belytschko, T., and Organ, D., *Element-free Galerkin methods for dynamic fracture in concrete.* Computational plasticity. Fundamentals and applications, 1997(Barcelona, Spain): p. 304-321.
32. Dolbow, J., and Belytschko, T. , *An introduction to programming the Meshless Element Free Galekin Method.* Computational Mechanics, 1998. **19**: p. 111-156.
33. Belytschko, T., and Tabbara, M. , *Dynamic fracture using element-free galerkin methods.* International Journal for Numerical Methods in Engineering 1995. **39**: p. 199-216.
34. Belytschko, T., Lu, Y.Y., and Gu, L., *Element-free Galerkin methods for static and dynamic fracture.* international Journal of Solids and Structures, 1995. **32**: p. 2547-2570.
35. Belytschko, T., Gu, L. and Lu, Y.Y., *Fracture and crack growth by element-free Galerkin method.* Modelling Simulations in Materials Science and Engineering, 1994. **2**: p. 519-534.
36. Belytschko, T., Lu, Y.Y., and Gu, L., *Crack propagation by element-free Galerkin methods.* Engineering Fracture Mechanics, 1995. **51**: p. 295-315.
37. Shepard, D., *A two-dimensional interpolation function for irregularly spaced points.* Proceeding 23rd ACM national conference, 1968. ACM Press, New York: p. 517-524.
38. Lancaster, P., and Salkauskas, K. , *Surfaces generated by moving least squares methods.* Math. Comput, 1981. **37**: p. 141-157.
39. Muravin, B., *The application of element free Galerkin method in the investigation of crack interaction.* Ph.D. Thesis, Tel-Aviv University, 2003.
40. mmlab. *Kernel function. available at:* *http://mmlab.disi.unitn.it/wiki/index.php/Super_Resolution:_a_survey*. [Accessed 28 December 2010].

41. Fleming, M.A., *The Element-Free Galerkin Method for Fatigue and Quasi-static Fracture*. Ph.D. Thesis, Northwestern University, 1997.
42. Organ D.J., *Numerical Solutions to Dynamic Fracture Problems Using the Element-Free Galerkin Method.* Ph.D. Thesis, Northwestern University, 1996.
43. Lu, Y.Y., Belytschko, T and Gu, L., *A new implementation of the Element Free Galerkin method* Computer Methods in Applied Mechanics and Engineering, 1994. **113**: p. 397-414.
44. Belytschko, T., Organ, D. and Krongauz, Y., *A coupled Finite element-Element free galerkin method.* computational Mechanics, 1995. **17**: p. 186-195.
45. Mohammadi, S., *Extended finite element method.* Blackwell Publishing Ltd, 2008.
46. Fries, T., and Belytschko,T., *The Intrinsic Partition of Unity method.* Computational Mechanics, 2006. **40**(4): p. 803-814.
47. Belytschko, T., and Fleming, M., *Smoothing, enrichment and contact in the element-free Galerkin method.* Computers and Structures, 1999. **71**: p. 173-195.

Chapter 3

MODELLING OF HETEROGENEOUS MATERIALS

3.1 Introduction

Most engineering materials produced in industry are heterogeneous on one or another spatial scale. Some of the common examples include metal alloys, porous media and composites. The particulate composites as discussed in chapter 1 are heterogeneous materials in nature. The effective physical behaviour of a heterogeneous structure strongly depends on the size, shape, spatial distribution and properties of the constituents and their respective interfaces.

To determine the macroscopic overall characteristics of heterogeneous media is an essential problem in many engineering applications. For example, material interfaces in composites are modelled to predict the mechanical behaviour and to establish macroscopic material properties [1]. Sometimes a heterogeneous structure is specifically created for a particular product or application. For instance, in aluminium metal matrix composites, silica fibres, fine stainless steel wires or small ceramic particles may be distributed throughout the matrix. This can produce vastly improved properties such as higher strength, enhanced toughness and weight reduction [2].

The different phases present in heterogeneous materials constitute a material microstructure. The relation between macroscopic behaviour and microstructural phenomena not only allows predicting the behaviour of existing multi-phase materials, but also provides a tool to design a material microstructure such that the resulting macroscopic behaviour exhibits the required characteristics [3].

The problem that will be carried out in the proposed study involves particulate composites as circular inclusion for heterogeneous materials. The governing equations have already been given in chapter 2 for single material. Due to the presence of heterogeneity (in this case, the inclusion), the EFG approximation is enriched by an additional function.

3.2 Implementation of the Enriched EFG method

Following are the necessary steps involved in the implementation of the enriched EFG method [4]:

1. Representation of the interface: The interface or discontinuity can be represented by using the level set method [5, 6]. Level set method will be described in detail later in this chapter.
2. Selection of enriched nodes: In case of local enrichment, only a subset of the nodes closer to the region of interest is enriched. The nodes that are needed to be enriched can be selected by using the nodal values of the level set function.
3. Choice of enrichment functions: Depending on the physics of the problem, different enrichment functions can be used.

3.3 Enrichment functions for the inclusions

Inclusions are inhomogeneities in material properties within a body, which can produce discontinuities in the gradient of the displacement field. In order to incorporate such discontinuities in the derivatives of the function, an enrichment function in the form of a ramp function was proposed in the frame work of enriched EFG method by Fleming et al. [7] and later, it was used by Sukumar et al. [1] within XFEM framework. It is worth mentioning that due to the problems in blending elements Sukumar et al. [1] have also proposed a modified enrichment function for inclusions.

One of the key steps in the implementation is the selection of region of interest, where the field is required to be enriched. This automatically implies the selection of enriched nodes, where additional degrees of freedom are added to the system. Although interfaces do not have to be re-meshed, the correct integration of the stiffness matrix, for nodes enriched by a discontinuous function along an interface, needs to be done carefully. Enrichment functions are usually defined with the help of the level set functions to access the distance to the interface at any given point, which will develop the local enrichment function for material interfaces. The level set

function will be discussed in detail later in this chapter. First the importance of numerical integration and discretisation of the governing equations for enriched EFG will be represented.

3.4 Discretisation in the weak form of enriched EFG method

3.4.1 Numerical integration

Accurate integration is one of the important factors in the accuracy of the solution, since the stiffness matrix and force vector are calculated by numerical integration. There are several schemes for numerical integration. One of them is the Gauss quadrature, which is used in this work. The method requires subdivision of the domain O on cells by means of a background mesh. Generally, the background mesh is independent of the nodal distribution. 4×4 Gauss quadrature points has been used for each regular cell in this proposed study.

Numerical integration of a two-dimensional function $f(x,y)$ over domain Ω can be expressed as [8]:

$$\int_{\Omega} f(x,y)d\Omega = \sum_{k=1}^{n} f(x_k,y_k)w_k \tag{3.1}$$

where (x_k,y_k) are the coordinates of a Gauss quadrature point, w_k is the weight of this Gauss quadrature point and $n = n_q^2$, where n_q is the order of the Gauss quadrature rule.

3.4.2 Discrete equation

The enriched EFG approximation is based on the decomposition of the displacement field into a continuous (standard) and discontinuous (enriched) part. The continuous EFG approximation is based on the MLS method and is shown in chapter 2. For the discontinuous part, also called the enriched part, of the displacement approximation due to all the enriched nodes is the sum of the discontinuous contribution associated

with each enriched node. Hence for the enriched EFG, the total approximation can be written as:

$$\begin{aligned}\mathbf{u}^h(\mathbf{x}) &= \mathbf{u}^h_{std}(\mathbf{x}) + \mathbf{u}^h_{enr}(\mathbf{x}) \\ &= \sum_{i=1}^{n} f_i(\mathbf{x})\mathbf{u}_i^{std} + \sum_{k=1}^{m} f_k(\mathbf{x})\, y\,(\mathbf{x})\mathbf{u}_k^{enr}\end{aligned} \tag{3.2}$$

where n is the number of all the nodes, m is the number of nodes that are enriched with the enrichment function y , f is the EFG shape function, $\mathbf{u}^{std}$ and $\mathbf{u}^{enr}$ are the standard and the enriched nodal variables associated with node i and k respectively.

Using the variational principle and assuming independent standard and enriched degrees of freedom $\mathbf{u}^{std}$ and $\mathbf{u}^{enr}$, lead to the following discrete system of linear equilibrium equation:

$$\mathbf{K}\mathbf{u} = \mathbf{f} \tag{3.3}$$

where $\mathbf{K}$ is the stiffness matrix, $\mathbf{u}$ is the vector of degrees of nodal freedom (for both standard and enriched nodes) and $\mathbf{f}$ is the vector of external forces. The global matrix and vectors are calculated by assembling the matrix and vectors for each node. For simplicity, it is assumed that the superscript u means standard part and e means enriched part. For example, $\mathbf{K}$ and $\mathbf{f}$ for node i and j are defined as:

$$\mathbf{K}_{ij} = \begin{bmatrix} \mathbf{K}_{ij}^{uu} & \mathbf{K}_{ij}^{ue} \\ \mathbf{K}_{ij}^{eu} & \mathbf{K}_{ij}^{ee} \end{bmatrix} \tag{3.4}$$

where $\mathbf{K}^{uu}$, $\mathbf{K}^{ee}$ and $\mathbf{K}^{ue}$ are the stiffness matrix associated with the standard EFG approximation, the enriched approximation and the coupling between the standard EFG and the enriched approximation respectively.

$$\mathbf{f}_i = \begin{Bmatrix} \mathbf{f}_i^{\,u} & \mathbf{f}_i^{\,e} \end{Bmatrix}^T \tag{3.5}$$

$$\mathbf{u} = \left\{ \mathbf{u}^u \quad \mathbf{u}^e \right\}^T \tag{3.6}$$

where

$$\mathbf{K}_{ij}^{uu} = \int_{\Omega} \left(\mathbf{B}_i^u \right)^T \mathbf{D} \mathbf{B}_j^u d\Omega \tag{3.7}$$

$$\mathbf{K}_{ij}^{ee} = \int_{\Omega_{enr}} \left(\mathbf{B}_{ij}^e \right)^T \mathbf{D} \mathbf{B}_{ij}^e d\Omega \tag{3.8}$$

$$\mathbf{f}_i^u = \int_{\Omega} f_i \mathbf{b} d\Omega + \int_{\Gamma_t} f_i \bar{\mathbf{t}} d\Gamma \tag{3.9}$$

$$\mathbf{f}_i^e = \int_{\Omega_{enr}} f_i y \ \mathbf{b} d\Omega + \int_{\Gamma_t} f_i \bar{\mathbf{t}} d\Gamma \tag{3.10}$$

In equation (3.7), **B** is the matrix of shape function derivatives,

$$\mathbf{B}_i = \left[\mathbf{B}_i^u \quad \mathbf{B}_i^e \right] \tag{3.11}$$

$$\mathbf{B}_i^u = \begin{bmatrix} f_{i,x} & 0 \\ 0 & f_{i,y} \\ f_{i,y} & f_{i,x} \end{bmatrix} \tag{3.12}$$

$$\mathbf{B}_i^e = \begin{bmatrix} (f_i y)_{,x} & 0 \\ 0 & (f_i y)_{,y} \\ (f_i y)_{,y} & (f_i y)_{,x} \end{bmatrix} \tag{3.13}$$

To accurately model interface discontinuity, various types of enrichment schemes are available in the literature. Some of them are described in the following section.

3.5 Enrichment schemes

3.5.1 Enrichment for strong discontinuity

For strong discontinuities (jumps), the sign-enrichment function $y_{sign}(\mathbf{x})$ is often used as the enrichment function leading to the following enriched EFG approximation:

$$\mathbf{u}^h(\mathbf{x}) = \sum_{i \in N} f_i(\mathbf{x})\mathbf{u}_i + \sum_{j \in N^{enr}} f_j(\mathbf{x})\, y_{sign}(\mathbf{x})\mathbf{a}_j \tag{3.14}$$

where $y_{sign}(\mathbf{x})$ is defined as:

$$y_{sign}(\mathbf{x}) = sign\ (j(\mathbf{x})) = \begin{cases} -1\ if\ \ j(\mathbf{x}) < 0 \\ 0\ if\ \ j(\mathbf{x}) < 0 \\ 1\ if\ \ j(\mathbf{x}) > 0 \end{cases} \tag{3.15}$$

3.5.2 Enrichment for weak discontinuity

Two types of enrichment functions are used in the literature in case of weak discontinuities. For the case of weak discontinuities (kinks), the abs-enrichment function $y_{abs}(\mathbf{x})$ is often chosen as the enrichment function leading to the following enriched EFG approximation:

$$\mathbf{u}^h(\mathbf{x}) = \sum_{i \in N} f_i(\mathbf{x})\mathbf{u}_i + \sum_{j \in N^{enr}} f_j(\mathbf{x})\, y_{abs}(\mathbf{x})\mathbf{a}_j \tag{3.16}$$

where $y_{sign}(\mathbf{x})$ is defined as:

$$y_{abs}(\mathbf{x}) = abs\ (j(\mathbf{x})) = |j(\mathbf{x})| \tag{3.17}$$

Hence the first choice for the enrichment function is defined as the absolute value of the level set function [1], which has a discontinuous first derivative on the interface.

Moes et al.[9] proposed another choice for the enrichment function given by:

$$y(\mathbf{x}) = \sum_i |j_i| f_i(\mathbf{x}) - \left| \sum_i j_i f_i(\mathbf{x}) \right| \tag{3.18}$$

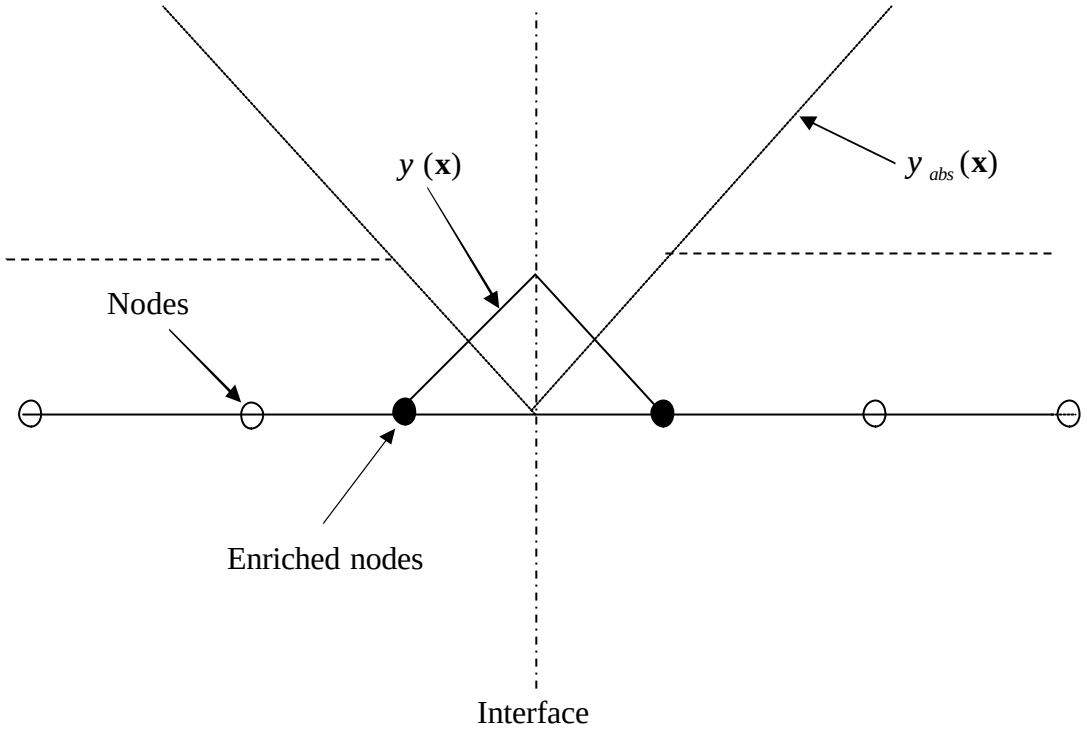

Figure 3.1: Weak discontinuity: different choices of enrichment functions [4]

Figure 3.1 shows the two choices of the enrichment function in the 1-D case. For two and three dimensional problems, the enrichment function proposed by Moes et al. [9] is a ridge centred on the interface and has zero value on the nodes which are not crossed by the interface.

3.6 Level set method

The level set method [10] is a numerical technique introduced by Osher and Sethian [6] for tracking moving interfaces. It is based upon the idea of representing the interface as a level set curve of a higher dimensional function. The key point in the level set method is to represent the geometric interface (for example, the boundary of a hole or inclusion) at any time *t*, with a zero level set function, i.e.

$$j(\mathbf{x},t)=0 \tag{3.19}$$

where $j(\mathbf{x},t)$ is the level set function.

The interface is located from the value of the level set information stored at the nodes. However, the level set function can be interpolated at any point **x** in the domain by the use of the shape function:

$$j(\mathbf{x}) = \sum_{i=1}^{n} f_i(\mathbf{x}) j_i \tag{3.20}$$

where the summation is over all the nodes that contains **x** and j_i are the nodal values of the level set function.

Since its introduction in [6], the above level set approach has been used in a wide collection of problems involving moving interfaces. Some of these applications include the generation of minimal surfaces [11], singularities and geodesics in moving curves and surfaces in [12], and shape reconstruction [13, 14].

Let Γ be an interface that divides the domain Ω into two non-overlapping sub domains, Ω_1 and Ω_2, as illustrated in Figure 3.2. The level set function j is defined as:

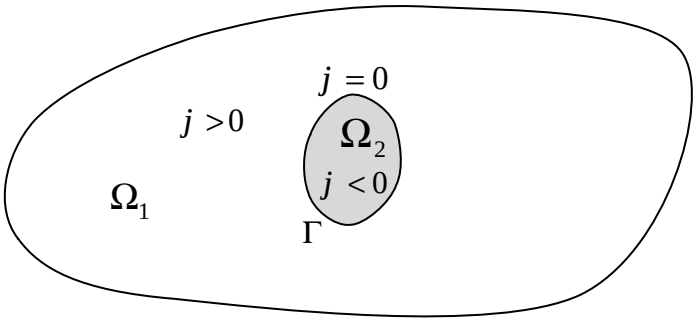

Figure 3.2: Definition of the level set function

$$j(\mathbf{x}) = \begin{cases} > 0, \mathbf{x} \in \Omega_1 \\ = 0, \mathbf{x} \in \Gamma \\ < 0, \mathbf{x} \in \Omega_2 \end{cases} \tag{3.21}$$

An interpretation of equation (3.21) is that the interface Γ can be regarded as the zero level contour of the level set function $j(\mathbf{x})$.

One of the common choices for the level set function, j, can then be simply defined in terms of the signed distance function:

$$j(\mathbf{x}) = \begin{cases} d, \mathbf{x} \in \Omega_1 \\ -d, \mathbf{x} \in \Omega_2 \end{cases} \tag{3.22}$$

The initial condition is usually taken as the signed distance function such that the level set function has positive values on one side of the interface and negative values at the other side of the interface and the interface is identified by the zero level set function. In order to construct a level set function using a signed distance function, we find the closest point on the discontinuity Γ such that $|\mathbf{x} - \mathbf{x}_\Gamma|$ is a minimum, where $\mathbf{x}$ is any query point and $\mathbf{x}_\Gamma$ is a point on the discontinuity Γ as shown in Figure 3.3. This actually defines a vector $\vec{\mathbf{d}} = (\mathbf{x} - \mathbf{x}_\Gamma)$ which is orthogonal to the discontinuity Γ at point $\mathbf{x}_\Gamma$. Next in order to construct the level set function we define a normal to the discontinuity at point $\mathbf{x}_\Gamma$. The level set function is then given as [15]:

$$\vec{\mathbf{d}} = (\mathbf{x} - \mathbf{x}_\Gamma) \tag{3.23}$$

$$j(\mathbf{x}, t = 0) = \vec{\mathbf{d}}.\hat{\mathbf{n}} \tag{3.24}$$

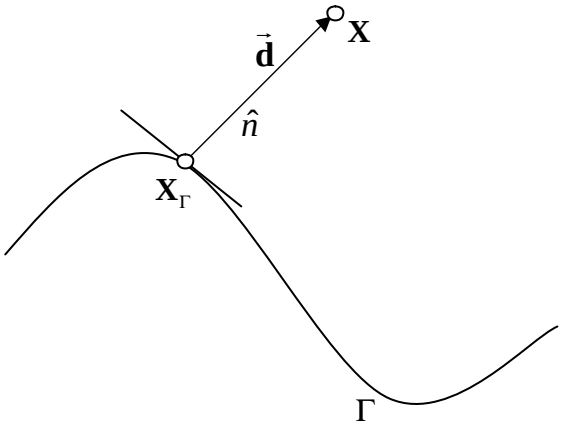

Figure 3.3: Signed distance function [15]

The following section will describe the implementation of circular discontinuity using the level set method.

3.6.1 Circular discontinuity

The signed distance function is one of the commonly used level set functions, and can be used to construct level set function for discontinuity of different types and shapes, such as circular, elliptical and polygonal voids. For a circular inclusion, we find the minimum signed distance to construct the level set function as follows:

$$j(\mathbf{x},0) = \|\mathbf{x} - \mathbf{x}_c\| - r_c \tag{3.25}$$

where $\mathbf{x}$ is any query point, $\mathbf{x}_c$ denotes the centre of the circle and r_c is the radius of the circle. The level set function can then simply be the signed distance function to the circular discontinuity. In this case, the level set function will have a positive value outside the circle and a negative distance value for any point inside the circle. The points that lie on the circle will be represented as a zero value of the function.

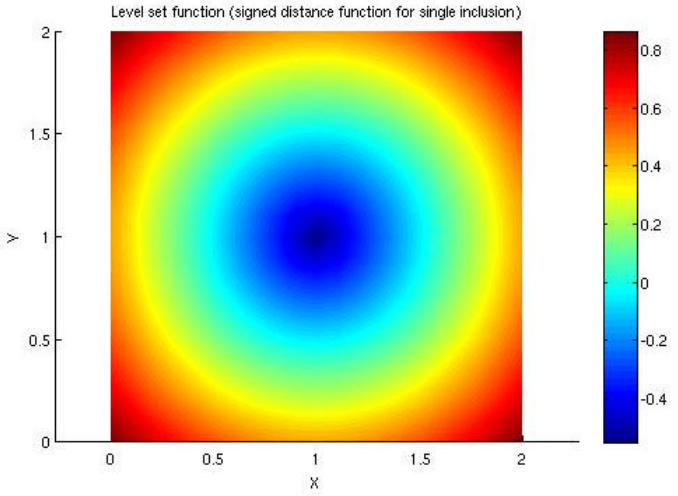

(a)

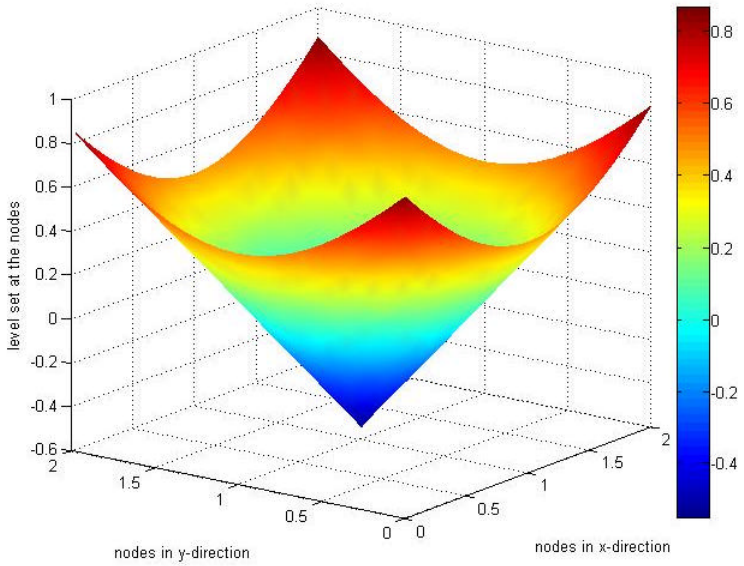

(b)

Figure 3.4: Level set function for single inclusion

If a body contains number of circular discontinuities then a single level set function for all the discontinuities can be defined as:

$$j(\mathbf{x},0) = \min_{i=1,2,3,....n_c} \left\{ \left\| \mathbf{x} - \mathbf{x}_c^i \right\| - r_c^i \right\} \tag{3.26}$$

where n_c is the total number of circular inclusions, $\mathbf{x}_c^i$ and r_c^i refers to the centre and radius of i-th inclusion respectively.

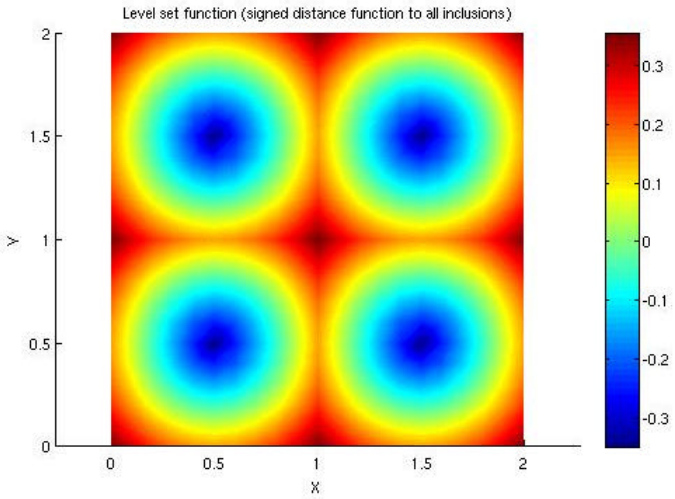

(a)

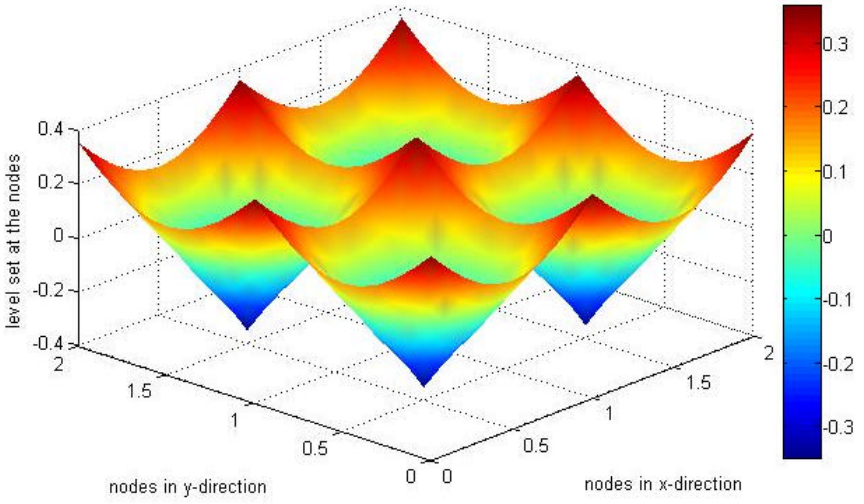

(b)

Fig. 3.5: Level set function for multiple inclusions

3.6.2 Complex shaped discontinuity

The signed distance function can also be used to construct level set function for complex shaped inclusions. A 'star' shape is considered for this particular case. First the implementation will be carried out for a single inclusion, and then for nine inclusions to illustrate multi-inclusions problem.

For complex shaped inclusion as shown in Figure 3.6, r_c^i in equation (3.26) is replaced by [4]:

$$r_c^i(q) = r_o^i + a^i \cos(b^i q) \tag{3.27}$$

where r_o is the reference radius, a^i and b^i are parameters that control the amplitude and period of oscillations for *i*-th inclusion.

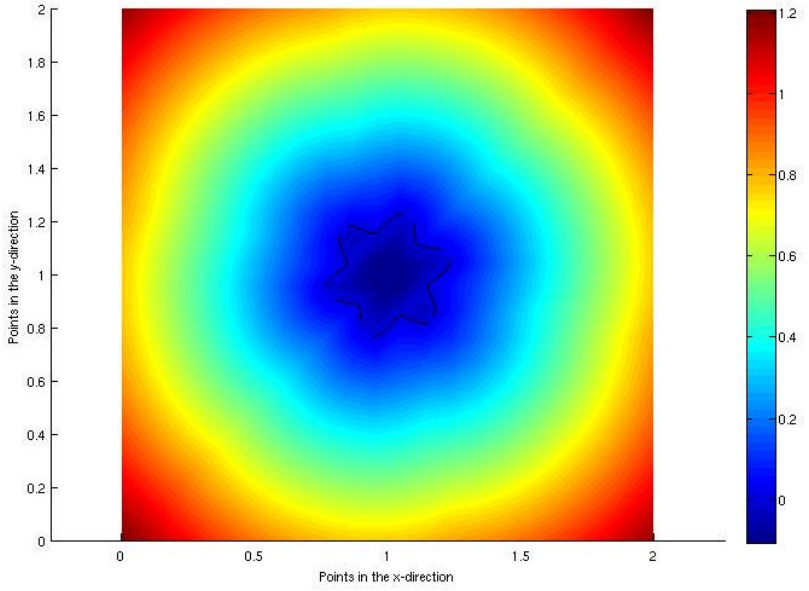

(a)

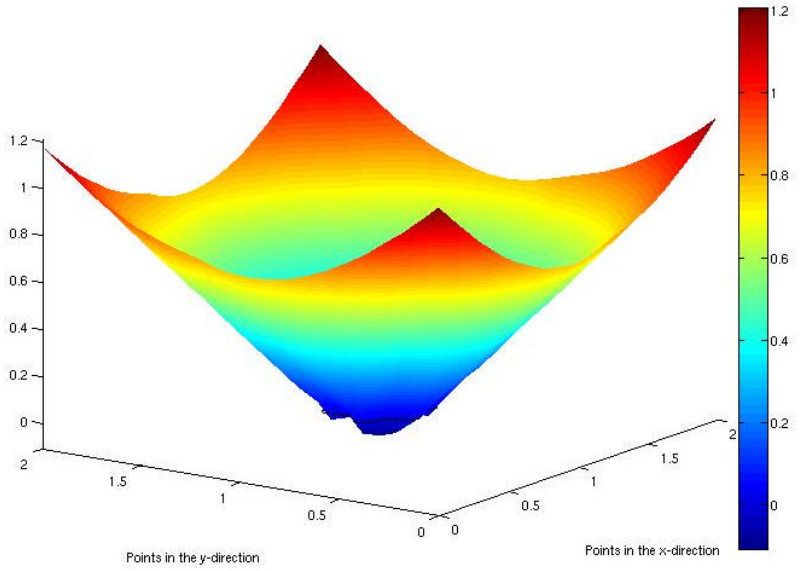

(b)

Figure 3.6: Level set function for complex shaped single inclusion

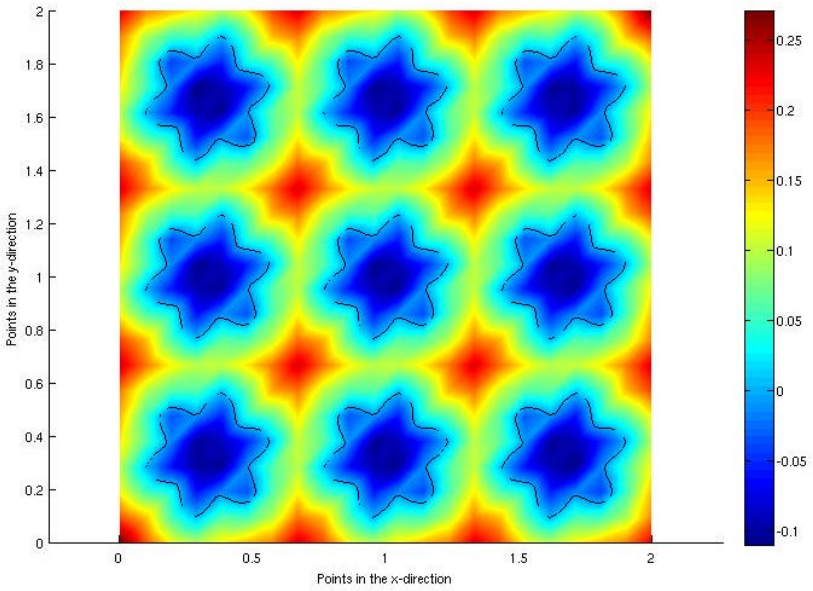

(a)

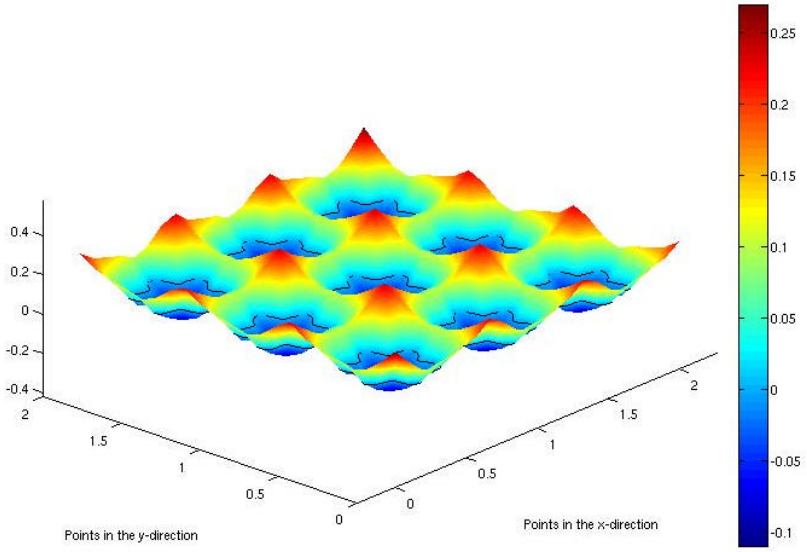

(b)

Figure 3.7: Level set function for complex shaped multiple inclusions

Another strategy to model heterogeneous materials is by using double nodes or pair nodes technique which does not need any enrichment function in the approximation space. The following section will illustrate the double nodes technique in detail.

3.7 Modelling heterogeneous materials using double nodes

Material discontinuity, for example, interface problem, can be treated through the use of the pair nodes near the region of the discontinuity in the EFG method. The following technique can be applied in implementing the interface discontinuity.

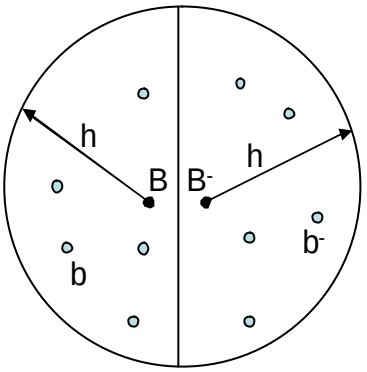

Figure 3.8: Pair nodes

For instance, a particle pair, B and B$^-$, located on opposite side close to an interface, are considered. The EFG approximation of the displacement and its derivative on particle B are (Figure 3.8) given by:

$$u^h(\mathbf{x}_B) = \sum_{b \in M_B} f_B(\mathbf{x}_B)\, \mathbf{u}_b \tag{3.28}$$

where f_B is the shape function

and $$\frac{\partial u^h(\mathbf{x}_B)}{\partial \mathbf{u}_a} = f_a(\mathbf{x}_B) \tag{3.29}$$

And the displacement approximation of particle B$^-$ can be expressed as:

$$u^h(\mathbf{x}_{B^-}) = \sum_{\langle b^- e M_{B^-} \rangle} f_{B^-}(\mathbf{x}_{B^-})\, \mathbf{u}_{b^-} \tag{3.30}$$

The spring potential function is defined by:

$$? _{bp} = \frac{1}{2} k_p \sum_{B=1}^{N_{bp}^B} A_B (\mathbf{u}_h(\mathbf{x}_B) - \mathbf{u}_h(\mathbf{x}_{B^-}))^2 \tag{3.31}$$

where k_p is the penalty value and N_{bp}^B are relevant boundary points.

Differentiating $?_{bp}$ with respect to $\mathbf{u}_a$ yields the interfacial traction as:

$$\mathbf{T}_a^{bp} = \frac{\partial ?_{bp}}{\partial \mathbf{u}_a} = \sum_{B \in M_a} k_p A_B (u_h(\mathbf{x}_B) - u_h(\mathbf{x}_{B^-}))\, f_a(\mathbf{x}_B) \tag{3.32}$$

Let,

$$\mathbf{K}_{ab}^{bp} = \sum_{B \in M_{ab}^{B}} k_p A_B \left[f_a(\mathbf{x}_B) \right] f_b(\mathbf{x}_B) \tag{3.33}$$

$$\mathbf{K}_{ab^-}^{bp} = \sum_{B^- \in M_{ab^-}^{B^-}} k_p A_B \left[f_a(\mathbf{x}_B) \right] f_{b^-}(\mathbf{x}_{B^-}) \tag{3.34}$$

Hence equation (3.5) can be re-written as:

$$\mathbf{T}_a^{bp} = \sum_{b=1}^{N_{bi}^{B}} \mathbf{K}_{ab}^{bp} \mathbf{u}_b - \sum_{b^-=1}^{N_{bi}^{B^-}} \mathbf{K}_{ab^-}^{bp} \mathbf{u}_{b^-} \tag{3.35}$$

As we know, the governing equation incorporating the essential boundary conditions can be written as:

$$\sum_{b=1}^{N} \left[\mathbf{K}_{ab} + \mathbf{K}_{ab}^{bp} \right] \mathbf{u}_b = \mathbf{T}_a + \mathbf{T}_a^{bp} \tag{3.36}$$

Substituting (3.34) into (3.35), the final system of equation on interfacial particles can be expressed in the following form:

$$\sum_{b=1}^{N} \left[\mathbf{K}_{ab} + \mathbf{K}_{ab}^{bp} \right] \mathbf{u}_b - \sum_{b^-=1}^{N} \mathbf{K}_{ab^-}^{bp} \mathbf{u}_{b^-} = 0 \tag{3.37}$$

where

$$\mathbf{K}_{ab} = \int_{\Omega} \mathbf{B}_a^T \mathbf{D} \mathbf{B}_b \, d\Omega \tag{3.38}$$

The numerical model established using the enriched EFG method will be validated with the XFEM. Hence a brief description of the XFEM method is given in the next section.

3.8 Extended finite element method (XFEM)

Within the finite element method, the domain Ω is divided into elements, called finite elements and constituting a mesh. The displacement field is approximated on these elements:

$$\mathbf{u}(\mathbf{x}) = \sum_{i}^{n} f_i(\mathbf{x})\mathbf{u}_i \tag{3.39}$$

where $f_i(\mathbf{x})$ are the finite element shape functions, and $\mathbf{u}_i$ the nodal displacements.

For the sake of mesh simplification, the extended finite element method (XFEM) was developed a decade ago, initially for crack propagation problem [16, 17]. Within XFEM, the mesh does not necessarily conform to internal discontinuities (such as holes, cracks, and material interfaces), which allows the use of simple meshes (structured or not). Moreover, the finite element approximation is enriched by additional functions (through the partition of unity [18]) that model the behaviour of boundaries, as follows:

$$\mathbf{u}^h(\mathbf{x}) = \sum_{i \in N} f_i(\mathbf{x})\mathbf{u}_i + \sum_{j \in N^{enr}} f_j(\mathbf{x})y(\mathbf{x})\mathbf{a}_j \tag{3.40}$$

Where $y(\mathbf{x})$ is the enrichment function, $\mathbf{a}_j$ are additional degrees of freedom, for enriched nodes; N represents the set of the nodes of the mesh, and N^{enr} the set of enriched nodes.

For example, in the case of material interfaces, only nodes belonging to elements crossed by the interface are enriched. If the mesh conforms to discontinuities, there is no enrichment on nodes, and classical finite element method is recovered [19]. Since the surfaces are not represented explicitly by mesh boundaries, level set is introduced to track them. This function usually gives the signed distance to the interface at any point of the domain (Figure 3.3).

3.9 Error analysis and convergence studies

The importance of error estimation when solving physical problems numerically (discretely) should be clear. The first source of error lies in the construction of the mathematical model, the second, is related to the error committed by the numerical model (discretised version of the mathematical model) [20]. Szabó and Babuška [21] suggest that knowledge of the error is essential to be able to correlate experimental and numerical results: one must ensure that the numerical results are close to the true solution of the mathematical model, to guarantee that any discrepancy between the numerical and experimental results can be ascribed to the unsuitability of the mathematical model.

For the purpose of error estimation and convergence studies, the relative error, L_2 and H_1 are used. The relative error in the displacement norm (L_2) is defined by:

$$\text{Displacement norm} = \frac{\left\{\int_{\Omega}(\mathbf{u}^{NUM}-\mathbf{u}^{EXACT})^{T}(\mathbf{u}^{NUM}-\mathbf{u}^{EXACT})d\Omega\right\}^{\frac{1}{2}}}{\left\{\int_{\Omega}\left(\mathbf{u}^{EXACT}\right)^{T}\left(\mathbf{u}^{EXACT}\right)d\Omega\right\}^{\frac{1}{2}}} \tag{3.41}$$

where $\mathbf{u}^{NUM}$ is the numerical displacement solution and $\mathbf{u}^{EXACT}$ is the analytical displacement solution, or a reference solution.

The rate of convergence in the energy norm (H_1) is calculated by using:

$$\text{Energy norm} = \left\{\frac{1}{2}\int_{\Omega}(\mathrm{e}^{NUM}-\mathrm{e}^{EXACT})^{T}\mathbf{D}(\mathrm{e}^{NUM}-\mathrm{e}^{EXACT})d\Omega\right\}^{\frac{1}{2}} \tag{3.42}$$

where e is defined as the symmetric gradient of the displacement **u.**

3.10 2-D program description

3.10.1 Enriched EFG method

MATLAB is used to develop the model for simulation of particulate composites within the framework of the enriched EFG method. A chart that shows the list of actions is illustrated below to represent the main algorithm used in the program [22].

Table 3.1: List of actions of 2-D enriched EFG program

a. Define the material properties and physical parameters.
b. Define the boundary condition.
c. Set up the nodal co-ordinates for a uniform mesh.
d. Determine the domain of influence for each node.
e. Set up quadrature cells in the domain.
f. Set up gauss points, weights and jacobian for each cell.
g. Determine the enriched nodes.
h. Loop over the gauss points to determine the neighbourhood nodes, weights, shape functions and shape function derivatives.
i. Assemble standard **B** matrix and additional **B** matrix due to the enrichment.
j. Add contributions to the **K** matrix.
k. Determine nodes on traction boundary and essential boundary.
l. Set up gauss points along traction boundary and essential boundary.
m. Integrate forces along traction boundary to form **f** vector.
n. Integrate Lagrange multipliers along essential boundary to form the **G** matrix and **q** vector.
o. Enforce essential boundary conditions using Lagrange multipliers.
p. Solve for nodal parameters.
q. Loop over gauss points to determine stress at quadrature point.

3.10.2 EFG method using double nodes

FORTRAN is used to develop the alternative model for simulation of particulate composites within the framework of the EFG method using double nodes technique. A chart that shows the list of actions is illustrated below to represent the main algorithm used in the program.

Table 3.2: List of actions of 2-D EFG program using double nodes

a. Define the material properties and physical parameters.
b. Define the boundary conditions.
c. Set up the nodal co-ordinates for a uniform mesh.
d. Determine the domain of influence for each node.
e. Set up quadrature cells in the domain.
f. Set up gauss points, weights and jacobian for each cell.
g. Loop over the gauss points to determine the neighbourhood nodes, weights, shape functions and shape function derivatives.
h. Assemble standard **B** matrix.
i. Add contributions to the **K** matrix.
j. Add the additional **K** matrix due to the pair nodes constrains.
k. Determine nodes on traction boundary and essential boundary.
l. Set up gauss points along traction boundary and essential boundary.
m. Integrate forces along traction boundary to form **f** vector.
n. Integrate Lagrange multipliers along essential boundary to form the **G** matrix and **q** vector.
o. Enforce essential boundary conditions using Lagrange multipliers.
p. Solve for nodal parameters.
q. Loop over gauss points to determine stress at quadrature point.

3.11 Conclusion

A numerical model has been developed using two different techniques namely the enriched EFG and EFG with double nodes. The detailed formulation for both the techniques has been presented, along with their governing equations. Level set method is described in details, which is applied to implement the enrichment function for the weak discontinuity.

The numerical simulation and the validation of the proposed model will be carried out in the next chapter. The results will be compared with some test cases for which the analytical solutions are available as well as with the results of other numerical techniques.

References

1. Sukumar, N., Chopp, D.L., Moës, N., and Belytschko, T., *Modeling holes and inclusions by level sets in the extended finite-element method.* Computational Methods in Applied Mechanics and Engineering, 2001. **190**: p. 6183-6200.
2. Kouznetsova, V.G., *Computational homogenization for the multi-scale analysis of multi-phase materials.* Ph.D. Thesis, Technische University Eindhoven, 2002.
3. Kouznetsova, V., Brekelmans, W.A.M., and Baaijens, F.P.T, *An approach to micro-macro modelling of heterogeneous materials.* Computational Mechanics, 2001. **27**: p. 37-48.
4. Natarajan, S., *Enriched finite element methods: Advances and applications.* Ph.D. Thesis, Cardiff University, 2011.
5. Sethian, J., *Level set methods and Fast marching methods: Evolving interfaces in computational geometry, fluid mechanics, computer vision and material science.* Cambridge University Press, 1999.
6. Osher, S., and Sethian, J., *Fronts propagating with curvature-dependent speed: Algorithms based on Hamilton-Jacobi formulations.* Journal of Computational Physics, 1988. **79(1)**: p. 12-49.

7. Fleming, M., Chu, Y.A., Moran, B., and Belytschko, T., *Enriched Element-free Galerkin methods for crack tip fields.* International Journal for Numerical Methods in Engineering, 1997. **40**: p. 1483-1504.
8. Muravin, B., *The application of element free Galerkin method in the investigation of crack interaction.* Ph.D. Thesis, Tel-Aviv University, 2003.
9. Moës, N., Cloirec, M., Cartraud, P., and Remacle, J.F, *A computational approach to handle complex microstructure geometries.* Computational Methods in Applied Mechanics and Engineering, 2003. **192**: p. 3163-3177.
10. Osher, S., and Fedkiw, R., *Level set methods and dynamic implicit surfaces.* Applied Mathematical Sciences, 2003. **153**(Springer).
11. Chopp, D.L., *Computing minimal surfaces via level set curvature flow.* Journal of Computational Physics, 1993. **106**: p. 77-91.
12. Chopp, D.L., and Sethian, J.A., *Flow under curvature: singularity formation, minimal surfaces, and geodesics.* Experimental Mathematics, 1993. **2(4)**: p. 235-255.
13. Malladi, R., and Sethian, J.A., *Image processing via level set curvature flow.* Proceedings of the National Academy of Science, USA, 1995. **92(15)**: p. 7046-7050.
14. Malladi, R., Sethian, J.A., and Vemuri, B.C., *Shape modeling with front propagation: A level set approach.* IEEE Trans. on pattern analysis and machine intelligence, 1995. **17(2)**: p. 158-175.
15. Ahmed, A., *Extended finite element method (XFEM) - Modeling arbitrary discontinuities and failure analysis.* Dissertation for the Maser Degree, Istituto Universitario di Studi Superiori di Pavia, 2009.
16. Belytschko, T., and Black, T., *Elastic crack growth in finite elements with minimal remeshing.* International Journal for Numerical Methods in Engineering, 1999. **45**: p. 601-620.
17. Moës, N., Dolbow, J., and Belytschko, T., *A finite element method for crack growth without remeshing.* International Journal for Numerical Methods in Engineering, 1999. **46**: p. 131-150.
18. Melenk, J.M., and Babuška, I., *The partition of unity finite element method: Basic theory and applications.* Computer Methods in Applied Mechanics and Engineering, 1996. **139**: p. 289-314.

19. Dreau, K., Chevaugeon, N., Moes, N., *Studied X-FEM enrichment to handle material interfaces with higher order finite element.* Computer Methods in Applied Mechanics and Engineering, 2010. **199**: p. 1922-1936.
20. Bordas, S., *Extended finite element meshfree methods.* Lecture notes, University of Glasgow, 2007.
21. Szabó, B.A., and Babuška, I., *Finite element analysis.* John Wiley & Sons: New York, 1991.
22. Dolbow, J., and Belytschko, T., *An introduction to programming the Meshless Element Free Galekin Method.* Computational Mechanics, 1998. **19**: p. 111-156.

Chapter 4

NUMERICAL SIMULATION AND DISCUSSIONS

4.1 Introduction

The main concept and formulation of the enriched EFG was discussed in chapter 3. Based on that, a reliable, accurate and efficient way of solving linear elastic material discontinuity problem will be performed. Following the validation of convergence and accuracy of the results in the applications with simple configurations, the model will be employed to test more complex problems. The chapter is organised as follows. Firstly particulate composites as a single inclusion in a square domain will be analysed and the results will be validated with the XFEM. Then the accuracy of the model will be compared with some test cases for which the analytical solutions are available. In order to demonstrate the capability of the model, multi-inclusion problems are going to be analysed and compared, where the model will be simulated for randomly distributed as well as complex shaped particles.

The numerical model will also be used in simulating syntactic foam and the results will be validated against the observation made from the FEM simulation. Homogenisation technique will be applied for multi-scale modelling of syntactic foam and will be compared with the experimental results. The XFEM will be applied to study the crack inclusion and interaction of crack propagation with particles in a particle reinforced composite material, where crack growth will be observed for different parameters including different positions of the inclusion and different ratio of Young's modulus for the matrix and the inclusion. The results obtained from the numerical study will be compared with the observations from the literature. Finally, the EFG technique using double nodes as described in chapter 3 will be applied to a simple configuration and compared with the results of the FEM to illustrate the capability of the technique to solve more complex problems.

4.2 Material discontinuity problem

The numerical model that was developed in the previous chapter to simulate particulate composites is going to be analysed for different orientation within the framework of the enriched EFG method. In order to perform the analysis, a two-

dimensional bi-material linear elastic problem is considered here. First the test will be carried out for single inclusion. Multi-inclusion problem will be performed following the validation and convergence study of the single inclusion problems.

4.2.1 Single inclusion problem

For the single inclusion problem, a heterogeneous material having a circular inclusion in a square matrix domain under uniform loading applied in the y-direction, as shown in Figure 4.1, is considered. The geometry, loading and boundary conditions are as follows:

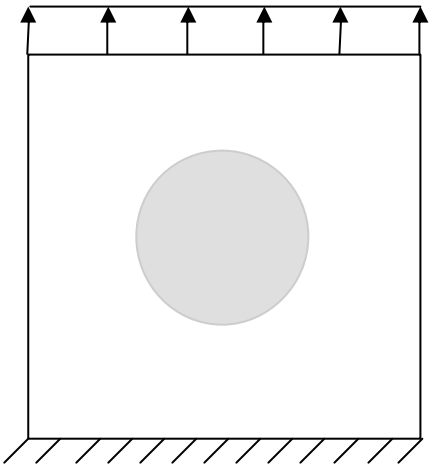

Figure 4.1: Bi-material single inclusion problem

The dimension of the square domain is 2×2. The inclusion is placed at the centre of the domain having a radius of 0.4. A uniform tension $P = 1$ is applied at the upper edge of the domain and the lower edge is fixed. Young's modulus of elasticity (E) for matrix is 1 and Poisson's ratio is 0.3; where as for inclusion they are 10 and 0.3 respectively. Plane stress conditions are assumed.

The selected EFG scheme includes a regular nodal distribution, a 4×4 Gauss quadrature rule and linear basis functions. The cubic spline weight functions are used for the construction of the weight functions and the domain of influence is chosen to be 1.5. Three different mesh sizes (h) are chosen, namely 0.2, 0.1 and 0.05. The nodal distributions for these three cases are 11×11, 21×21 and 41×41 respectively. For all

cases, 12% volume fraction is considered. Nodal distribution for h = 0.1 is shown in Figure 4.2 to indicate the distribution of all the nodes and selection of the enriched nodes. Normal nodes are shown by the circles, where as stars in the circles depicting enriched nodes.

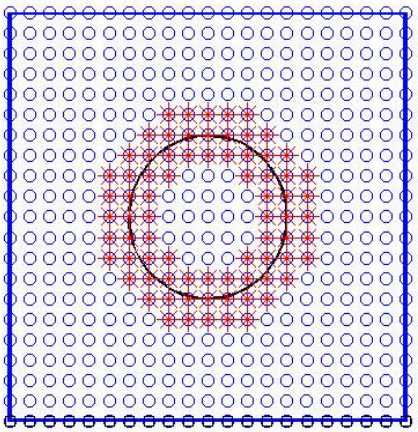

Figure 4.2: Distribution of nodes and location of enriched nodes for single inclusion

Numerical results are computed and compared with the results generated by the XFEM. The comparison between the XEFG and the XFEM is shown below by plotting the y co-ordinates of centre line nodes along the Y axis in the horizontal direction to the y-displacement of centre line nodes along the Y axis in the vertical direction for 3 different mesh sizes:

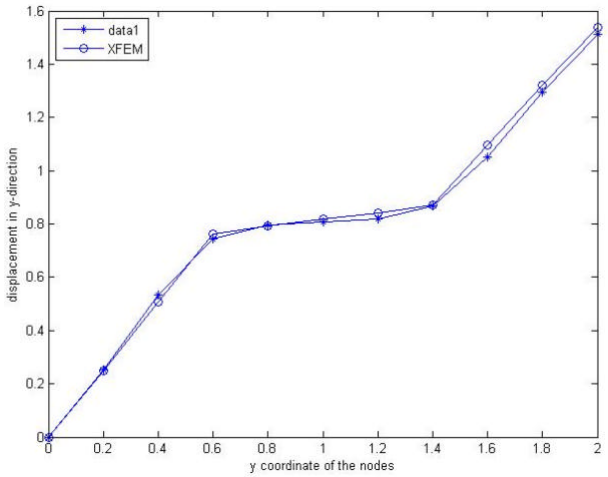

(a) Mesh size, h = 0.2

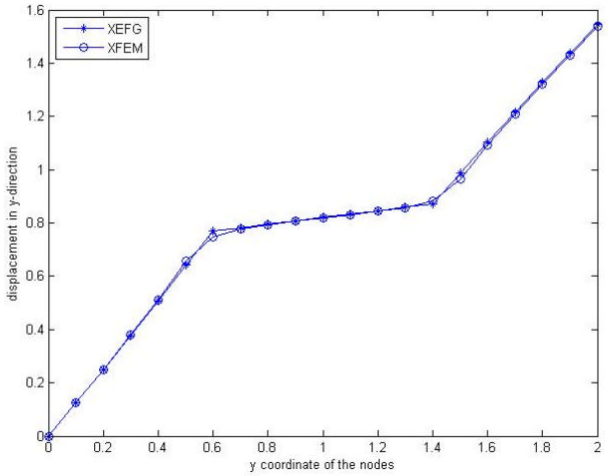

(b) Mesh size, h = 0.1

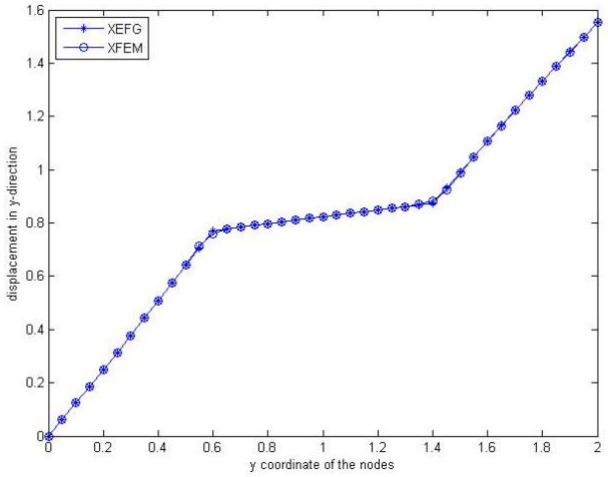

(c) Mesh size, h = 0.05

Figure 4.3: Comparison of the y-displacement along the Y axis between XEFG and XFEM for different mesh sizes (a) 0.2 (b) 0.1 and (c) 0.05

As it can be seen from Figure 4.3 above that for the finer mesh (h = 0.05), the y-displacement values at the node points in the XEFG exactly match with those produced in the XFEM. Hence the proposed model can be implemented further for more complex configurations. Figures 4.4 and 4.5 will show the displacement and stress contour in the y-direction for both the methods (mesh size is used as h = 0.05).

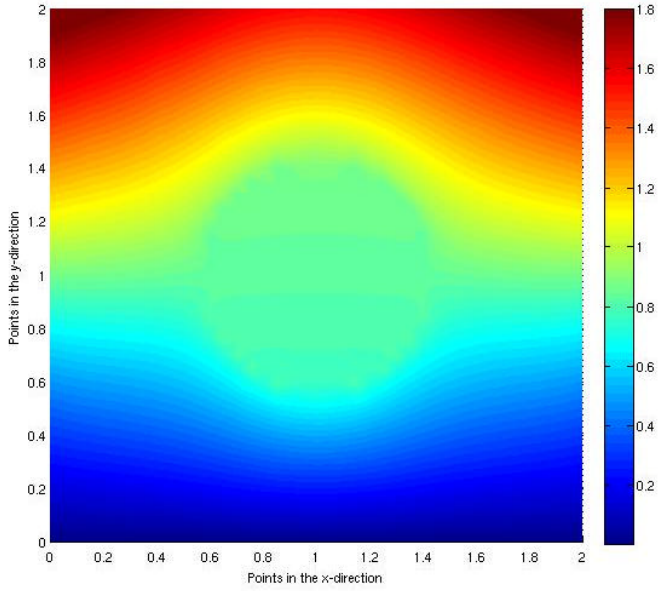

(a)

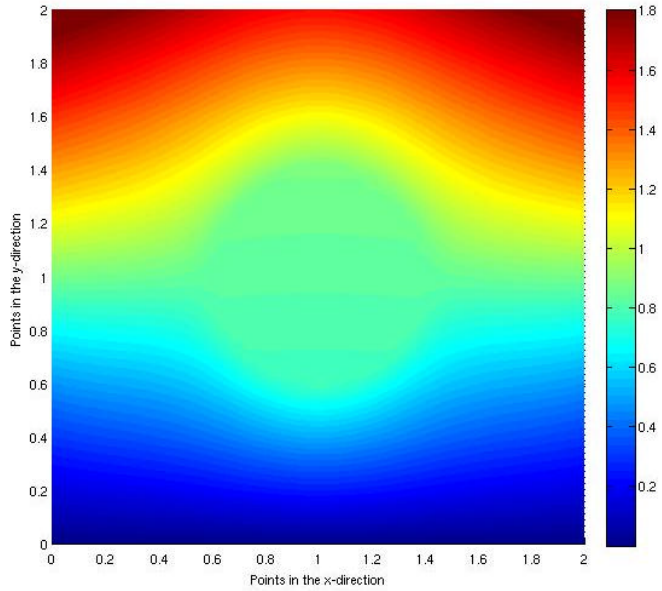

(b)

Figure 4.4: Displacement contour in the y-direction of single inclusion for (a) XEFG and (b) XFEM

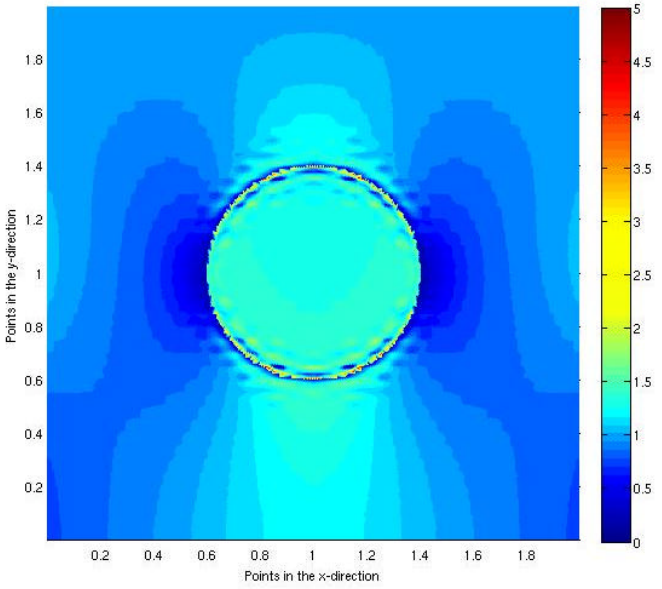

(a) XEFG

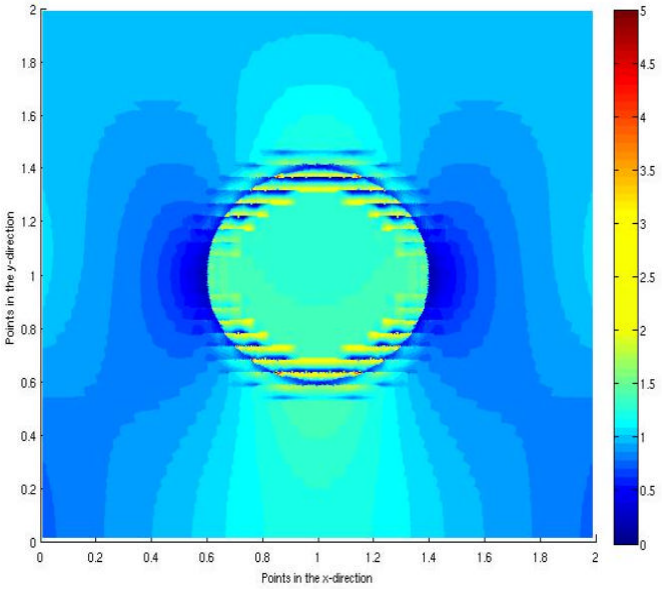

(b) XFEM

Figure 4.5: Stress contour in the y-direction of single inclusion for (a) XEFG and (b) XFEM

As it can be observed from these figures, there is a good agreement in terms of displacement contour between the XEFG and the XFEM. Regarding the stress plot, it is understandable that the derivative of displacement plot will not be as smooth as displacement plot. However, the XEFG shows better convergence than the XFEM as

more oscillations are observed around the interface region in case of the XFEM. In the following section, this numerical model will be validated with analytical solutions available in the literature.

4.2.2. Test case: Bi-material boundary value problem - elastic circular inhomogeneity

In this example, an analytical solution for the elastostatic response of a circular material inhomogeneity under radially symmetric loading, as shown in Figure 4.6, is examined within the framework of the enriched EFG. Inside a circular plate of radius *b*, whose material is defined by $E_1 = 10$ and $u_1 = 0.3$, a circular inclusion with radius '*a*' of a different material with $E_2 = 1$ and $u_2 = 0.25$ are considered. The material properties are constant within each domain, Ω_1 and Ω_2, but there is a material discontinuity across the interface $\Gamma_1(r = a)$. The Lame constants in Ω_1 and Ω_2 are: $c_1 = 0.4,\ m_1 = 0.4$ and $c_2 = 5.7692,\ m_2 = 3.8461$, respectively. A linear displacement field: $u_1 = x_1, u_2 = x_2$ ($u_r(b,q) = r$ and $u_q(b,q) = 0$) on the outer boundary $\Gamma_2(r = b)$ is imposed.

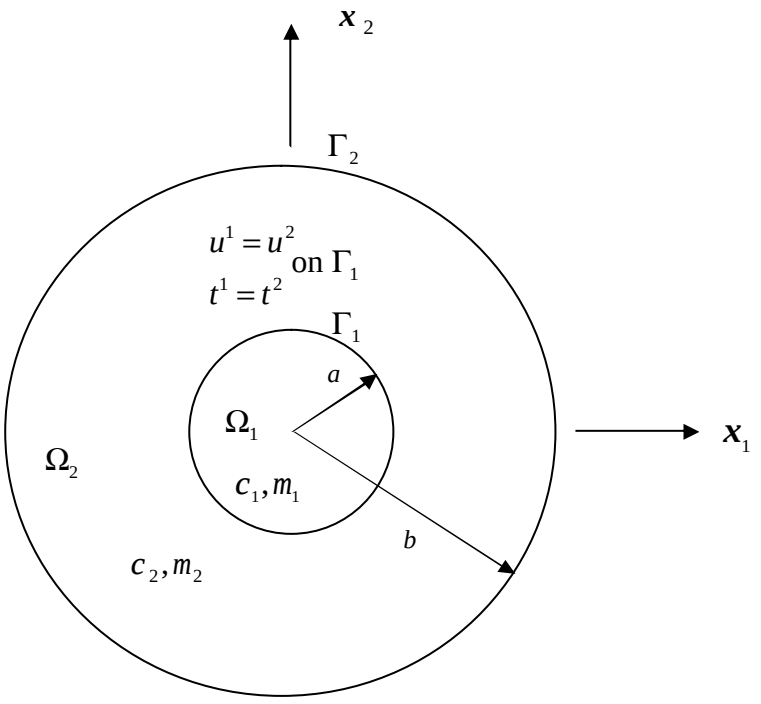

Figure 4.6: Bi-material boundary value problem

By considering displacement and traction continuity across the interface, the exact displacement solutions can be written as [1]:

$$u_r(r,q)=\begin{Bmatrix}[(1-\frac{b^2}{a^2})a+\frac{b^2}{a^2}]r, & 0\le r\le a,\\ (r-\frac{b^2}{r})a+\frac{b^2}{r}, & a\le r\le b,\end{Bmatrix} \tag{4.1}$$

$$u_q(r,q)=0 \tag{4.2}$$

The parameter a involved in these definitions is:

$$a=\frac{(c_1+m_1+m_2)b^2}{(c_2+m_2)a^2+(c_1+m_1)(b^2-a^2)+m_2b^2} \tag{4.3}$$

The radial $e_{rr}(r)$ and hoop $e_{qq}(r)$ strains are given by:

$$e_{rr}(r)=\begin{Bmatrix}(1-\frac{b^2}{a^2})a+\frac{b^2}{a^2}, & 0\le r\le a,\\ (1+\frac{b^2}{r^2})a-\frac{b^2}{r^2}, & a\le r\le b,\end{Bmatrix} \tag{4.4}$$

$$e_{qq}(r)=\begin{Bmatrix}(1-\frac{b^2}{a^2})a+\frac{b^2}{a^2}, & 0\le r\le a,\\ (1-\frac{b^2}{r^2})a+\frac{b^2}{r^2}, & a\le r\le b,\end{Bmatrix} \tag{4.5}$$

For the present numerical study, a square domain of size $L\times L$ with L = 2 is considered, where the outer radius is chosen to be as b = 2 and the inner radius as a = 0.4. Closed-form displacements are imposed along the outer boundary. Plane strain conditions are assumed. A convergence study is conducted using equi-spaced rectangular $L_h\times L_h$ meshes for nodes, where L_h =10, 20, 40, 80, 160. Hence five different mesh sizes - 0.2, 0.1, 0.05, 0.025 and 0.0125 are used respectively.

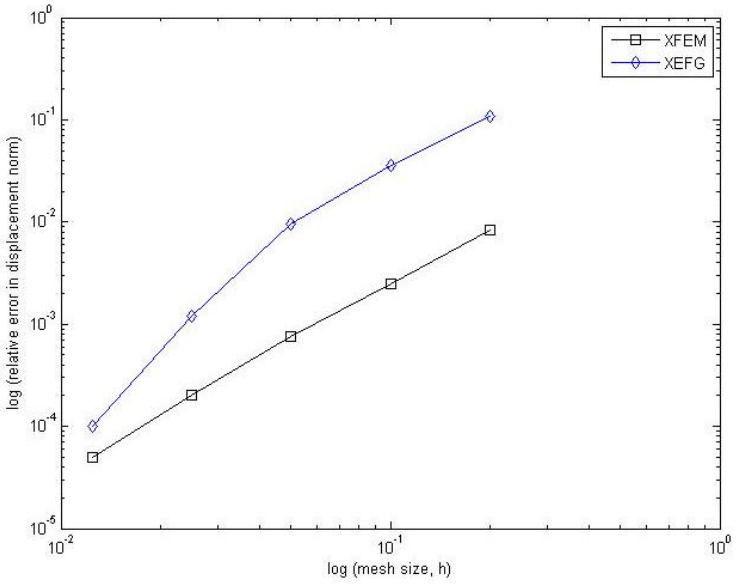

Figure 4.7: Rate of convergence in displacement norm

Figure 4.7 shows the rate of convergence in the displacement norm (L^2) for the enriched EFG method, in which the accuracy is improved as the number of degrees of freedom is increased. Also the convergence is compared with the XFEM for the same problem. The enriched EFG method achieves a convergence rate of 1.80 where as the XFEM achieves 1.84. Thus, sufficient accuracy in the enriched EFG method can be achieved compared to the XFEM and other approximation methods.

In addition, the computed displacement, and radial and hoop strains along the line y=0 are compared with the analytical ones given in equation (4.1) to (4.5). Figure 4.8 and 4.9 show the results with the model for mesh sizes h = 0.1 and 0.05 respectively. Although when relatively coarse mesh is used (h = 0.1), a lot of oscillations are observed in the strain diagrams in Figure 4.8. However, using finer mesh (h = 0.05) generally cures those oscillations. As it can be seen, both displacement and strains are successfully reproduced by the enriched EFG in Figure 4.9.

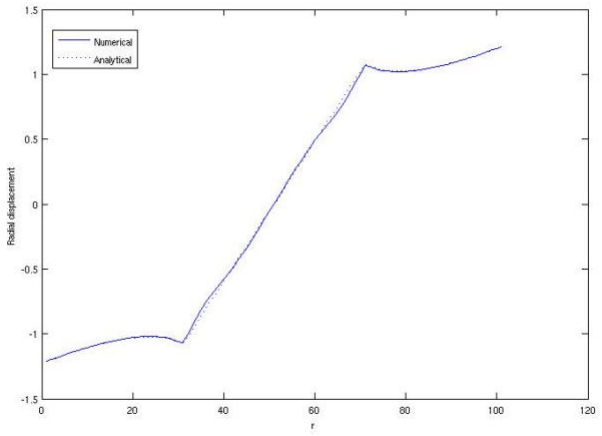

(a)

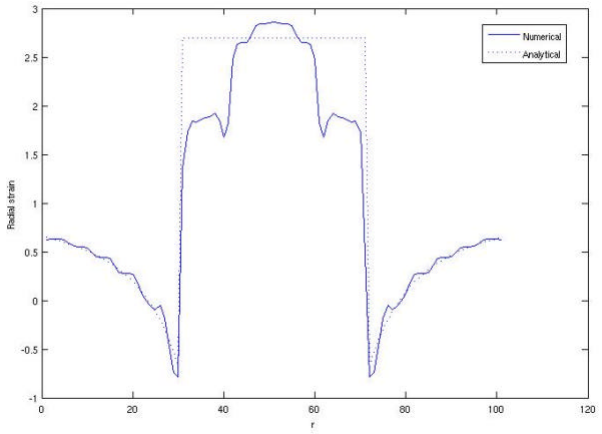

(b)

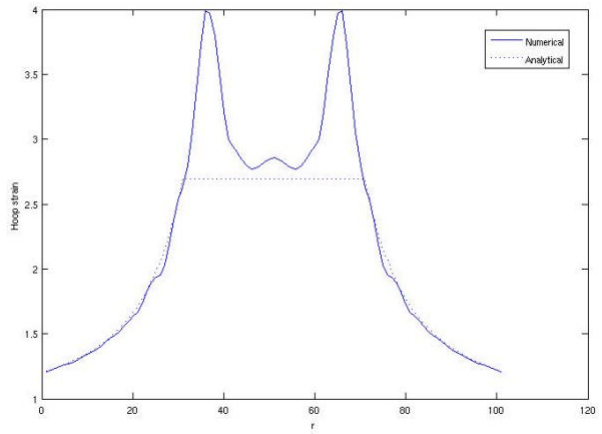

(c)

Figure 4.8: Comparison of the displacement and strains calculated by the enriched EFG with the analytical solution for mesh size 0.1: (a) displacement in the *r*-direction, u_r ; (b) radial strain, e_{rr} ; (c) hoop strain, e_{qq}

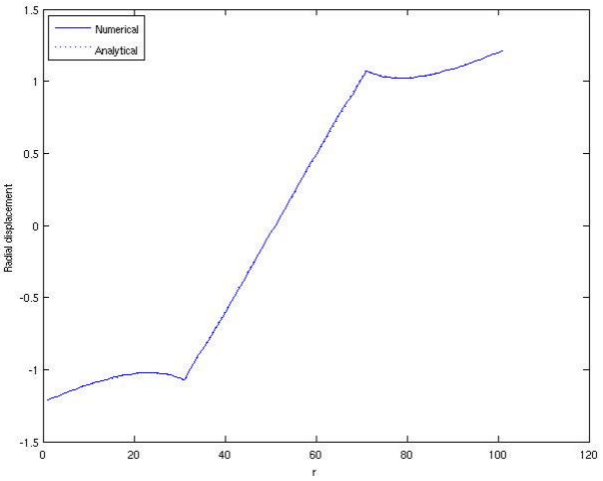

(a)

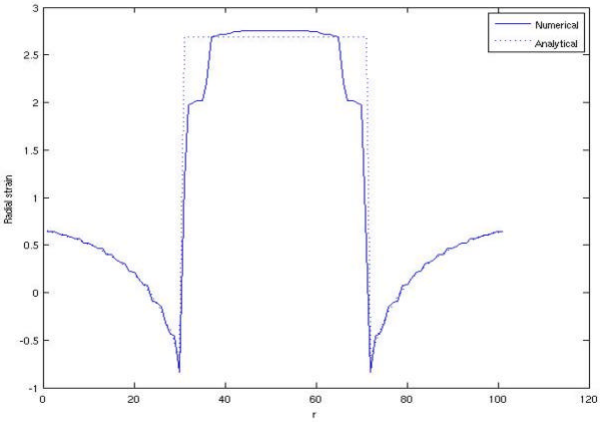

(b)

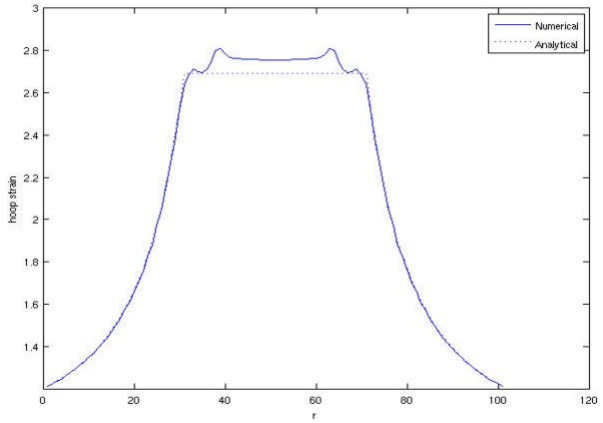

(c)

Figure 4.9: Comparison of the displacement and strains calculated by the enriched EFG with the analytical solution for mesh size 0.05: (a) displacement in the *r*-direction, u_r ; (b) radial strain, e_{rr} ; (c) hoop strain, e_{qq}

Previous results have shown the robustness of this numerical technique for single inclusion problem. In order to demonstrate the effectiveness and capability of the proposed model, analyses of the multi-inclusion problems will be carried out next. Two problems are going to be considered – one having four inclusions and the other having nine inclusions.

4.2.3 Multi-inclusion problem

4.2.3.1 *Four inclusions problem*

In case of four inclusions, radius of each circle is chosen to be 0.2 for 12% volume fraction. Domain of influence is 1.5. Nodal distribution for h = 0.1 is shown below to indicate the position of the circles and selection of the enriched nodes.

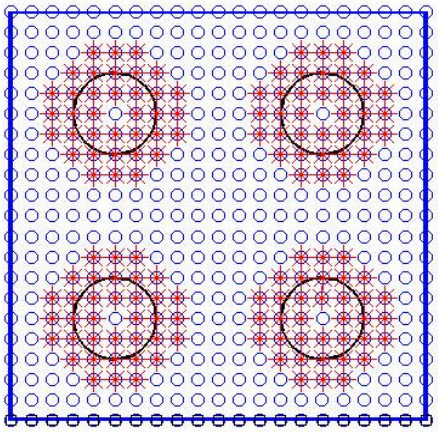

Figure 4.10: Distribution of nodes and location of enriched nodes for four inclusions

The dimension of the square domain is 2×2. A uniform tension P = 1 is applied at the upper edge of the domain and the lower edge is fixed. Young's modulus of elasticity (E) for matrix is 1 and Poisson's ratio is 0.3; where as for inclusion they are 10 and 0.3 respectively. Plane stress conditions are assumed. The comparison between the XEFG and the XFEM for the same criterion is shown in Figure 4.11:

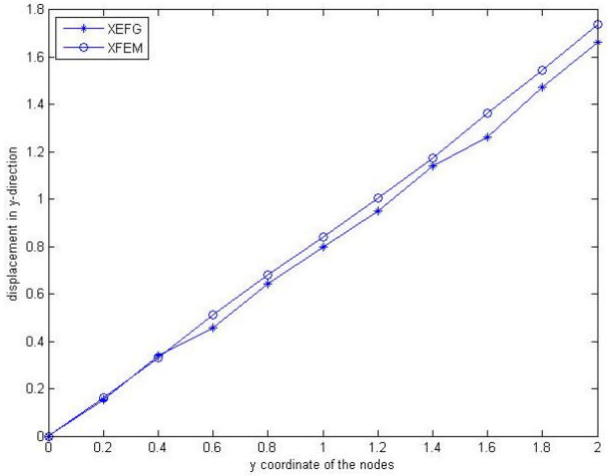

(a) Mesh size, h = 0.2

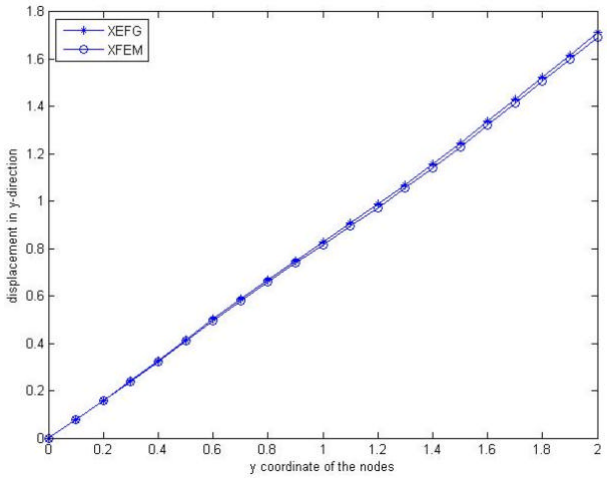

(b) Mesh size, h = 0.1

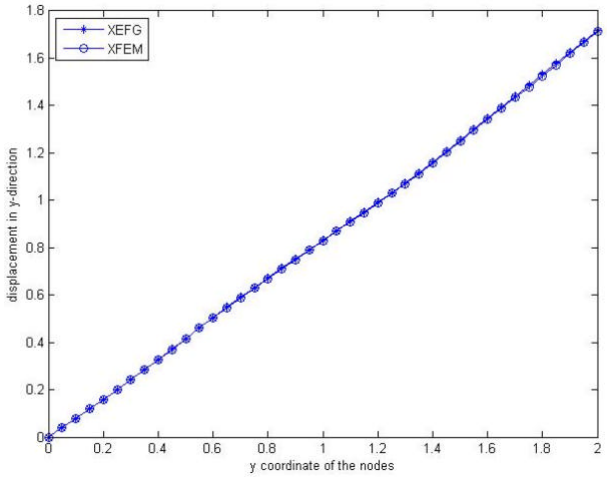

(c) Mesh size, h = 0.05

Figure 4.11: Comparison of the y-displacement along the Y axis between XEFG and XFEM for different mesh sizes (a) 0.2 (b) 0.1 and (c) 0.05

In case of four inclusions, a high convergence of the XEFG is observed. As it can be seen from Figure 4.11 that for the finer mesh (h = 0.05), the y-displacement values at the node points in the XEFG exactly match with those produced in the XFEM. The following diagrams show the displacement contour in the y-direction for both the methods (mesh size is used as h = 0.05).

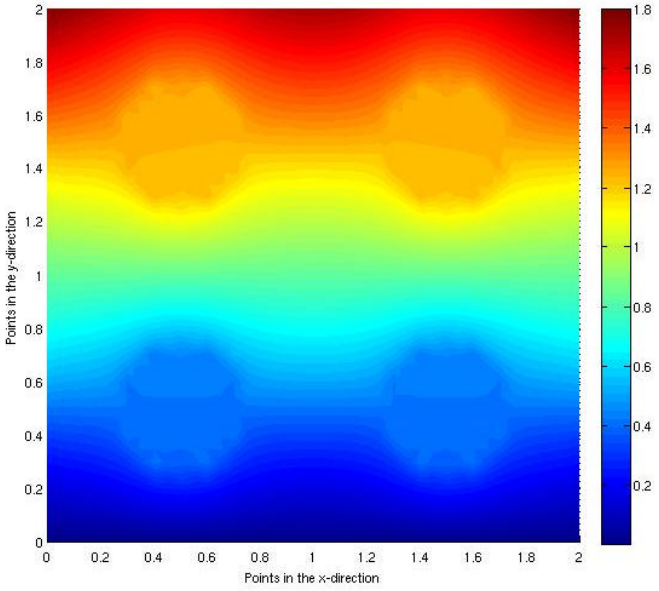

(a) XEFG

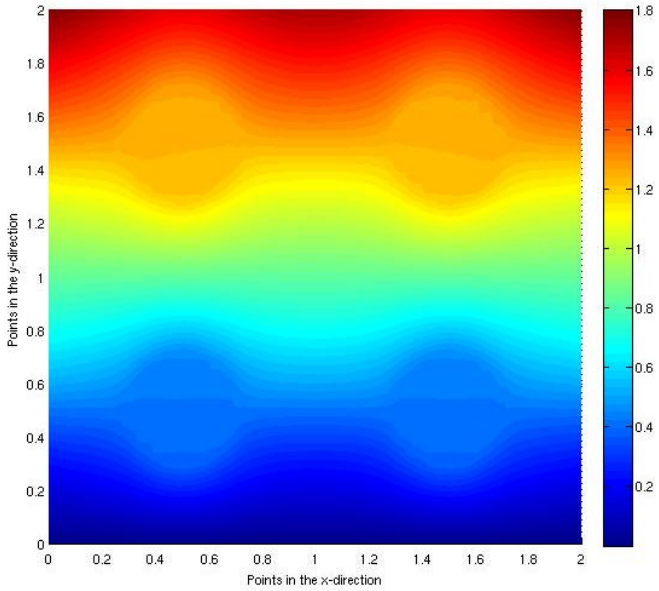

(b) XFEM

Figure 4.12: Displacement contour in the y-direction of four inclusions for (a) XEFG and (b) XFEM

4.2.3.2 *Nine inclusions problem*

In case of nine inclusions, radius of each circle is chosen to be 0.133 for 12% volume fraction. Domain of influence is 1.4 for h=0.1 and 1.2 for h=0.05, respectively. The loading condition and material properties are exactly the same as in the case of four inclusions. Nodal distribution for h = 0.1 is shown in Figure 4.13 to indicate the position of the circles and selection of the enriched nodes.

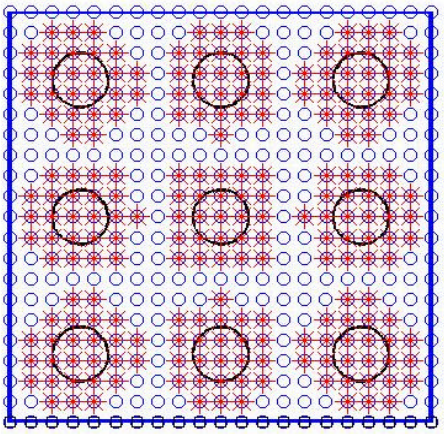

Figure 4.13: Distribution of nodes and location of enriched nodes for nine inclusions

The comparison between XEFG and XFEM for the same criterion is given below:

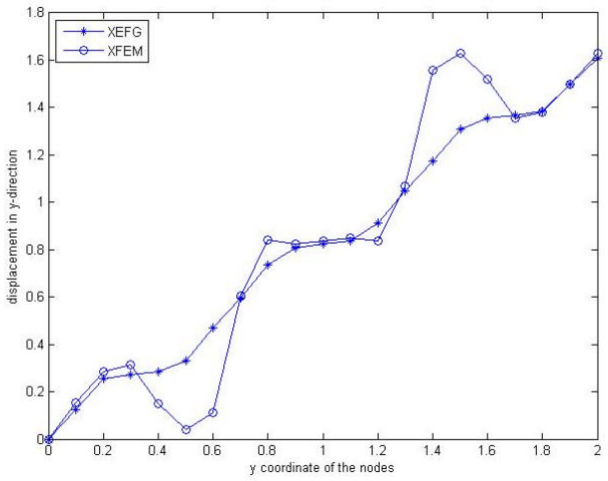

(a) Mesh size, h = 0.1

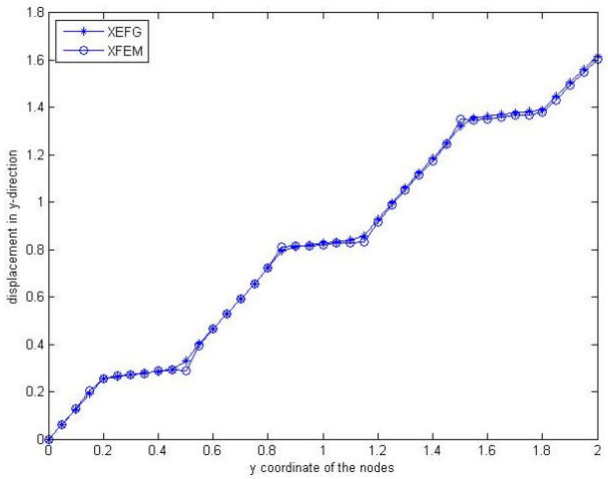

(b) Mesh size, h = 0.05

Figure 4.14: Comparison of the y-displacement along the Y axis between XEFG and XFEM for different mesh sizes (a) 0.1 and (b) 0.05

There is a good overall agreement between the two methods is observed in case of nine inclusions as well. As it can be seen from Figure 4.14 that for the finer mesh (h = 0.05), the y-displacement values at the node points in the XEFG generally match with those constructed in the XFEM. Figure 4.15 shows the displacement contour in the y-direction for both the methods (mesh size is used as h = 0.05). The displacement contour plots are very much comparable between the two methods.

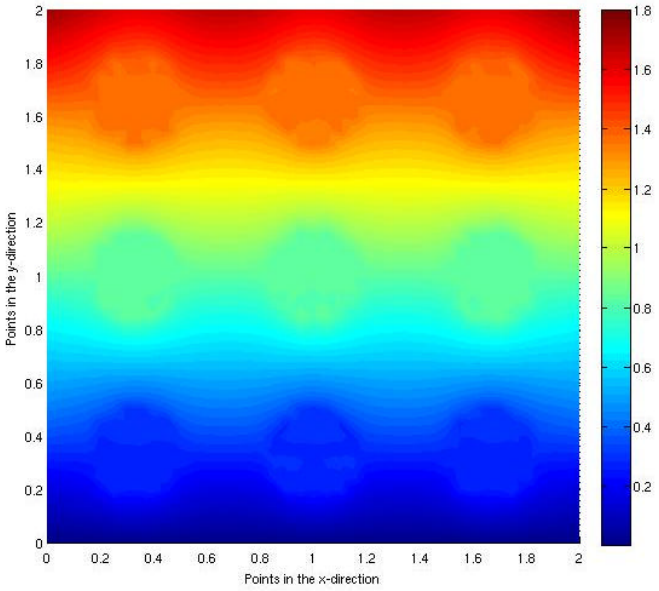

(a) XEFG

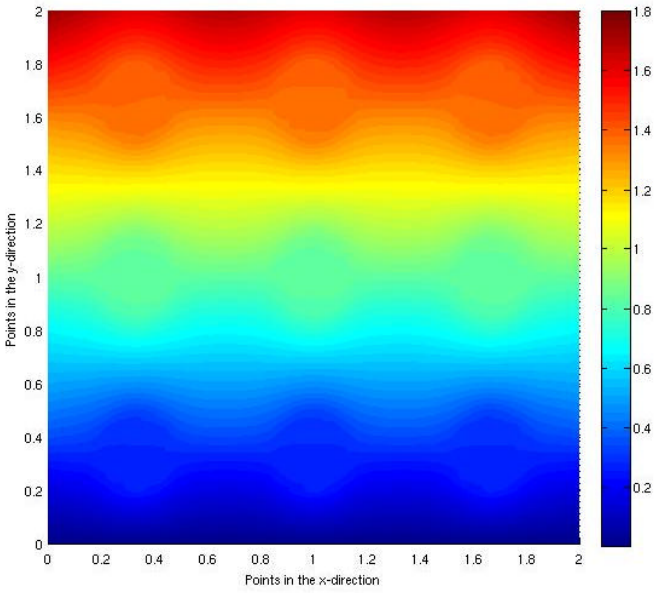

(b) XFEM

Figure 4.15: Displacement contour in the y-direction of nine inclusions for (a) XEFG and (b) XFEM

In order to establish the effectiveness of the proposed numerical tool, soft inclusions compared to the matrix material are considered too. In this case young's modulus of elasticity (E) for matrix is 10 and Poisson's ratio is 0.3; where as for inclusion they are 1 and 0.3 respectively. Three different cases will be considered just like the previous test cases – single inclusion, four inclusions and nine inclusions. The domain size and nodal distributions will remain exactly the same. Numerical results are computed and compared with the XFEM. The comparison between the XEFG and the XFEM is shown below by plotting the y co-ordinates of centre line nodes along the Y axis in the horizontal direction to the y-displacement of centre line nodes along the Y axis in the vertical direction for 3 different mesh sizes:

1. For single inclusion:

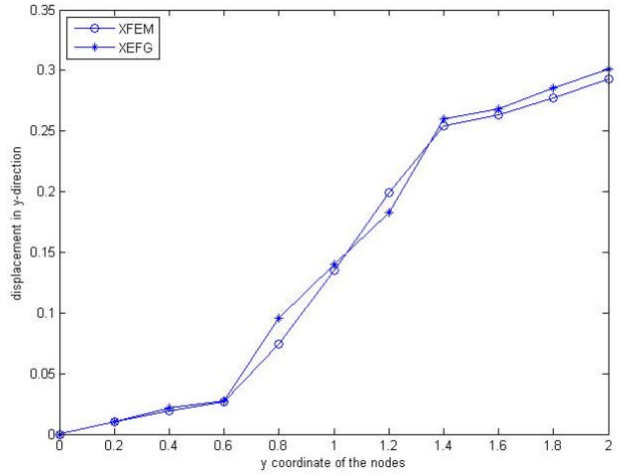

(a) Mesh size, h = 0.2

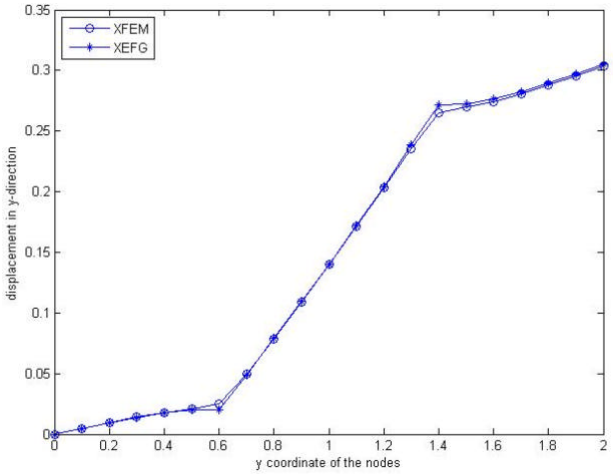

(b) Mesh size, h = 0.1

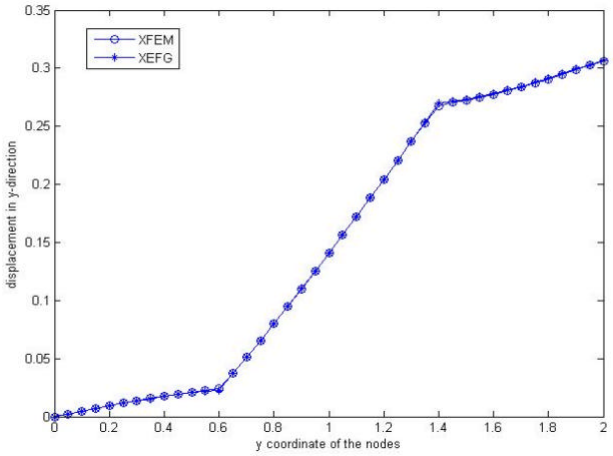

(c) Mesh size, h = 0.05

Figure 4.16: Comparison of the y-displacement along the Y axis between XEFG and XFEM for different mesh size (a) 0.2 (b) 0.1 and (c) 0.05

2. For four inclusions:

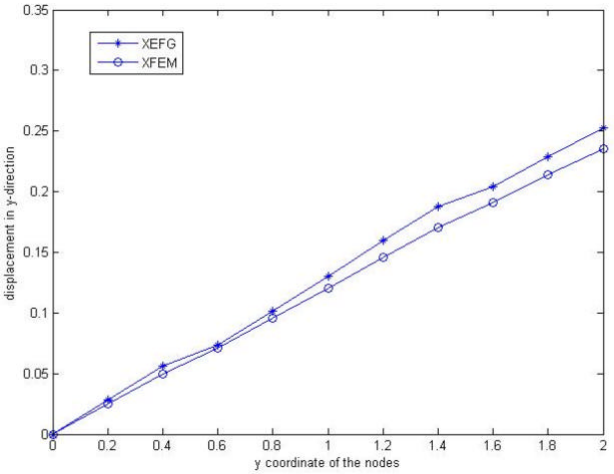

(a) Mesh size, h = 0.2

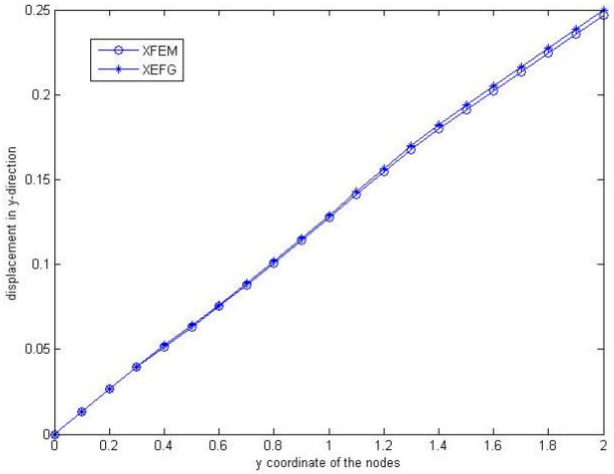

(b) Mesh size, h = 0.1

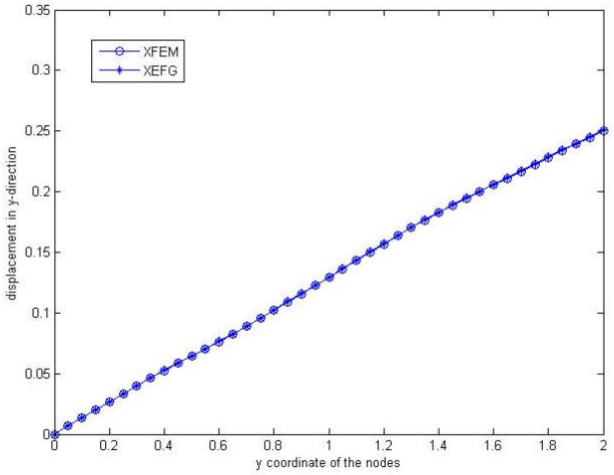

(c) Mesh size, h = 0.05

Figure 4.17: Comparison of the y-displacement along the Y axis between XEFG and XFEM for different mesh size (a) 0.2 (b) 0.1 and (c) 0.05

3. For nine inclusions:

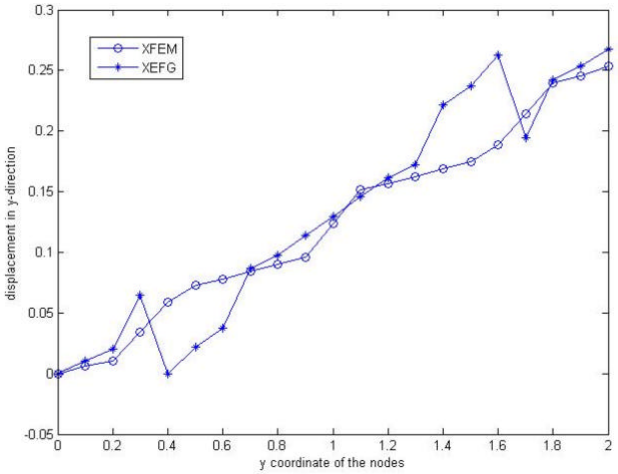

(a) Mesh size, h = 0.1

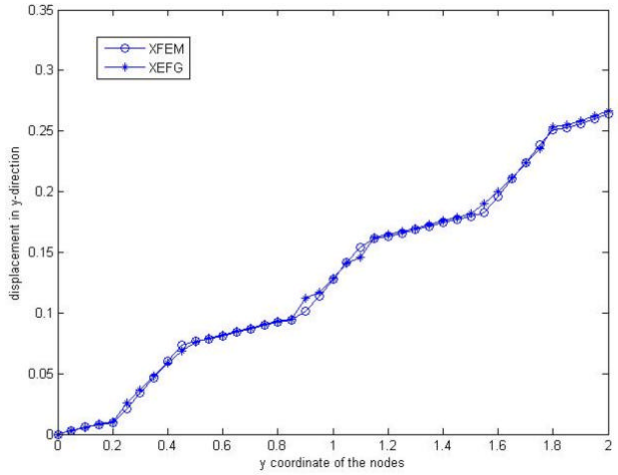

(b) Mesh size, h = 0.05

Figure 4.18: Comparison of the y-displacement along the Y axis between XEFG and XFEM for different mesh sizes (a) 0.1 and (b) 0.05

From the above analyses, it can be concluded that this numerical model can predict the behaviour of particulate composites of any given properties accurately. In the next section, randomly distributed particles are going to be analysed.

4.3 Randomly distributed particles

The proposed model can also be utilised for randomly distributed particles. A brief description is presented here to show the efficiency of the enriched EFG in modelling randomly distributed particles. The geometry and boundary conditions are as follows:

The selected domain size is 2×2. A uniform tension $P = 1$ is applied at the upper edge of the domain and the lower edge is fixed. Young's modulus of elasticity (E) for matrix is 1 and Poisson's ratio is 0.3; where as for inclusion they are 10 and 0.3 respectively. Plane stress conditions are assumed. The implementation can be divided in 2 parts:

1) To keep the radii size same of all the inclusions for a particular volume fraction, which is 12% in this case. The y displacement contours are shown below for this case:

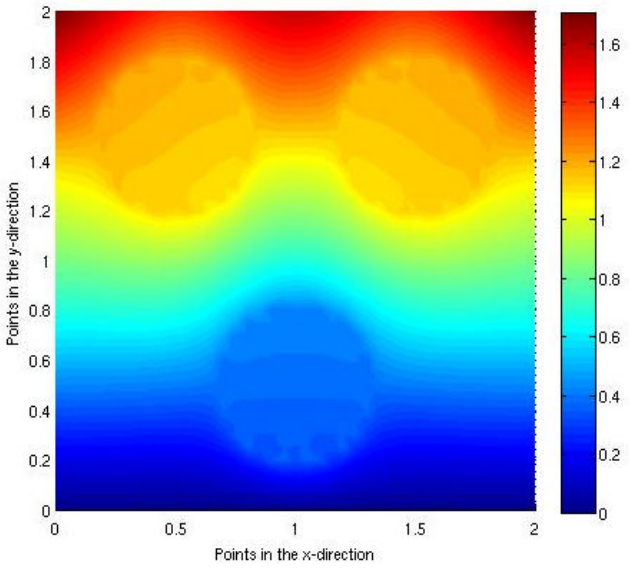

(a)

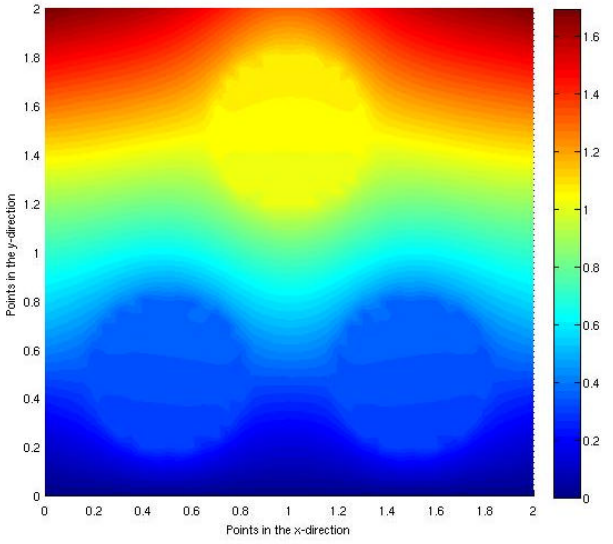

(b)

Figure 4.19: Displacement contour for randomly distributed particles with same radii size

2) To change the radii size of all the inclusions for the same volume fraction, which is 12%. The y-displacement contours are shown below for this case:

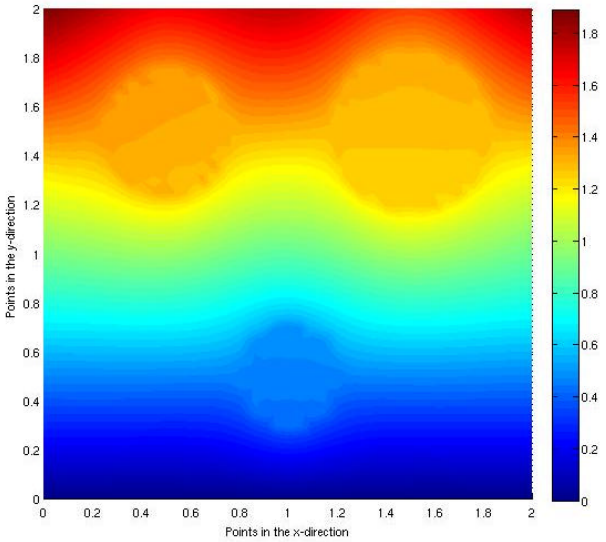

(a)

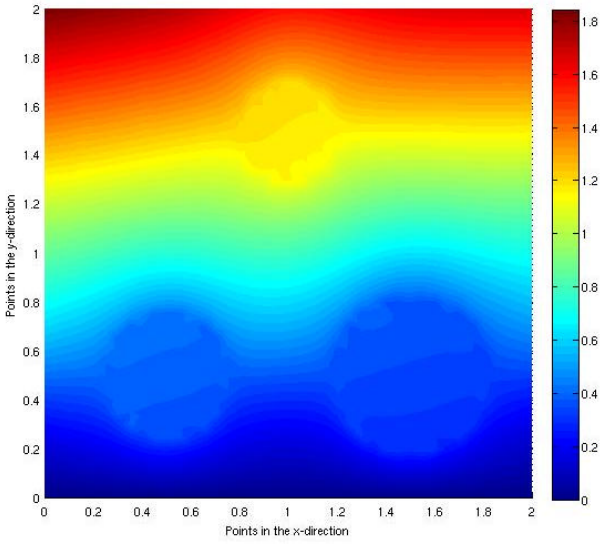

(b)

Figure 4.20: Displacement contour for randomly distributed particles with different radii size

From the displacement contours shown above, it can be seen that the displacements in both cases are very smooth regardless the sizes and positions of the inclusions. In the next section, configurations involving complex shaped inclusions will be investigated to further demonstrate the effectiveness of this method.

4.4 Complex shaped inclusion

One of the major advantages in using the enriched EFG method is to overcome the tedious job of meshing for complex shaped inclusion as opposed to mesh based methods. An irregular shape of 'star' is modelled as particulate composites within the framework of the enriched EFG to demonstrate the potential of this method. Two different cases are considered – single inclusion and nine inclusions. The geometry, loading and boundary conditions are as follows:

The selected domain size is 2×2. The 'star' shaped inclusion is placed at the centre of the domain for single inclusion. A uniform tension $P = 1$ is applied at the upper edge of the domain and the lower edge is fixed. Young's modulus of elasticity (E) for matrix is 1 and Poisson's ratio is 0.3; where as for inclusion they are 10 and 0.3 respectively. Plane stress conditions are assumed. The displacement contour along the x- and y-direction is shown in the following diagrams:

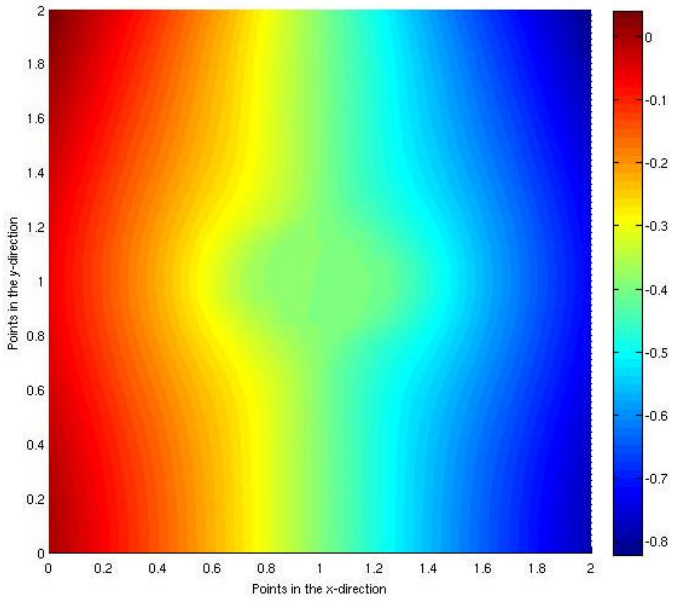

Figure 4.21: Displacement contour in the x-direction for single inclusion

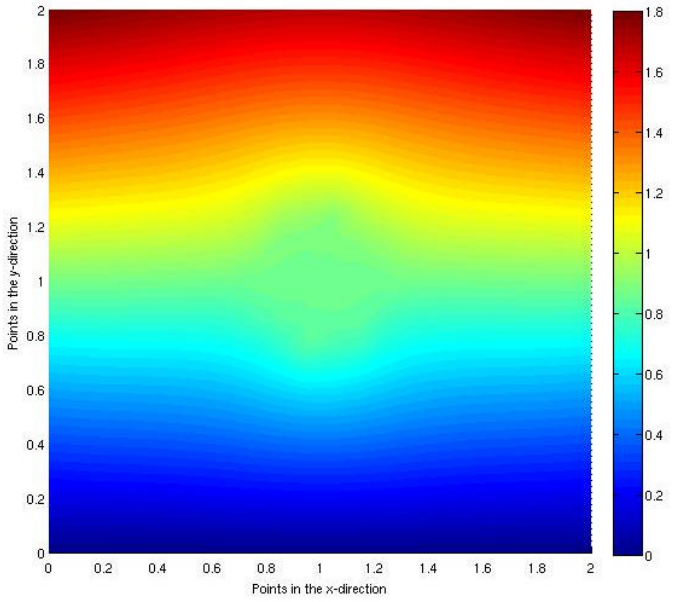

Figure 4.22: Displacement contour in the y-direction for single inclusion

As it can be seen from Figure 4.21 and Figure 4.22 that the displacements are very smooth and are in good agreement with the displacements of regular shaped inclusion.

In order to demonstrate the effectiveness and capability of this method, a problem involving multi-inclusions is also performed, for which the displacement contour along the x- and y-direction are shown in the following diagrams:

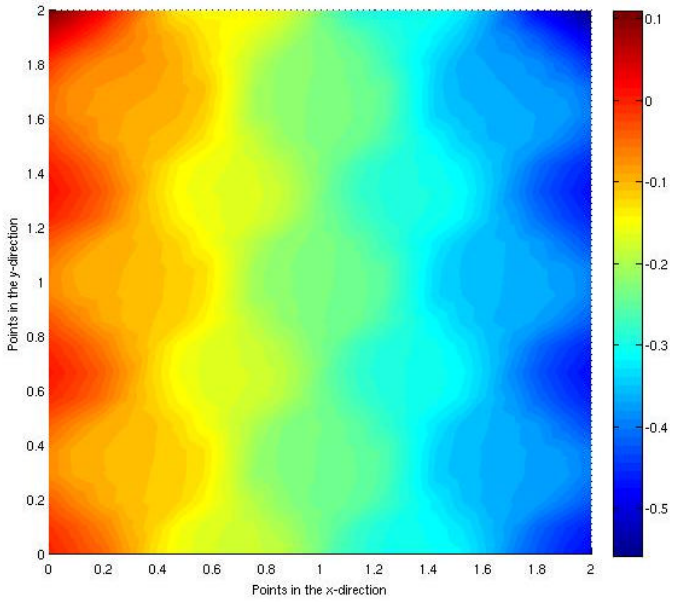

Figure 4.23: Displacement contour in the x-direction for nine inclusions

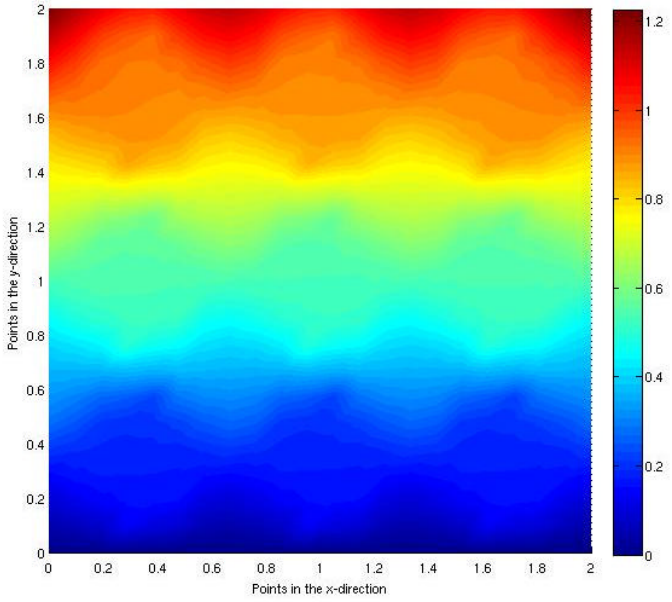

Figure 4.24: Displacement contour in the y-direction for nine inclusions

4.5 Syntactic foams

4.5.1 Introduction

Syntactic foams are a special kind of particulate composite materials made by a matrix ("binder") and a gas-filled aggregate ("filler") consisting of hollow spherical microspheres [2]. These composite materials are classified as foams since they possess a structure formally similar to that of a cellular, gas-expanded, solidified liquid. The term syntactic (from the Greek "s*yntaktikos*" - orderly disposed system) indicates a constructed foam, in the sense that the material is manufactured by a specific mixing procedure of fillers and binders with appropriate volume fractions [3]. However, the filler is randomly dispersed in the matrix, in a way to obtain a homogeneous and isotropic macroscopic behaviour.

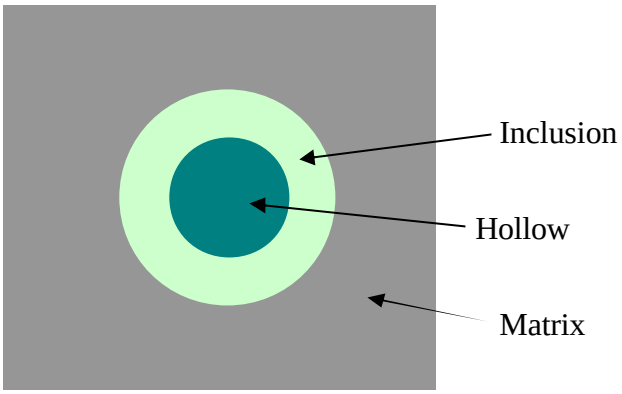

Figure 4.25: Syntactic foam

Syntactic foams are normally tertiary systems, since matrix and gas-filled aggregate are usually made of different materials. Thermosetting polymers such as epoxy and phenolic resins and silicons are often used as binders; where as glass, carbon, metal, and resin made of microbubbles are frequently taken as fillers. However, syntactic foams are basically classified as two-phase systems, when they do not contain dispersed air bubbles between binder and filler, or as three-phase systems, when air bubbles are included, in some cases on purpose, in view of lowering the foam density [4, 5].

The structure of syntactic foams comprises two constituents: matrix material and microballoons. In experimental studies such structure is termed as a two-phase structure based on the two physical phases present in the material [6]. The void enclosed inside microballoons is not considered as a separate phase. Some fundamental differences are present between solid and hollow particles, which cause significant deviation of predictions based on theories developed for solid particle filled composites from the experimental results. For particulate composites comprising solid or hollow particle of the same material, shape and size, the effective elastic moduli are different. In the case of hollow particles, the effective Young's modulus depends on the wall thickness of the particles and, more specifically, on the wall thickness to particle size ratio. Hence, wall thickness must appear in the theoretical models. This requires that the void enclosed inside the microballoons should be considered as a separate phase. Hence, the microstructure of syntactic foams is considered to be composed of three phases, namely matrix, microballoon shell and the air void inside the microballoon.

4.5.2 Significance in the properties of syntactic foams

Additionally, the moisture absorption is significantly lower in these composites compared to the matrix material and other foam types due to the presence of porosity only inside the hollow inclusions [7, 8]. It mainly depends on the chemical and physical properties of filler and binder and their volume ratio. Thermal properties are normally dominated by the matrix characteristics. Syntactic foams are also characterized by good thermal insulation and dielectric properties [6]. Glass microbubbles are frequently preferred due to mechanical strength, smoothness and regularity of the surface, good wetting characteristics and low viscosity of the resulting foam [3].

4.5.3 Application of syntactic foams

Syntactic foams are known for their low weight, high specific compressive strength, low moisture absorption, and impact resistance coupled with excellent damping characteristics [9]. They are used in many applications due to the flexibility in tailoring the material to provide a combination of desired mechanical properties. The spectrum of engineering applications of syntactic foams is quite broad as significant applications of syntactic foams date back a long way. Syntactic foams are used as core materials in sandwich composites for aerospace and marine structural applications [10, 11]. Syntactic foams made with glass and more often carbon microbubbles are widely used in aeronautical and aerospace engineering as fillers of alveolate structures [12] and as protection shields for space vehicles and missile heads [13]. Syntactic foams are extensively used in deep sea, marine structures and offshore applications due to their light weight structure, buoyancy and water insulation properties [9, 14]. Syntactic foams are often used in civil and industrial engineering, in construction and as an imitation of wood and marble [6]; often they are employed as core materials due to good shear stiffness and strength, fatigue and impact resistance [15, 16].

4.5.4 Modelling of syntactic foams

In this section, the present numerical technique is applied to model syntactic foam. The following geometry and material properties are considered:

The selected domain has the dimension of 2×2. A uniform tension $P = 1$ is applied at the upper edge of the domain and the lower edge is fixed. Young's modulus of elasticity (E) for matrix is 1 and Poisson's ratio is 0.3; where as for the microballons, they are 150 and 0.3 respectively. For the hollow part, Young's modulus of elasticity and Poisson's ratio are considered zero. The radius is taken as 0.3 and 0.4 for the inner and outer circle respectively. Plane stress conditions are assumed.

The selected EFG scheme includes a regular nodal distribution, a 4×4 Gauss quadrature rule and linear basis functions. The cubic spline weight functions are used for the construction of the weight functions and the domain of influence is chosen to be 1.5. The distribution of nodes and selections of enriched nodes are shown below for mesh size, $h = 0.1$.

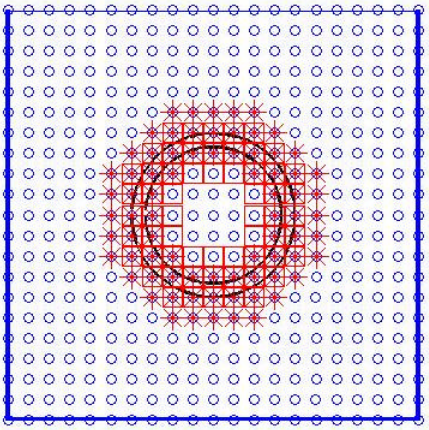

Figure 4.26: Distribution of nodes for syntactic foam

The results are validated and compared with the FEM results. The comparison between the XEFG and FEM is shown below by plotting the y co-ordinates of centre line nodes along the Y axis in the horizontal direction to the y-displacement of centre line nodes along the Y axis in the vertical direction:

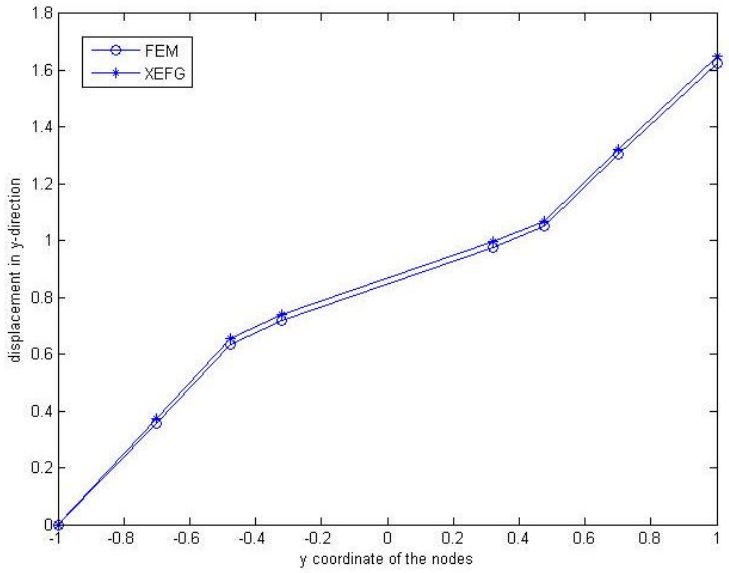

Figure 4.27: Comparison of the y-displacement along the Y axis between XEFG and FEM

It can be seen from Figure 4.27 that the model that has been developed using the enriched EFG technique has shown very good agreement and is very much comparable with the FEM. The y-displacement contour for this particular case is shown in Figure 4.28 below:

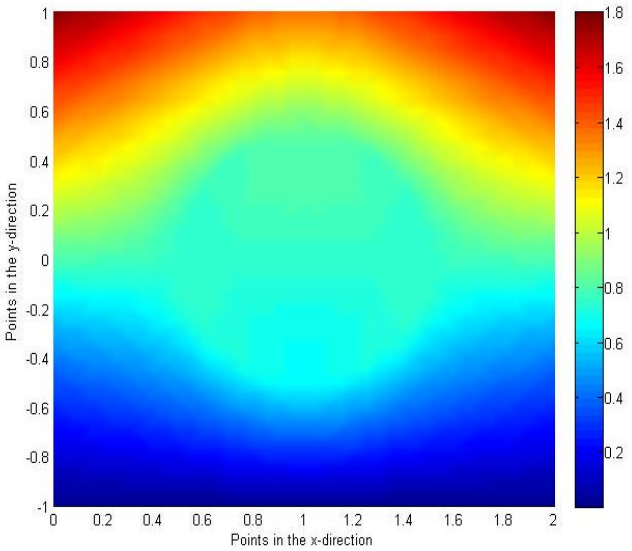

(a) XEFG

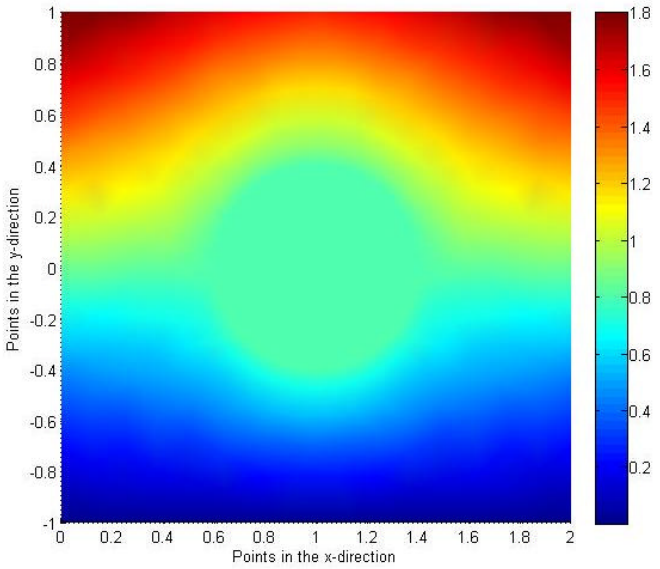

(b) FEM

Figure 4.28: Comparison of y-displacement contour between (a) XEFG and (b) FEM

Once the model is established, then the results are compared for different radii positions of the inner and outer circle. Stress contour in the y-direction for some of the cases are shown below:

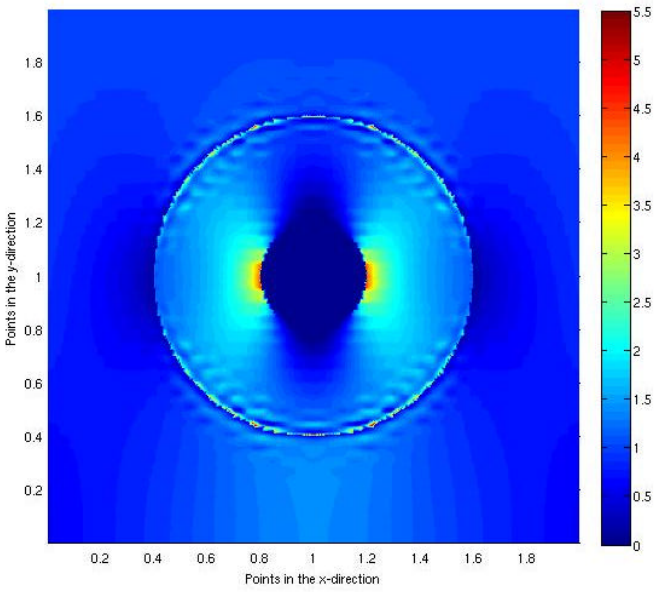

Figure 4.29: Stress contour in the y-direction for inner radius 0.2 and outer radius 0.6

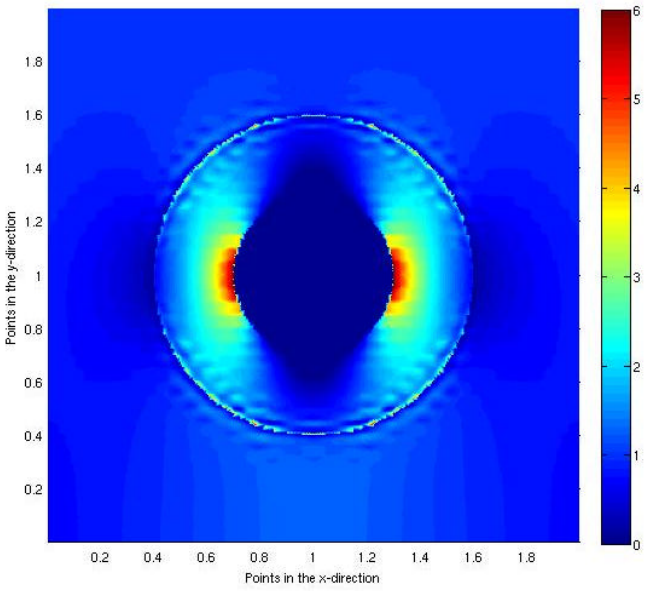

Figure 4.30: Stress contour in the y-direction for inner radius 0.3 and outer radius 0.6

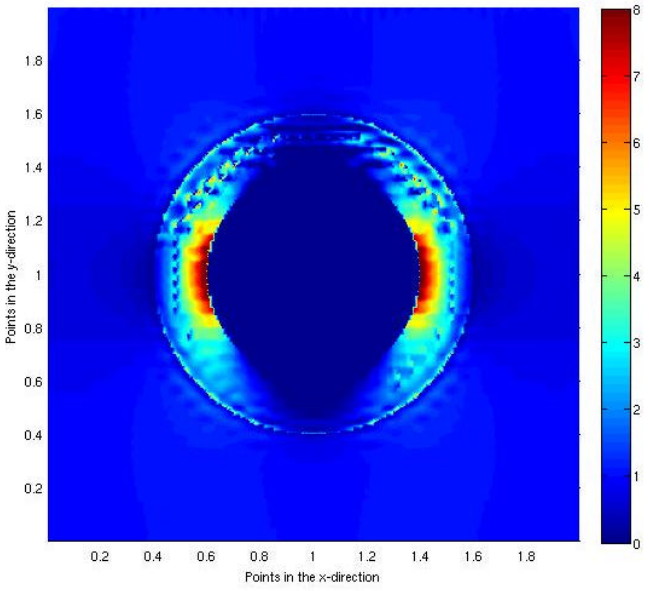

Figure 4.31: Stress contour in the y-direction for inner radius 0.4 and outer radius 0.6

It can be seen from the diagrams above that when the distance between the inner and outer circle is sufficiently large, the stress distribution is very smooth. However, when the distance is very small, i.e., they are close to each other; oscillation starts forming in the stress plot within the inclusion and makes it unsmooth.

4.6 Homogenisation technique for syntactic foams

In order to compute the effective elastic properties of particulate composites, this section will focus on investigating the correlations among material parameters, mechanical properties and microstructural parameters of syntactic foams. First order homogenisation technique is applied assuming the materials are linear elastic, micro scale is prescribed with a constant strain, and using Hill Mandel condition combined with stress/strain averaging. First-order homogenization assumes that the RVE is infinitely small compared to the macroscopic characteristic length scale and that there is clear separation of scales.

The inner and outer radii of the microballoon are called r_i and r_o. The volume fraction of microballoon is denoted by Φ, where as the wall thickness is denoted as *t*. for matrix and microballoons, the elastic properties are represented by same notations with subscripts *m* and *b* respectively. Hollow particles can be characterized based on their wall thickness. A parameter named 'radius ratio' is defined for hollow particles as [17]:

$$h = \frac{r_i}{r_o} \tag{4.6}$$

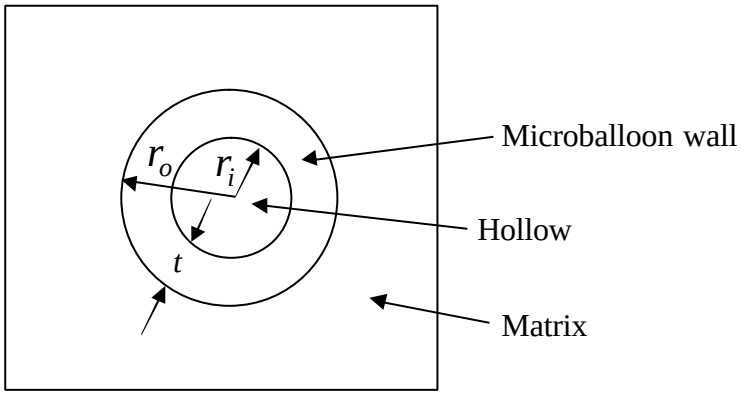

Figure 4.32: Notations used to define various physical parameters for microballoons [17]

The following material properties are used for the investigation:

Young's modulus of elasticity (E) for matrix is 3.060×10^9 and Poisson's ratio is 0.3; where as for microballoons, they are 60×10^9 and 0.21 respectively. For the hollow part, Young's modulus of elasticity and Poisson's ratio are considered zero. Plane stress conditions are assumed. The result obtained from the numerical simulation is compared with the experimental data of glass embedded microballoons in a vinyl ester resin matrix. The properties of the resin are taken from [17].

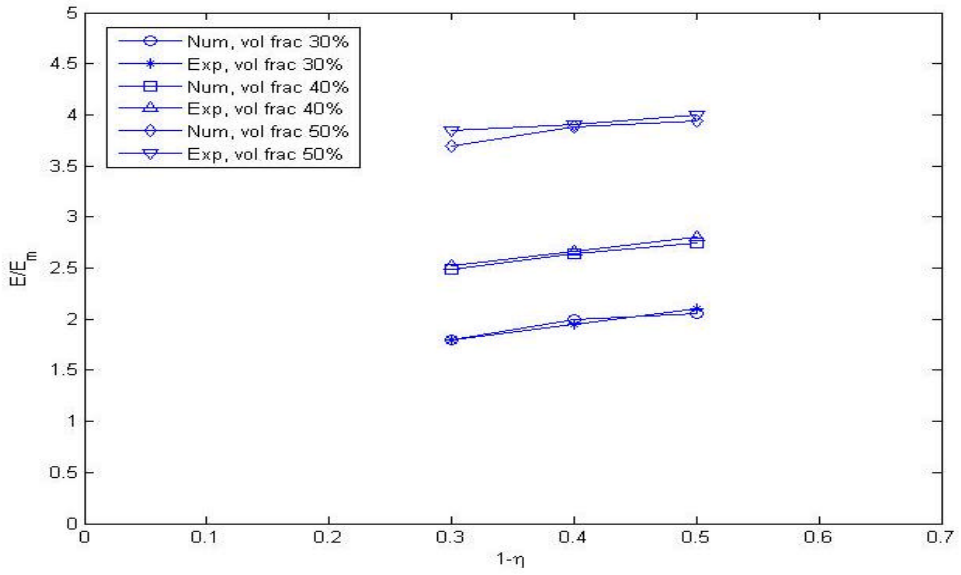

Figure 4.33: Change in the elastic modulus with respect to the microballoon wall thickness

The variation in E/E_m for epoxy matrix syntactic foams in the range of 0.3-0.5 for $(1-h)$ is shown in Figure 4.33 for three different volume fractions. It is signified from the figure that the rate of increase of the Young's modulus decreases as h decreases. The values of E/E_m are strongly dependant on Φ [14]. The effect of h diminishes faster at lower values of Φ.

Next, the effect of microballoon wall thickness on the modulus of syntactic foams is compared in Figures 4.34 to 4.37 for vinyl ester resin matrix syntactic foams, containing Φ in the range of 0.3-0.6. In these figures, non-dimensional wall thickness of microballoons in the form of $(1-h)$ is plotted on the horizontal axis. The relative

modulus of the composite with respect to the modulus of the matrix material (E / E_m) is plotted on the vertical axis.

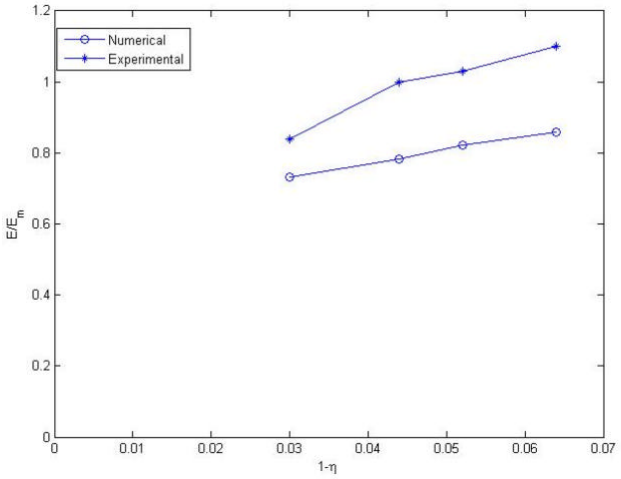

Figure 4.34: Effect of microballoon wall thickness on Young's modulus for Φ = 0.3

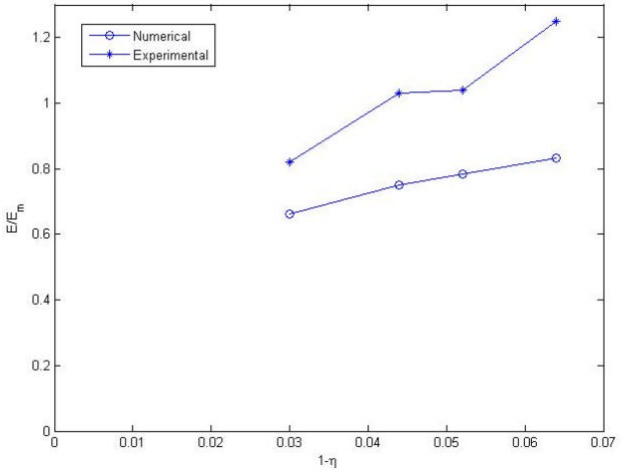

Figure 4.35: Effect of microballoon wall thickness on Young's modulus for Φ = 0.4

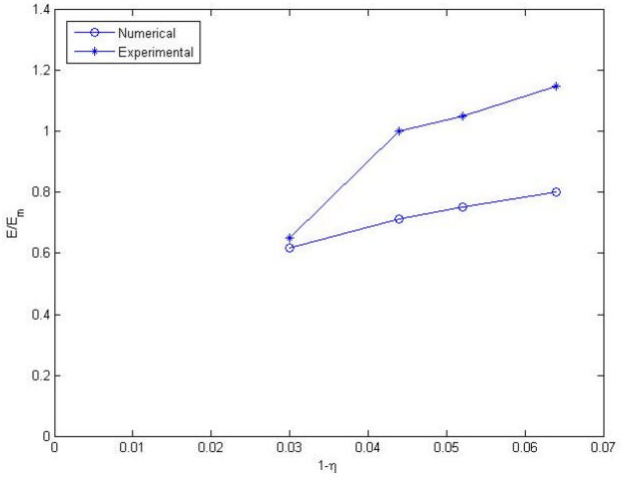

Figure 4.36: Effect of microballoon wall thickness on Young's modulus for Φ = 0.5

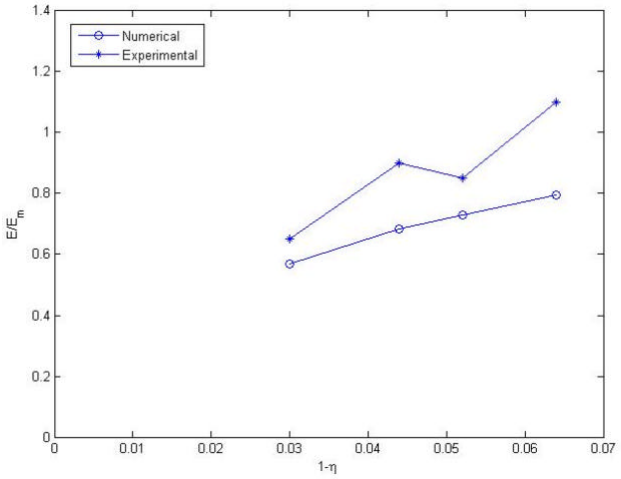

Figure 4.37: Effect of microballoon wall thickness on Young's modulus for Φ = 0.6

It can be observed from these figures shown above that as the value of $(1-h)$ increases, the dependence of the relative Young's modulus on the wall thickness decreases, i.e., the slope of the curves decreases. Although the experimental values are higher in magnitude, there is an overall agreement between the predicted and measured values. One of the reasons for that is the quantity of microballoons used in the numerical simulation is less than they are in the experimental data. In addition to that, numerical models are developed for a constant particle size, where as the particle size varies over a certain range in the experimental studies.

4.7 Crack growth

In this section, the XFEM is applied to study a quasi-static crack growth. The crack growth is governed by the maximum hoop stress criterion [18], which states that the crack will propagate from its tip in the direction q_c where the circumferential (hoop) stress is maximum. The critical angle is calculated by solving the following equations:

$$K_I \sin(q_c) + K_{II}(3\cos(q_c) - 1) = 0 \tag{4.7}$$

Solving equation (4.7) gives the crack propagation angle [19]:

$$q_c = 2\arctan\left[\frac{-2\left(\frac{K_{II}}{K_I}\right)}{1+\sqrt{1+8\left(\frac{K_{II}}{K_I}\right)^2}}\right] \tag{4.8}$$

where K_I and K_{II} are Mode I and II stress intensity factors.

In this particular study, the amount by which the crack advances at each step is fixed in advance, rather than being computed at each step based on some crack growth law.

4.7.1 Crack inclusion interaction

Crack growth in presence of an inclusion is studied in the following example. A square plate of dimension 2×2, subjected to a uniform tensile load, $P = 1$ at the upper edge of the plate and lower edge being fixed is considered. An inclusion of radius 0.166 is situated at the centre of the plate. The geometry and boundary conditions are shown in Figure 4.38. The length of the crack is considered to be 0.2; crack growth increment is taken to be 0.1 for this study and crack growth is simulated for 13 steps. A mesh size of 41×41 is used in this case.

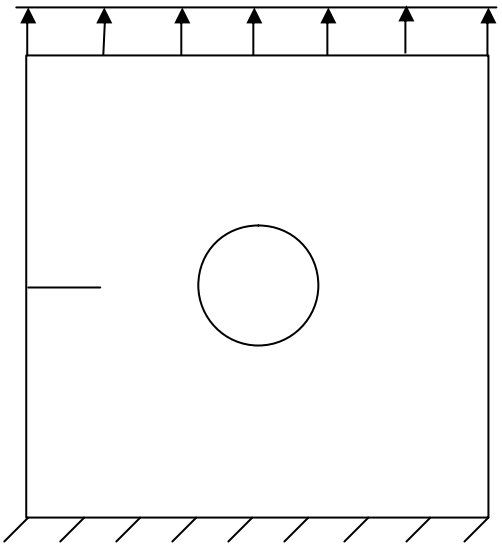

Figure 4.38: Crack inclusion interaction: geometry and boundary conditions

Let $E_{ratio} = E_{matrix} / E_{inclusion}$ be the ratio of Young's modulus between the matrix and the inclusion. The crack growth around the inclusion is studied for two different ratios of Young's modulus: (a) soft inclusion (for which E_{ratio} is taken as 0.01) and (b) stiff inclusion (E_{ratio} is taken as 100). The crack path for both the inclusions (soft and stiff) is shown in Figure 4.39 and 4.40. It can be seen that in case of the soft inclusion, the crack is attracted towards the inclusion where as the crack is deflected in the presence of stiff inclusion. The results obtained are consistent with the results available in the literature [20].

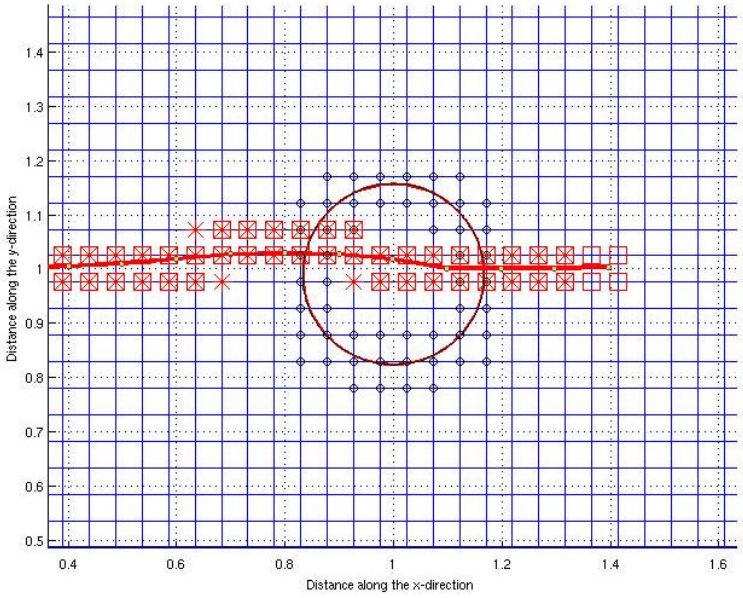

Figure 4.39: Numerically computed crack path for soft inclusion

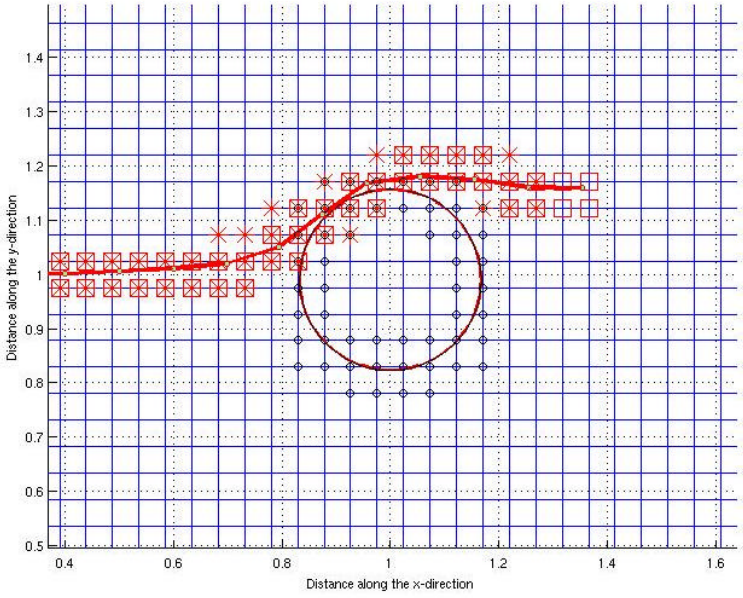

Figure 4.40: Numerically computed crack path for stiff inclusion

Next, another example is carried out where the inclusion is off-centred in the square plate. Apart from the change in the position of the inclusion, the geometry, loading and boundary conditions are kept exactly the same as in the previous case which is shown in Figure 4.41.

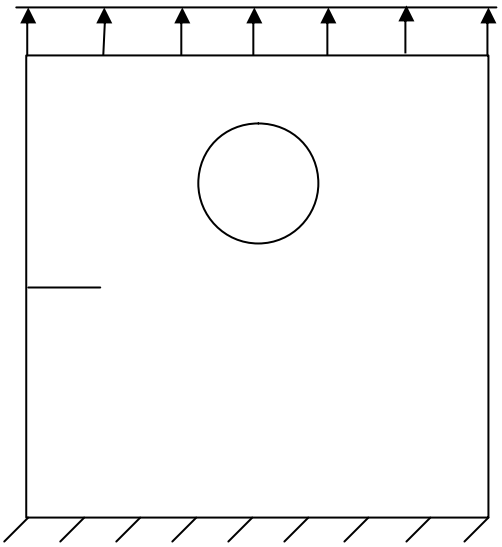

Figure 4.41: Crack inclusion interaction: geometry and boundary conditions

It can be seen from the figures below that crack path follows the same pattern in this case as well. The crack is attracted towards the inclusion if the inclusion is less rigid than the matrix. But if the inclusion is more rigid than the matrix, then the crack is moving away from the inclusion.

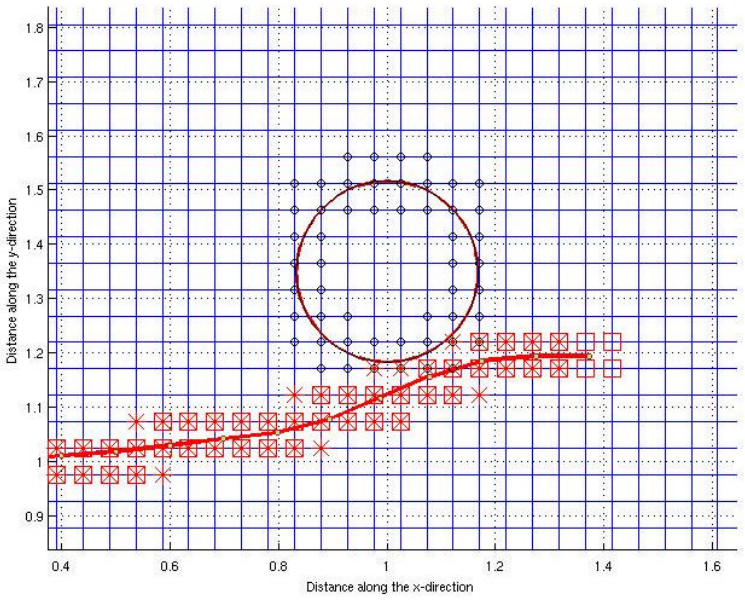

Figure 4.42: Numerically computed crack path for soft inclusion

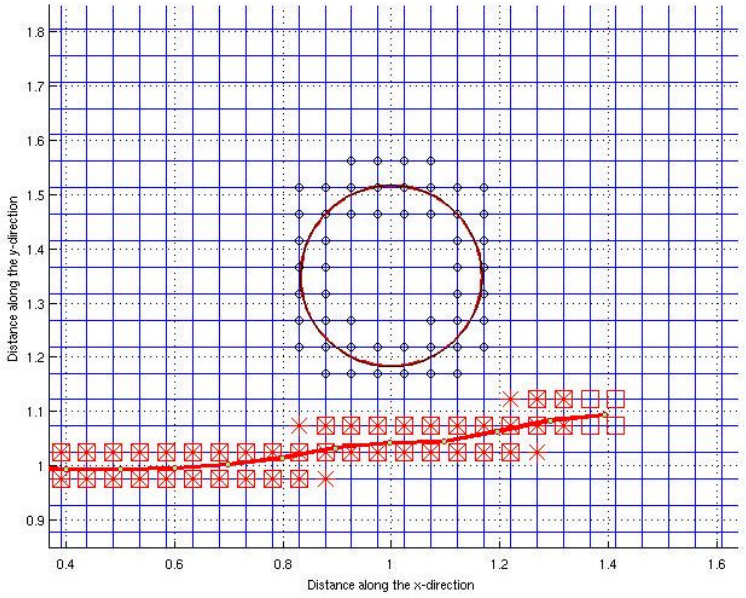

Figure 4.43: Numerically computed crack path for stiff inclusion

An edge crack containing in a square plate of 2×2 interacts with two inclusions (one is a star-shaped and the other one is circular) is considered as the next example. The plate is subjected to a uniform tensile load, $P = 1$ at the upper edge of the plate and the lower edge is fixed. The length of the crack is considered to be 0.2; crack growth increment is 0.1 and crack growth is simulated for 13 steps. A mesh size of 41×41 is used in this study. Young's modulus of elasticity (E) for matrix is 1 and Poisson's ratio is 0.3; where as for inclusions they are 100 and 0.3 respectively.

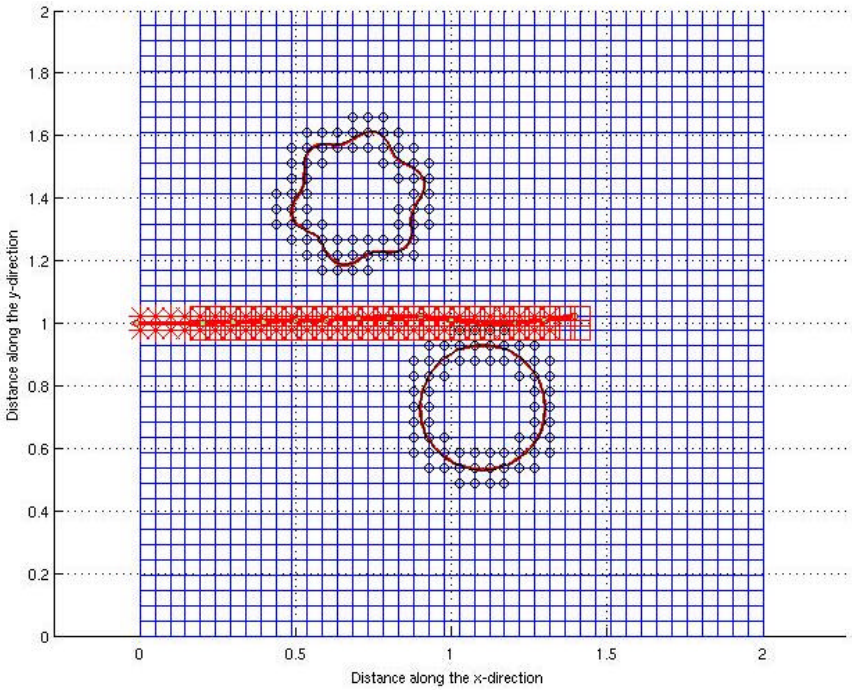

Figure 4.44: Crack propagation phenomenon for soft inclusion

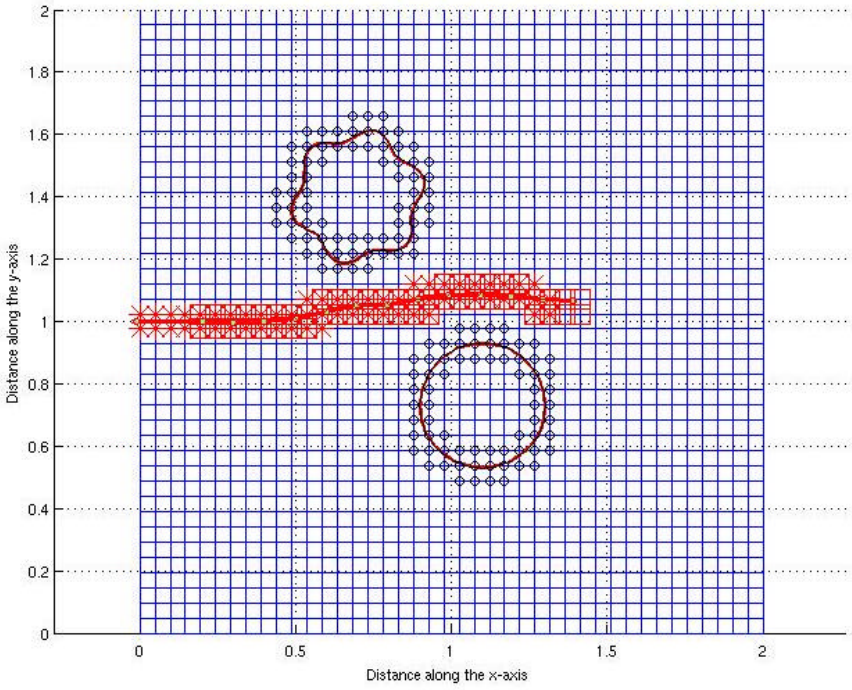

Figure 4.45: Crack propagation phenomenon for stiff inclusion

The computed crack trajectories are shown in Figure 4.44 and 4.45. It can be seen that for soft inclusion, the crack tends to move straight, where as for stiff inclusion, it tends to move away from the inclusions.

4.7 Comparison between EFG using double nodes and FEM

A comparative study is performed between the EFG using double nodes, as discussed in section 3.7, and the FEM to highlight the efficiency and reliability of this technique. The selected domain has width 0.01 and height 0.01. The inclusion is placed at the centre of the domain having a radius of 0.0018. A uniform tension $P = 1$ is applied at the upper edge of the domain and the lower edge is fixed. Young's modulus of elasticity (E) for matrix is 1×10^6 and Poisson's ratio is 0.4; where as for inclusion they are 150×10^6 and 0.4 respectively. Plane stress conditions are assumed. The displacement contour along the x and y-direction is shown in the following diagrams:

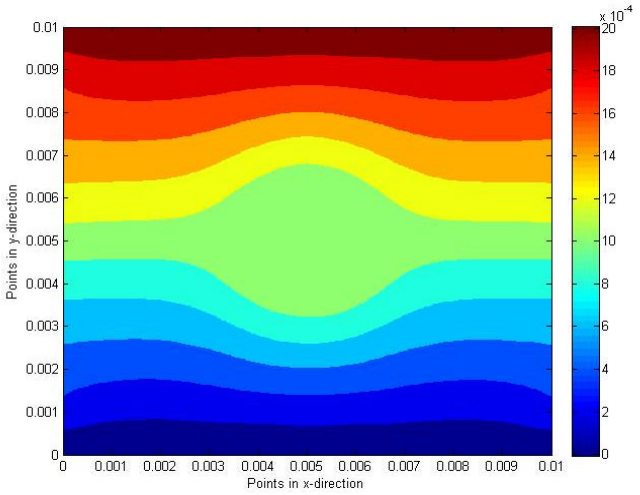

(a)

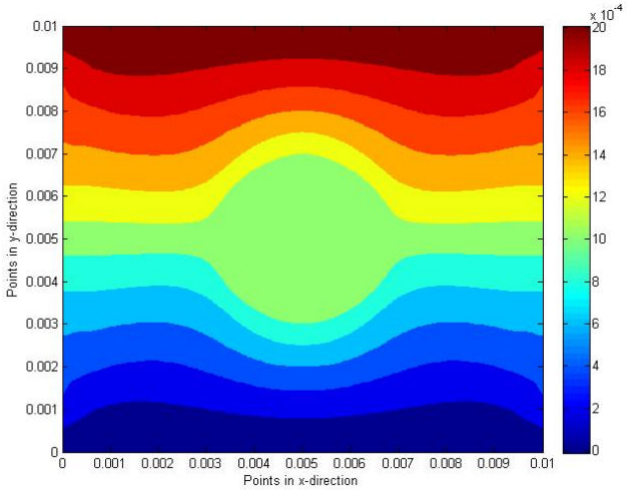

(b)

Figure 4.46: y-displacement contour in (a) XEFG (b) FEM

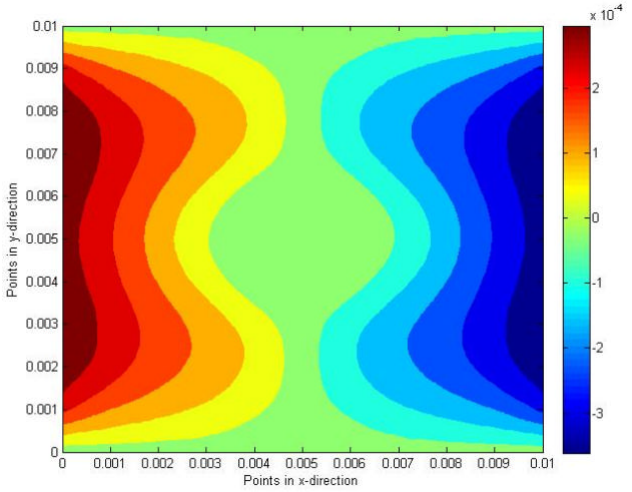

(a)

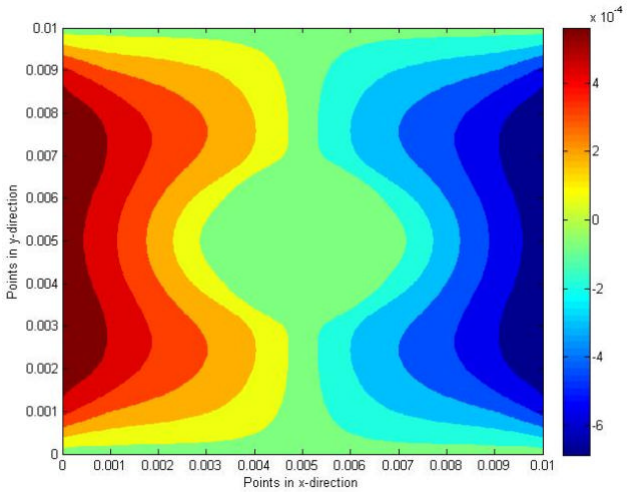

(b)

Figure 4.47: x-displacement contour in (a) XEFG (b) FEM

From the above diagrams, it can be seen that this EFG method using double nodes is highly comparable with the FEM for problems involving material discontinuities and hence the technique can be utilised further to predict the behaviour of particulate composites.

References

1. Sukumar, N., Chopp, D.L., Moës, N., and Belytschko, T., *Modeling holes and inclusions by level sets in the extended finite-element method.* Computational Methods in Applied Mechanics and Engineering, 2001. **190**: p. 6183-6200.
2. Luxmoore, A.R., and Owen, D.R.J., *Syntactic foams. In: Hilyard, N.C. (Ed.).* Mechanics of Cellular Plastics. Applied Science Publishers, London, 1982: p. 359-391.
3. Rizzi, E., Papa, E., and Corigliano, A., *Mechanical behaviour of a syntactic foam: experiments and modelling.* International Journal of Solids and Structures, 2000. **37**: p. 5773-5794.
4. Puterman, M., Narkis, M., and Kenig, S., *Syntactic foam. Part I: Preparation, structure and properties.* Journal of Cellular Plastics, 1980. **16**: p. 223-229.
5. Narkis, M., and Puterman, M., and Kenig, S., *Syntactic foam. Part II: Preparation and characterization of three-phase systems* Journal of Cellular Plastics, 1980. **16**: p. 326-330.
6. Shutov, F.A., *Syntactic polymer foams.* Advances in Polymer Science, 1986. **73(74)**: p. 63-123.
7. Gupta, N., and Woldesenbet, E., *Hygrothermal studies on syntactic foams and compressive strength determination.* composite Structures, 2003. **61(4)**: p. 311-320.
8. Sauvant-Moynot, V., Gimenez, N., Sautereau, H., *Hydrolytic ageing of syntactic foams for thermal insulation in deep water: degradation mechanisms and water uptake model.* Journal of Materials Science, 2006. **41(13)**: p. 4047-4054.
9. Marur, P.R., *Effective elastic moduli of syntactic foams.* Materials Letters, 2005. **59**: p. 1954-1957.
10. Gupta, N., and Woldesenbet, E., *Characterization of flexural properties of syntactic foam core sandwich composites and effect of density variation.* Journal of Composite Materials, 2005. **39(24)**: p. 2197-2212.
11. Bardella, L., and Genna, F., *Elastic design of syntactic foamed sandwiches obtained by filling of three-dimensional sandwich-fabric panels.* International Journal of Solids and Structures, 2001. **38(2)**: p. 307-333.

12. Lee, H., and Neville, K. , *Epoxy-resin foams. In: Frisch, K.C., Saunders, J.H. (Eds.).* Plastic foams. Marcel Dekker, New York, 1973: p. 701-733.
13. Chen, Y.P., Lee, J.D., and Eskandarian, A., *Dynamic meshless method applied to nonlocal crack problems.* Theoretical and Applied Fracture Mechanics, 2002. **38**: p. 293-300.
14. Porfiri, M., and Gupta, N., *Effect of volume fraction and wall thickness on the elastic properties of hollow particle filled composites.* Composites: Part B, 2009. **40**: p. 166-173.
15. Hiel, C., Dittman, D., Ishai, O., *Composite sandwich construction with syntactic foam core. A practical assessment of post-impact damage and residual strength.* . Composites, 1993. **24(5)**: p. 447-450.
16. Scarponi, C., Briotti, G., Barboni, R., Marcone, A., Iannone, M., *Impact testing on composites laminates and sandwich panels.* Journal of Composite Materials, 1996. **30(17)**: p. 1873-1911.
17. Gupta, N., and Nagorny, R., *Tensile properties of glass microballoon-epoxy resin syntactic foams.* Journal of Applied Polymer Science, 2006. **102**(2): p. 1254-1261.
18. Erdogan, F., and Sih, G., *On the crack extension in plates under plane loading and transverse shear.* Journal of Basic Engineering, 1963. **85**: p. 519-527.
19. Sukumar, N., and Prevost, J.H., *Modeling quasi-static crack growth with the extended finite element method part i: Computer implementation.* International Journal of Solids and Structures, 2003. **40**: p. 7513-7537.
20. Bouchard, P., Bay, F., and Chastel, Y., *Numerical modelling of crack propagation: automatic remeshing and comparison of different criteria.* Computer Methods in Applied Mechanics and Engineering, 2003. **192**: p. 3887-3908.

Chapter 5

CONCLUSION

5.1 General conclusion

This thesis focussed on the development, comparison and validation of two enriched numerical methods: the enriched EFG method and the enriched/extended finite element method (XFEM). Both methods are weak form based and rely on enriching the approximation space with special functions representing knowledge about the solution which is known a priori. It is noteworthy to mention that any type of function describing the general behaviour of the solution can be used as an enrichment function. It can be polynomial or non-polynomial functions, discontinuous functions or even data obtained experimentally about the characteristic behaviour of the solution.

This thesis presented the potential of the enriched EFG method for the numerical simulation of particulate composites. The efficiency and accuracy of this method were illustrated with a number of numerical examples by comparing with available analytical solutions and other numerical methods. The work also set strategy for more complicated problems and future work. Separate conclusions were drawn at the end of each chapter. The important contributions and key findings of the thesis are summarized below:

- A novel numerical technique namely the enriched EFG method was studied to model particulate composites. The accuracy and efficiency of this method was validated by satisfactory comparison with other numerical techniques. Hence a simple, reliable and robust EFG scheme for solving problems in linear elastic solid mechanics was developed.

- The use of a single level set for all inclusions affords modelling any number of inhomogeneities present in a linear elastic body of any physical shape and location. Hence the material discontinuities for multiple inclusions were dealt with minimum computational efforts and complexity.

- This numerical technique was applied in modelling syntactic foams, which are nothing but particulate composites with microballons used as filler materials. The investigation was limited to simple configurations; however, the initial tests showed that the results were satisfactory.

- Multi-scale modelling of syntactic foam was performed using homogenisation technique in order to find out the effective properties. The numerical results, compared with the experimental results, provide evidence that the model can be effectively utilised to establish macro-micro structure property relation for multi-phase materials.

- The XFEM was applied to study the crack inclusion interaction in a particle reinforced composite material, where crack trajectories were observed for different parameters. The results obtained from the numerical study were consistent with the results available in the literature.

- Another form of the EFG method was developed to account for the interface discontinuity between the matrix and the inclusion to model particulate composites. This technique involves double nodes or pair nodes around the region of discontinuity (interface) to create continuity condition between the matrix and the inclusion. The numerical investigation was limited to simple configurations due to the problems of enforcing penalty method in the interface region. However, if corrected, this technique can also be applied to predict the behaviour of particulate composites.

5.2 Future work

The enriched EFG method has a lot of potential and presents a wider area of its implementation for the solution of numerous problems. Performing numerical study either to verify some experimental test results or to develop some numerical models presents motivation to develop a numerical tool, where such analysis could be done with accuracy and computational efficiency. Enriched EFG method in this sense is quite appealing as the arbitrary discontinuities can be treated independent of the mesh. Some future recommendations are listed below:

- Generating the initial particle distribution from digital images would be beneficial to study actual microstructures and compare the numerical results to experimentally observed force displacement curves for various

microstructures. The flexibility brought by the lack of conforming meshing of the interfaces will make this image-based analysis simpler. Applications are also expected in biomechanics, where the numerical model could be obtained simply using medical resonance imagery (MRI) or other imaging modalities.

- Because the microstructure is fully parameterised using a single level set function, two phase microstructural optimisation, for example based on topological derivatives would be a natural extension of the method. Similarly to the more recently introduced isogeometric analysis, the boundary between the matrix and the inclusions could be optimised for a given objective function (which could be measured on the macro scale) without any changes in the mesh. However, it would be necessary to ensure the accuracy of each evaluation of the objective function using adaptivity and mesh refinement driven by sound error estimators. The method could then be compared with Cartesian-based FEM.

- More sophisticated models can obviously be looked at, for example including the models for debonding and crack propagation phenomena. Also problems related to various particles having different material properties within the same matrix can be explored. That would help in understanding on the quality and life span of particulate composites, hence could be beneficiary for the design of particulate composites and the relative manufactured products.

- The model can be employed further for investigating more complex problems. For example, large deformation problems where mesh distortion can be burdensome, the enriched EFG will hold high potential to solve those problems.

- The work has been done using a simple 2-D model. The present model has the potential to be extended into 3-D, where various aspects like crack propagation can be explored.

- There has been a lot of research work being carried out on syntactic foam experimentally, however numerically very limited amount of research has been performed. Enriched EFG has the potential to model and analyse the fracture properties of syntactic foam, e.g., the debonding of the microballoons.

- It was observed that the XFEM was applied to study the crack inclusion interaction. Different crack propagation problems can also be investigated using the enriched EFG method, for example graded mesh to observe crack growth within the inclusion, inclined crack, multiple cracks, effect of distance between the crack and the inclusion to name a few.

Publications

1. Islam, M.S., Kulasegaram, S., and Chen, Y.Q., *Computational modelling of particulate composites using Element Free Galerkin method.* 17th UK Conference on Computational Mechanics (ACME-UK), Nottingham, 6-9 April, 2009.